Assessment of an Innovative Compressor Design

Master Thesis
by
Christoph Niederseer, MSc.

MONTAN UNIVERSITÄT
WWW.UNILEOBEN.AC.AT

Strömungsforschung GmbH
ICE
Innovative Computational Engineering

MAGNA STEYR

Submitted at the
Department of Mineral Resources and Petroleum Engineering
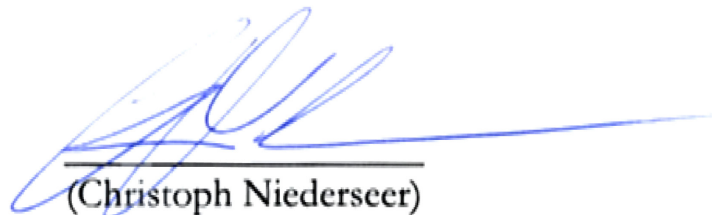at the
University of Leoben

Leoben, 18th of December 2013

EIDESSTATTLICHE ERKLÄRUNG

Ich erkläre an Eides statt, dass ich diese Arbeit selbstständig verfasst, andere als die angegebenen Quellen und Hilfsmittel nicht benutzt und mich auch sonst keiner unerlaubten Hilfsmittel bedient habe.

AFFIDAVIT

I declare in lieu of oath, that I wrote this thesis and performed the associated research myself, using only literature cited in this volume.

(Christoph Niederseer)

Leoben, 18th of December 2013

ABSTRACT:

Viktor Schauberger became over the course of his life a remarkable natural scientist, inventor and philosopher. He established the theory that if water flows in an inwardly spiralling copper pipe, great losses due to resistance and friction occurs. Prof. Pöpel experimentally confirmed this hypothesis in the year 1952. This result from the experiment was the motivation for the master thesis. Based on them and Schauberger's theories a feasibility study was made. It was investigated if these theories can be applied in the automotive industry for forced induction and further research in this direction is meaningful.

By using computational fluid dynamics the assertion from Schauberger could not be confirmed in the course of this work. According to the expectations the simulation's results show a linear relationship between flow rate and flow losses in pipes. The pipes with the smallest wall surfaces and thus with the lower friction areas are having the highest flow rate. The results from 1952 can only be explained by a faulty experimental set up and a very unscientific evaluation of the measurements.

The idea of Mr. Franz Mayr, employee of the company Magna Steyr, was to construct an absolutely new kind of compressor with spiral channels. For the investigation a turbocharger was used as a reference, where the pressure ratio increases with increasing revolutions per minute and air flow. The concept with spiral channels shows the opposite behaviour and is able to defeat the turbocharger at low rotation speeds. According to the results a second reference turbocharger with higher flow rates at lower rotational speeds was used for further comparison. The analysis of the behaviour of the new concept at lower rotation speeds lead to the same result. Again at lower rotation speeds the spiral compressor defeats the reference until a certain number of revolutions.

The results of the simulations have shown that the first considerations towards to turbochargers were proved to be false. The spiral concept should be investigated in the area of superchargers, compressors with low speed of rotation.

Further fluid flow simulation research is necessary and should be improved and verified experimentally.

ACKNOWLEDGEMENT

Christoph Niederseer

TABLE OF CONTENT

LIST OF FIGURES

LIST OF TABLES

LIST OF ABBREVIATIONS

A	area
AFD	Analytic Fluid Dynamics
C	carbon
CDT	Compressor Discharge Temperature
CFD	Computational Fluid Dynamics
CPU	Central processing unit
DNS	Direct Numerical Simulation
EFD	Experimental Fluid Dynamics
f.	and the following one
ff.	following pages
F	force
H	hydrogen
l	length
m	mass
mm	millimetre
$\dot{m}$	mass flow rate
No	number
O	Oxygen
psi	pounds per square inch
Q	volumetric flow rate
RANS	Reynolds-Averaged Navier-Stokes
RNG	Renormalization-group
Re	Reynolds Number
RPM	rotations per minute
u	mean velocity
v	velocity
μ	dynamic viscosity
ν	kinematic viscosity
ρ	density
τ	shear stress
Φ	mass flux

1 INTRODUCTION

1.1 OBJECTIVE OF THE STUDY

Based on an idea by Viktor Schauberger a new compressor concept for automotive applications should be developed and optimized using advanced simulation methods. Viktor Schauberger (1885-1958) was an Austrian forester, scientist and inventor. He observed nature in the smallest detail, and tried to use the principles from nature in his inventions. The cornerstone of his career was sat with his first brilliant invention, a log flume. The construction reduced the carrying costs of wood drastically and worked despite all scientific theories. Schauberger justified the functionality of his log flumes with his thesis on the "law of the water movement". His theories about the movement of water system were confirmed later in a laboratory, the so called "Stuttgart or Pöpel experiment". He was in the opinion that the cycloid space curve movement, a spiral movement from the outside to the inside in direction to the center of movement is the ideal form of motion. According to Schauberger with this form of movement and under specific conditions the frictional resistance can be reduced to a minimum. This result from the experiment was the motivation for this master thesis. Based on this experiment and Schauberger's theories a feasibility study was made. It should be investigated if these theories can also be applied to car compressors and further research in this direction is meaningful.

Schauberger's theories stand in contrast to the current thermodynamic theories. The master thesis should discuss the application and validity of these theories specifically for new automotive compressors. In certain circumstances it could bring significant improvements for turbochargers and could revolutionize the auto world.

The objectives for the thesis were:

- literature about Schauberger's life and his inventions

- collecting data and making investigations about the Stuttgart experiment

- literature about forced induction for the automotive industry

- creation of the geometries with the Software Rhino

- defining the boundary conditions

- various simulations with the Flow Modelling Software ANSYS Fluent to

  o confirm or refute the Stuttgart experiment

  o develop a compressor based on the Schauberger concept

- evaluation of the results and chances to success of the different approaches

1.2 STRUCTURE OF THE THESIS

Basically the diploma thesis consists of three parts, in the first the theoretical fundamentals are formulated, followed by a chapter about Viktor Schauberger and the new idea of automotive compressors. In the last chapter the empirical work is described by ending with the interpretations of the results.

The theoretical fundamentals start with a short overview of computational fluid dynamics in general. It includes basic knowledge, such as the governing equations derived to the Navier-Stokes equations, which has to be known for further simulations. A brief biography about Viktor Schauberger introduces the next chapter. Some of his inventions are described with the focus of the "Stuttgart experiment". After a short introduction in forced induction the idea of a new compressor concept is explained, based on the assertions of Schauberger.

In this work historical experimental data from the so called Pöpel or Stuttgart experiment has to be understood and reproduced. Based on the fundamental understanding of fluid flow itself, a major task of the thesis is to reproduce the experiment with CFD methods.

The main part of the master thesis is the feasibility study from the new concept of the automotive compressor based on the Stuttgart data. More than one construction were planned and investigated for their functionality. The interpretations of the results and further suggestions are ending the master thesis.

2 THEORETICAL FUNDAMENTALS

The chapter should give a very short introduction in the theoretical fundamentals of fluid dynamics. It is kept short with deliberate and points to the numerous books which exist in this area.

2.1 FLUID DYNAMICS IN GENERAL

Fluid mechanics is the study of all fluids either at rest, called fluid statics, or in motion, called fluid dynamics and the subsequent effects of the fluid upon the boundaries, which may be either solid surfaces or interfaces with outer fluids. The study of fluid mechanics contents several fields that have no exact boundaries between them (see following Figure 1). Likely it will be classified between laminar flow and turbulent flow, but fluid mechanics can also be distinguished between a single phase flow and multiphase flow. All boundaries in fluid mechanics aren't sharp, because fluid can switch from a single phase to a multiphase flow, or moreover, a flow with two phases can be treated as a single phase (for example air with dust particle).[1]
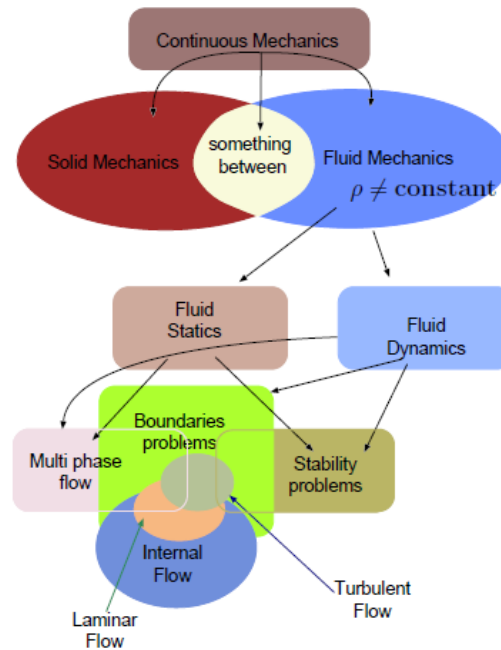
Figure 1 Relationships of fluid mechanics fields *(Bar-Meir (2013), p.2)*

Astronomers, geophysicist, biologist and many more have to deal with fluids and study them. The number of fluids engineering applications is enormous. It is one of the most important areas of physics. Life as we know it would not exist without fluids and without the behaviour that fluids exhibit. There is essentially no part of our daily lives that is not influenced by fluids. Fluids are in general classified as both gases and liquids. For example the air we breathe and the water we drink and which makes up most of our body mass are fluids.[2]

---

[1] Bar-Meir (2013), p.2
[2] McDonough (2009), p. 1

The study of fluid mechanics goes back at least to the days of ancient Greece, when Archimedes investigated fluid statics and buoyancy and formulated his famous law known now as the Archimedes principle. Basic practical understanding of the behaviour of fluids was available much earlier, at least by the time of the ancient Egyptians. Also the Romans had flushing toilets not very different from modern houses and their aqueducts are still considered a tremendous engineering feat. Thus, already by the time of the Roman Empire enough practical information had been accumulated to permit quite sophisticated applications of fluid dynamics.

Rapid advancement in fluid mechanics was made by Leonardo da Vinci with his observations and experiments. He made several attempts to study the flight and developed some concepts on the origin of the forces. He also built the first chambered canal lock near Milan. Knowledge increasingly gained then by the contributions of Galileo Galilei and with inventing the barometer by Evangelista Torricelli. Defining the viscosity by Isaac Newton and the hydrostatic research by Blaise Pascal were also notable milestones. The modern understanding of fluid motion began several centuries ago with the work of Leonhard Euler and the Bernoullis (father and son) with the introduction of the Bernoulli equation.

Of crucial importance in fluid dynamics are the Navier-Stokes equations, which were introduced by Navier in the 1820s, and the complete system of equations representing essentially all fluid motions were given by Stokes in the 1840s.[3] The Navier-Stokes equations were considered unsolvable during the mid-nineteen century because of the high complexity. So theoreticians tried to simplify the equations and experimentalists at the same time proposed many correlations to many fluid mechanic problems, for example, resistance by Darcy or Weisbach. The industrial revolution at the end of the twenty century lead to new several novel concepts like the theoretical and experimental researches by Reynolds and the development of dimensional analysis by Rayleigh, which changed the science of the fluid mechanics. Perhaps the most radical concept that affects the fluid mechanics is Prandtl's idea of boundary layer which is a combination of the modelling and dimensional analysis. This concept leads to mathematical basis for many approximations and transformed the fluid mechanics to today modern science.[4]

Today engineers have different kinds of tools available for solving fluids engineering systems: as mentioned above, study could be done theoretically, called "Analytic Fluid Dynamics" (AFD), experimentally, named "Experimental Fluid Dynamics" (EFD) and because of the power of modern digital computers in these days there is a third way to study fluid dynamics, the "Computational Fluid Dynamics" (CFD). Today CFD has moved to the forefront in engineering analysis of fluid flow, because most of what can be done theoretically has already been done, and experiments are generally difficult and expensive.[5]

---

[3] McDonough (2009), p. 4
[4] Bar-Meir (2013), p.4
[5] McDonough (2009), p. 4

2.2   COMPUTATIONAL FLUID DYNAMICS

CFD is the analysis of systems in terms of fluid flow, heat transfer and associated phenomena such as chemical reactions by means of computer-based simulation. All CFD codes contain three main elements: a pre-processor, a solver and a post-processor.[6]

Pre-processing consists of the input of a flow problem to a program by means of an operator-friendly interface and the subsequent transformation of this input into a form suitable for use by the solver. Activities that have to be done at the pre-processing stage are the definition of the geometry, the grid generation, which divides the geometry into a number of smaller cells, and the selection of the physical and chemical phenomena that need to be modelled. Also the fluid properties have to be defined with setting the boundary conditions.

The solution to a flow problem is defined at nodes inside each cell. The accuracy of a CFD solution is governed by the number of cells in the grid. In general, the larger the number of cells the better the solution accuracy, but resulting in a longer calculation time. About 50 % of the time from a CFD project is spent in the definition of the geometry and generating the mesh.[7]

Numerical solution techniques for a solver can be divided into: finite difference, finite element and spectral methods. Finite volume method is a special finite difference formulation and is the most well-established and thoroughly validated general purpose CFD technique. The CFD software used for this master thesis is also based on this formulation. The numerical algorithm consists of the following three main steps:

- Formal integration of the governing equations of fluid flow over all the (finite) control volumes of the solution geometry
- Discretisation involves the substitution of a variety of finite-difference-type approximations for the terms in the integrated equation representing flow processes such as convection, diffusion and sources. This converts the integral equations into a system of algebraic equations.
- Solution of the algebraic equations by an iterative method.

The first step, the control volume integration, distinguishes the finite volume method from all other CFD techniques. The resulting statements express the exact conservation of relevant properties for each finite size cell. This clear relationship between the numerical algorithm and the underlying physical conservation principle forms one of the main attractions of the finite volume method and makes its concepts much simpler to understand than finite element and spectral methods.

CFD codes contain discretisation techniques suitable for the treatment of the key transport phenomena, convention and diffusion as well as for the source terms and the rate of change with respect to time. The underlying physical phenomena are complex and non-linear so an iterative solution approach is required. One of the most popular solution procedures is the SIMPLE algorithm to ensure correct linkage between pressure and velocity. SIMPLE was also used for this work.[8]

---

[6] Versteeg (1995), p. 1ff.
[7] Versteeg (1995), p. 1ff.
[8] Versteeg (1995), p. 1ff.

Post-processing means to use visualisation tools to interpret the results. Therefore geometry and grid displays, vector plots, contour plots, surface plots, particle tracking and animations are available to illustrate the solution.

In solving fluid flow problems the underlying physics is complex and the results generated by a CFD code are at best as good as the physics embedded in it and at worst as good as its operator. A good understanding of the numerical solution algorithm is crucial. For determining the success of such algorithm the mathematical concept convergence can be used. Convergence is the property of a numerical method to produce a solution which approaches the exact solution as the grid spacing, control volume size or element size is reduced to zero.[9]

---

[9] Versteeg (1995), p. 1ff.

2.3   CONSERVATION LAWS OF FLUID FLOW

The governing equations of fluid flow represent mathematical statements of the conservation laws of physics:

- The mass of a fluid is conserved.
- Newton's second law, the rate of change of momentum equals the sum of the forces on a fluid particle.
- First law of thermodynamics, the rate of change of energy is equal to the sum of the rate of heat addition to and the rate of work done on a fluid particle.[10]

Before taking a closer look to the conservation laws we have to discuss the continuum hypothesis. This continuum assumption, however, considers fluids to be continuous.

2.3.1 THE CONTINUUM HYPOTHESIS

The Continuum Hypothesis is necessary to provide the framework in which essentially all analysis of fluids were conducted. The assumption, however, says that when we dealing with fluid flow at macroscopic length scales we can ignore the fact that fluids are composed of billions of individual molecules that collide with one another. The molecular structure of matter and molecular motions can be disregarded. The behaviour of the fluid is described in terms of macroscopic properties, such as velocity, pressure, density and temperature, and their space and time derivatives. They may be assumed to vary continuously from one point to the next and are averaged values within the fluid. A fluid particle or point in a fluid is then the smallest possible element of fluid whose macroscopic properties are not influenced by individual molecules. The fact that the fluid is made up of discrete molecules is ignored.[11]
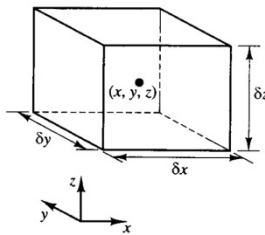
Figure 2 A small element of fluid *(Versteeg (1995), p. 11)*

Considering a small element of fluid with the sides δx, δy and δz (Figure 2). The centre of the element is located at position (x,y,z). A systematic account of changes in the mass, momentum and energy of the fluid element due to fluid flow across its boundaries and, where appropriate, due to the action of sources inside the element, leads to the fluid flow equations.

All fluid properties are functions of space and time so it would strictly need to write ρ(x,y,z,t), p(x,y,z,t), T(x,y,z,t) and u(x,y,z,t) for the density, pressure, temperature and the velocity vector. The element under consideration is so small that fluid properties at the faces can be expressed accurately enough by means of the first two terms of a Taylor series expansion. For example, the pressure at the left and right side, which are both at a distance of 1/2δx from the element centre, can be expressed as[12]

$$p - \frac{\partial p}{\partial x}\frac{1}{2}\delta x \ \ and \ \ p + \frac{\partial p}{\partial x}\frac{1}{2}\delta x \,.$$

---

[10] Versteeg (1995), p. 10
[11] McDonough, p. 11
[12] Versteeg (1995), p. 11

2.3.2 CONSERVATION OF MASS

The rate of increase of mass in a fluid element is equal to the net rate of flow of mass into the fluid element. This is known as the mass balance for the fluid element.

$$\frac{\partial}{\partial t}(\rho \partial x \partial y \partial z) = \frac{\partial \rho}{\partial t}(\partial x \partial y \partial z),$$

defines the rate of increase of mass in the fluid element. The mass flow rate across a face of the element is given by the product of density, area and the velocity component normal to the face. The figure below shows the mass flows in and out of the fluid element.
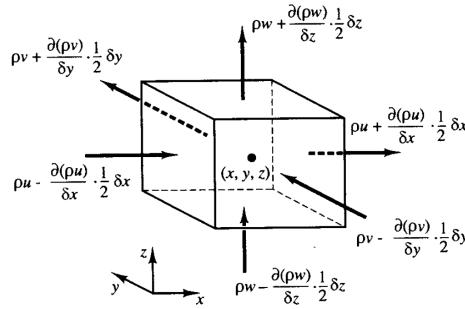
Figure 3 Mass flows in and out of the fluid element *(Versteeg (1995), p. 12)*

Now the rate of increase of mass is equated to the net rate of flow of mass into the element across its faces. All terms of the resulting mass balance are arranged on the left hand side of the equals sign and the expression is divided by the element volume δxδyδz. This yields to

$$\boldsymbol{\frac{\partial \rho}{\partial t} + \frac{\partial(\rho u)}{\partial x} + \frac{\partial(\rho v)}{\partial y} + \frac{\partial(\rho w)}{\partial z} = 0}$$

or in a more compact vector notation:

$$\boldsymbol{\frac{\partial \rho}{\partial t} + \nabla (\rho v) = 0}$$

The above expression is known as the continuity equation. It is the unsteady, three dimensional mass conservation at a point in a compressible fluid. The first term on the left hand side is the rate of change in time of the density in mass per unit volume. The second term describes the net flow of mass out of the element across its boundaries and is called the convective term.[13]

The derivative of conservation of mass is summarized from Versteeg and Malalasekera (1995). For a more detail explanation see chapter "2.1.1 Mass conservation in three dimensions" in their book "An introduction to computational fluid dynamics".

---

[13] Versteeg (1995), p. 11ff.

2.3.3 MOMENTUM BALANCE

Newton's second law states that the rate of change of momentum of a fluid particle equals the sum of the forces on the particle.

The rates of increase of x-, y- and z- momentum per unit volume of a fluid particle are given by

$$\rho \frac{Du}{Dt} \qquad\qquad \rho \frac{Dv}{Dt} \qquad\qquad \rho \frac{Dw}{Dt}$$

Forces on fluid particles can be distinguished between surface forces and body forces. Both types also can be further divided in:

- surface forces
    - pressure forces
    - viscous forces
- body forces
    - gravity force
    - centrifugal force
    - Coriolis force
    - electromagnetic force

In practice the contributions due to the surface forces are often highlighted as separate terms in the momentum equation and the effects of body forces are included as source terms.

The pressure, denoted by p, and the nine viscous stress components, which were denoted by $\tau_{i,j}$, are defining the state of stress of a fluid element seen in the figure below.
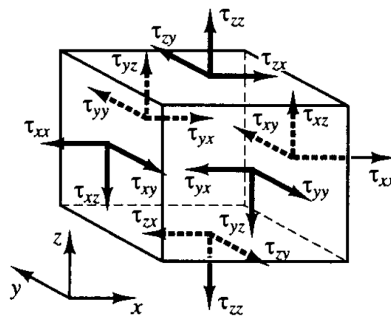
Figure 4 Stress components on the fluid element *(Versteeg (1995), p. 12)*

The x-component of the momentum equation is found by setting the rate of change of x-momentum of the fluid particle equal to the total force in the x-direction on the element due to surface stresses plus the rate of increase of x-momentum due to sources.

$$\rho \frac{Du}{Dt} = \frac{\partial(-p + \tau_{xx})}{\partial x} + \frac{\partial(\tau_{yx})}{\partial y} + \frac{\partial(\tau_{zx})}{\partial z} + S_{Mx}$$

The y-component of the momentum equation looks similar and is given by

$$\rho \frac{Dv}{Dt} = \frac{\partial(\tau_{xy})}{\partial x} + \frac{\partial(-p + \tau_{yy})}{\partial y} + \frac{\partial(\tau_{zy})}{\partial z} + S_{My}$$

and the z-component of the momentum equation by

$$\rho \frac{Dv}{Dt} = \frac{\partial(\tau_{xz})}{\partial x} + \frac{\partial(\tau_{yz})}{\partial y} + \frac{\partial(-p + \tau_{zz})}{\partial z} + S_{Mz}$$

The source terms S_{Mx}, S_{My} and S_{Mz} include contributions due to body forces only. For example the body force due to gravity would be modelled by $S_{Mx}=0$, $S_{My}=0$ and $S_{Mz}=-\rho g$.[14]

Also this chapter was summarized from Versteeg and Malalasekera (1995). A deeper discussion can be found in their book "An introduction to computational fluid dynamics", chapter "2.1.3 Momentum equation in three dimensions".

---

[14] Versteeg (1995), p. 14ff.

2.3.4 ENERGY CONSERVATION

The first law of thermodynamics says that the rate of change of energy of a fluid particle is equal to the rate of heat addition to the fluid particle plus the rate of work done on the particle.

The rate of heat addition to the fluid particle due to heat conduction across element boundaries is defined by:

$$-\nabla q = \nabla(k \ grad \ T)$$

The rate of work done on the fluid particle in the element by a surface force is equal to the product of the force and velocity component in the direction of the force. So the total rate of work done on the fluid particle by surface stresses is given by:

$$-\nabla(\rho u) + \left[\frac{\partial(u\tau_{xx})}{\partial x} + \frac{\partial(u\tau_{yx})}{\partial y} + \frac{\partial(u\tau_{zx})}{\partial z} + \frac{\partial(v\tau_{xy})}{\partial x} + \frac{\partial(v\tau_{yy})}{\partial y} + \frac{\partial(v\tau_{zy})}{\partial z} + \frac{\partial(w\tau_{xz})}{\partial x} + \frac{\partial(u\tau_{yz})}{\partial y} + \frac{\partial(u\tau_{zz})}{\partial z} \right]$$

The energy of a fluid is defined as the sum of internal (thermal) energy i, kinetic energy ½(u²+v²+w²) and gravitational potential energy. It is possible to regard the gravitational force as a body force which does work on the fluid element as it moves through the gravity field.

So the rate of change of energy of a fluid particle per unit volume is given by the sum of the net rate of work done on the fluid particle and the net rate of heat addition to the fluid and the rate of increase of energy due to sources. [15]

$$\rho \frac{DE}{Dt} = -\nabla(\rho u) + \left[\frac{\partial(u\tau_{xx})}{\partial x} + \frac{\partial(u\tau_{yx})}{\partial y} + \frac{\partial(u\tau_{zx})}{\partial z} + \cdots \right]$$

$$\left[\cdots + \frac{\partial(v\tau_{xy})}{\partial x} + \frac{\partial(v\tau_{yy})}{\partial y} + \frac{\partial(v\tau_{zy})}{\partial z} + \frac{\partial(w\tau_{xz})}{\partial x} + \frac{\partial(u\tau_{yz})}{\partial y} + \frac{\partial(u\tau_{zz})}{\partial z} \right] + \cdots$$

$$\cdots + \nabla(k \ grad \ T) + S_E$$

The chapter is an outlook from Versteeg and Malalasekera (1995), chapter "2.1.4 Energy equation in three dimensions" from their book "An introduction to computational fluid dynamics".

---

[15] Versteeg (1995), p. 19ff.

2.4 EQUATION OF STATE

The five partial differential equations mentioned in the chapters (the mass conservation, the x-, y- and z-momentum equations and the energy equation) are describing the motion of a fluid in three dimensions. Among the unknowns there are four thermodynamic variables: p, ρ, i and T. Relationships between the thermodynamic variables can be obtained through the assumption of thermodynamic equilibrium, because fluids always remain in thermodynamic equilibrium.

Describing the state of a substance in thermodynamic equilibrium can be made by just two state variables. Equations of state relate the other variables to the two state variables. If using ρ and T as state variables leads to state equations for pressure p and specific internal energy i: [16]

$$p = p\,(\rho, T) \quad \text{and} \quad i = i\,(\rho, T)$$

For a perfect gas the following equations of state can be used:

$$p = \rho RT \quad \text{and} \quad i = C_V T$$

where R is the gas constant ($8,314\ \text{J mol}^{-1}\ \text{K}^{-1}$), and C_V the specific heat at constant volume.

The assumption of thermodynamic equilibrium eliminates all but the two thermodynamic state variables. In the flow of compressible fluids the equations of state provide the linkage between the energy equation on the one hand and mass conservation and momentum equations on the other. This linkage arises through the possibility of density variations as a result of pressure and temperature variations in the flow field.

Liquids and gases flowing at low speeds behave as incompressible fluids. Without density variations there is no linkage between the energy equation and the mass conservation and momentum equations. The flow field can often be solved by considering mass conservation and momentum equations only. The energy equation only needs to be solved alongside the others if the problem involves heat transfer. [17]

---

[16] Versteeg (1995), p. 21

[17] Versteeg (1995), p. 21

2.5 NAVIER-STOKES EQUATIONS

The governing equations contain as further unknowns the viscous stress components $\tau_{i,j}$. The most useful forms of the conservation equations for fluid flows are obtained by introducing a suitable model for the viscous stresses $\tau_{i,j}$. In many fluid flows the viscous stresses can be expressed as functions of the local deformation rate. In three dimensional flows the local rate of deformation is composed of the linear deformation rate and the volumetric deformation rate. The rate of linear deformation of a fluid element has nine components in three dimensions.

In a Newtonian fluid the viscous stresses are proportional to the rates of deformation. The three-dimensional form of Newton's law of viscosity for compressible flows involves two constants of proportionality. The dynamic viscosity, μ, to relate stresses to linear deformations, and the second viscosity λ to relate stresses to the volumetric deformation. Not much is known about the second viscosity λ, because its effect is small in practice. For gases a good working approximation can be obtained by taking value $\lambda = 2/3\ \mu$.[18] Liquids are incompressible so the mass conservation equation is $\nabla u = 0$ and the viscous stresses are just twice the local rate of linear deformation times the dynamic viscosity.

Substitution of the nine viscous stress components into the momentum equations from the chapter 2.3.3 "Momentum balance" yields to the Navier-Stokes equations: [19]

$$\rho \frac{Du}{Dt} = -\frac{\partial p}{\partial x} + \frac{\partial}{\partial x}\left[2\mu\frac{\partial u}{\partial x} + \lambda\nabla u\right] + \frac{\partial}{\partial y}\left[\mu\left(\frac{\partial u}{\partial y} + \frac{\partial v}{\partial x}\right)\right] + \frac{\partial}{\partial z}\left[\mu\left(\frac{\partial u}{\partial z} + \frac{\partial w}{\partial x}\right)\right] + S_{Mx}$$

$$\rho \frac{Dv}{Dt} = -\frac{\partial p}{\partial y} + \frac{\partial}{\partial x}\left[\mu\left(\frac{\partial u}{\partial y} + \frac{\partial v}{\partial x}\right)\right] + \frac{\partial}{\partial y}\left[2\mu\frac{\partial v}{\partial y} + \lambda\nabla u\right] + \frac{\partial}{\partial z}\left[\mu\left(\frac{\partial v}{\partial z} + \frac{\partial w}{\partial x}\right)\right] + S_{My}$$

$$\rho \frac{Dw}{Dt} = -\frac{\partial p}{\partial z} + \frac{\partial}{\partial x}\left[\mu\left(\frac{\partial u}{\partial z} + \frac{\partial w}{\partial x}\right)\right] + \frac{\partial}{\partial y}\left[\mu\left(\frac{\partial v}{\partial z} + \frac{\partial w}{\partial y}\right)\right] + \frac{\partial}{\partial z}\left[2\mu\frac{\partial w}{\partial z} + \lambda\nabla u\right] + S_{Mz}$$

The Navier-Stokes equations can also be written in the more useful form for the development of the finite volume method:

$$\rho \frac{Du}{Dt} = -\frac{\partial p}{\partial x} + \nabla(\mu\ grad\ u) + S_{Mx}$$

$$\rho \frac{Dv}{Dt} = -\frac{\partial p}{\partial y} + \nabla(\mu\ grad\ v) + S_{My}$$

$$\rho \frac{Dw}{Dt} = -\frac{\partial p}{\partial z} + \nabla(\mu\ grad\ w) + S_{Mz}$$

---

[18] Schlichting (1979)

[19] Versteeg (1995), p. 21ff.

By using the Newtonian model for viscous stresses in the internal energy equation it yields to:

$$\rho \frac{Di}{Dt} = -\mathbf{p}\nabla\mathbf{u} + \nabla(\boldsymbol{\mu}\ grad\ T) + \Phi + S_i$$

All effects due to viscous stresses in this internal energy equation are described by the dissipation function Φ, which represents a source of internal energy due to deformation work on the fluid particle. This work is extracted from the mechanical agency which causes the motion and is converted into internal energy or heat.[20]

To summarize, the governing equations of the flow of a compressible Newtonian fluid are:

Mass

$$\frac{\partial \rho}{\partial t} + div(\rho u) = 0$$

x-momentum

$$\frac{\partial(\rho u)}{\partial t} + \nabla(\rho u \boldsymbol{u}) = -\frac{\partial p}{\partial x} + \nabla(\mu\ grad\ u) + S_{Mx}$$

y-momentum

$$\frac{\partial(\rho v)}{\partial t} + \nabla(\rho v \boldsymbol{u}) = -\frac{\partial p}{\partial y} + \nabla(\mu\ grad\ v) + S_{My}$$

z-momentum

$$\frac{\partial(\rho w)}{\partial t} + \nabla(\rho w \boldsymbol{u}) = -\frac{\partial p}{\partial z} + \nabla(\mu\ grad\ w) + S_{Mz}$$

Internal energy

$$\frac{\partial(\rho i)}{\partial t} + \text{div}(\rho i \boldsymbol{u}) = -p\ \text{div}\ \boldsymbol{u} + \nabla(k\ grad\ T) + \Phi + S_i$$

Equations of state

$$p = \rho RT \qquad \text{and} \qquad p = C_V T$$

This short explanation about the Navier-Stokes equations was summarised from Versteeg and Malalasekera (1995), chapter "2.3 Navier-Stokes equations for a Newtonian fluid" from their book "An introduction to computational fluid dynamics".

---

[20] Versteeg (1995), p. 24

2.6 TRANSPORT EQUATION

Introducing a general variable $\emptyset$ in the various fluid flow equations before leads us to the so-called transport equation for property $\emptyset$:

$$\frac{\partial(\rho\emptyset)}{\partial t} + \nabla(\rho\emptyset\mathrm{u}) = \nabla(\Gamma\ grad\ \emptyset) + S_\emptyset$$

In words it means that the rate of increase of $\emptyset$ of the fluid element plus the net rate of flow of $\emptyset$ out of the fluid element equals the rate of increase of $\emptyset$ due to diffusion (Γ is the diffusion coefficient) and the rate of increase of $\emptyset$ due to sources.

The equation is used as the starting point for computational procedures in the finite volume method. By integration of the equation over a three dimensional control volume CV and using Gauss' divergence theorem (see Versteeg (1995), p. 25) it leads us to:

$$\frac{\partial}{\partial t}\left(\int_{CV} \rho\emptyset\ dV\right) + \int_A\ n\,.\,(\rho\emptyset u)\ dA = \int_A\ n\,.\,(\Gamma\ grad\ \emptyset)\ dA + \int_{CV} S_\emptyset\ dV$$

On the left hand side the first term signifies the rate of change of the total amount of fluid property $\emptyset$ in the control volume. The product $n\,.\,(\rho\emptyset u)$ expresses the flux component of property $\emptyset$ due to fluid flow along the outward normal vector n, so the second term on the left hand side, the connective term, is therefore the net rate of decrease of fluid property $\emptyset$ of the fluid element due to convection. The first term on the right hand side of the equation above, the diffusive term, is thus associated with a flux into the element and represents the net rate of increase of fluid property $\emptyset$ of the fluid element due to diffusion. The final term on the right hand side of this equation gives the rate of increase of property $\emptyset$ as a result of sources in the fluid element.

In steady state the rate of change term is equal to zero. This fact leads to the integrated form of the steady transport equation:[21]

$$\int_A\ \boldsymbol{n}\,.\,(\boldsymbol{\rho\emptyset u})\ \boldsymbol{dA} = \int_A\ \boldsymbol{n}\,.\,(\boldsymbol{\Gamma\ grad\ \emptyset})\ \boldsymbol{dA} + \int_{CV} \boldsymbol{S_\emptyset}\ \boldsymbol{dV}$$

The derivation of the transport equation in detail can be found in Versteeg and Malalasekera (1995), chapter "2.5 Differential and integral forms of the general transport equations" in their book "An introduction to computational fluid dynamics".

---

[21] Versteeg (1995), p. 25f.

2.7 TURBULENCE AND ITS MODELLING

All flows, both simple ones such as pipe flows and flat boundary layers and more compli-
cated ones, become unstable above a certain Reynolds number. At low Reynolds numbers
flows are laminar. At higher Reynolds numbers flows are observed to become turbulent. So
to characterize whether the flow regime is laminar or turbulent, the Reynolds number can
be used. It is a dimensionless number that gives a measure of the ratio of inertial forces to
viscous forces. If viscous forces are dominant, a low Reynolds number would be the result
and indicates laminar flow. High Reynolds numbers are the result by dominating of inertial
forces and a chaotic and random state of motion develops in which the velocity and pres-
sure change continuously with time within substantial regions of flow.

The Reynolds number is defined as

$$Re = \frac{\rho * u * l}{\mu} = \frac{u * l}{v} \ ,$$

where u is the mean velocity, l the characteristic length (for flow in pipe it is the hydraulic
diameter), ρ the density of the fluid, v the kinematic viscosity and μ the dynamic viscosity.

Experimental observations have shown that for a fully developed flow in a pipe, laminar
flow occurs when Re is smaller than 2300 and turbulent flow occurs when Re is bigger than
4000. The interval between 2300 and 4000 is called transition flow, in which laminar and
turbulent flow can be possible.[22]

The transition between laminar and turbulence is strongly affected by factors such as pres-
sure gradient, disturbance levels, wall roughness and heat transfer, but the discussion only
apply to subsonic incompressible flows. The appearance of significant compressibility ef-
fects complicates the theory.[23]

All fluids are compressible to some extent, because changes in pressure or temperature will
result in changes in density. However, in many situations the changes in pressure and tem-
perature are sufficiently small that the change in density is negligible. In this case the flow
can be modelled as an incompressible flow.[24]

Compressibility effects are typically considered significant if the Mach number (the ratio of
the flow velocity to the local speed of sound) of the flow exceeds 0.3, or if the fluid under-
goes very large pressure changes.[25] When the flow velocity reaches the speed of sound or
when the pressure change in the system is large, the variation of the gas density with pres-
sure has a significant impact on the flow velocity, pressure, and temperature. Compressible
flows create a unique set of flow physics and are not further discussed in this work.

While turbulence is, in principle, described by the Navier-Stokes equations, it is not feasible
in most situations to resolve the wide range of scales in time and space by Direct Numeri-
cal Simulation (DNS) as the CPU requirements would by far exceed the available compu-
ting power for any foreseeable future. For this reason, averaging procedures have to be
applied to the Navier-Stokes equations to filter out all, or at least, parts of the turbulent
spectrum. The most widely applied averaging procedure is Reynolds-averaging (which, for

---

[22] http://en.wikipedia.org/wiki/Reynolds_number

[23] Versteeg (1995), p. 48

[24] http://en.wikipedia.org/wiki/Fluid_dynamics#Compressible_vs_incompressible_flow

[25] http://en.wikipedia.org/wiki/Compressible_flow

all practical purposes is time-averaging) of the equations, resulting in the Reynolds-Averaged Navier-Stokes (RANS) equations. By this process, all turbulent structures are eliminated from the flow and a smooth variation of the averaged velocity and pressure fields can be obtained. However, the averaging process introduces additional unknown terms into the transport equations (Reynolds Stresses and Fluxes) which need to be provided by suitable turbulence models. The quality of the simulation can depend crucially on the selected turbulence model.[26]

---

[26] ANSYS 14.5 Help, Fluent, User's Guide, chapter 12.1 Introduction

2.7.1 BOUNDARY LAYER

In flows along solid boundaries there is a substantial region of inertia dominated flow far away from the wall and a thin layer within which viscous effects are important.

Close to the wall the flow is influenced by viscous effects. The mean flow velocity only depends on the distance y from the wall, fluid density ρ and viscosity μ and the wall shear stress τ_w. Dimensional analysis shows that

$$u^* = \frac{U}{u_\tau} = f\left(\frac{\rho u_\tau y}{\mu}\right) = f(y^*)$$

This is the **law of the wall** and contains the definitions of two important dimensionless groups u^* and y^*, where

$$u_\tau = \left(\frac{\tau_W}{\rho}\right)^2$$

is the so called friction velocity.

Far away from the wall the velocity at a point is influenced by the retarding effect of the wall through the value of the wall shear stress, but not by the viscosity itself. The length scale appropriate to this region is the boundary layer thickness δ and leads us to the **velocity-defect law**:

$$\frac{U_{max} - U}{u_\tau} = g\left(\frac{y}{\delta}\right)$$

At the solid surface the fluid is stationary. Turbulent eddying motions must also stop very close to the wall. In the absence of turbulent shear stress effects the fluid closest to the wall is dominated by viscous shear. This layer is in practice extremely thin ($y^* < 5$) and assume that the shear stress is approximately constant and equal to the wall shear stress throughout the layer. This leads to a linear relationship between velocity and distance from the wall and so the fluid layer adjacent to the wall is often called as the **linear sub-layer.**

Outside the viscous sublayer ($30 < y^* < 500$) a region exists where viscous and turbulent effects are both important. The shear stress varies slowly with distance from the wall and within this inner region it is assumed to be constant and equal to the wall shear stress. The relationship between u^* and y^* is then given by

$$U^* = \frac{1}{\kappa}\ln(Ey^*)$$

and is called the **log-law** because of the logarithmic relationship and the layer the log-law layer.[27]

---

[27] Versteeg (1995), p. 57ff.

Figure 5 shows the close agreement between theoretical equations and their respective areas of validity and experimental data.[28]
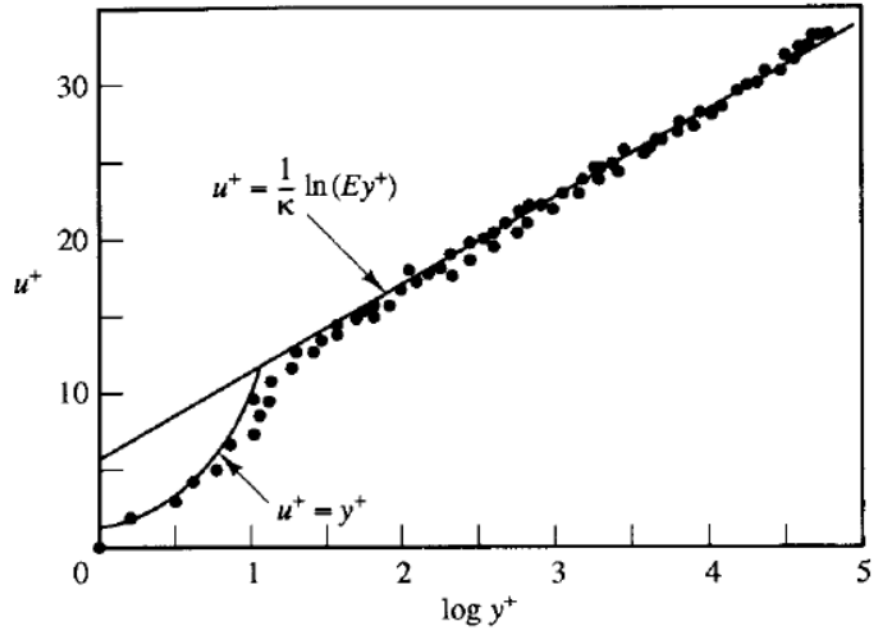

Figure 5 Subdivision of the Near-Wall Region[29]

---

[28] Schlichting (1979)

[29] Versteeg (1995), p. 61

2.7.2 TURBULENCE MODELS

There are a numerous turbulence models available. In simple they can be classified between classical models and Large eddy simulations. Classical models use the Reynolds equations (see Versteeg (1995), p. 49ff.). Large eddy simulations are turbulence models where the time-dependent flow equations are solved for the mean flow and the largest eddies and where the effects of the smaller eddies are modeled. The focus of this master thesis is on a classical model, the so called k-ε model, because it is presently by far the most widely used and validated one.

THE k-ε MODEL

The standard k-ε model allows the determination of both, a turbulent length and time scale by solving two separate transport equations. This model has become the workhorse of practical engineering flow calculations in the time since it was proposed by Launder and Spalding (1974).

Robustness, economy, and reasonable accuracy for a wide range of turbulent flows explain its popularity in industrial flows. It is a semi-empirical model, and the derivation of the model equations relies on phenomenological considerations and empiricism.

In the derivation of the k-ε model, the assumption is that the flow is fully turbulent, and the effects of molecular viscosity are negligible. The standard k-ε model is therefore valid only for fully turbulent flows.

As the strengths and weaknesses of the standard k-ε model have become known, modifications have been introduced to improve its performance. Two of these variants are available in the RNG k-ε model (see ANSYS 14.5 Help, Fluent, User's Guide, chapter 4.3.2 RNG k-ε Model) and the realizable k-ε model (see ANSYS 14.5 Help, Fluent, User's Guide, chapter 4.3.3 Realizable k-ε Model).

The standard k-ε model is a model based on model transport equations for the turbulence kinetic energy k and its dissipation rate ε. The model transport equation for k is derived from the exact equation, while the model transport equation for ε was obtained using physical reasoning and bears little resemblance to its mathematically exact counterpart.[30]

The turbulent (or eddy) viscosity is computed by combining k and ε as follows:

$$\mu_t = C\rho\vartheta l = \rho C_\mu \frac{k^2}{\varepsilon}$$

where C_μ is a dimensionless constant.

---

[30] ANSYS 14.5 Help, Fluent, User's Guide, chapter 4.3.1 The Standard k-ε Model

The standard model uses the following transport equations used for k and ε:

$$\frac{\partial(\rho k)}{\partial t} + \nabla(\rho k U) = \nabla\left[\frac{\mu_t}{\sigma_k} grad\ k\right] + 2\mu_t E_{ij}.E_{ij} - \rho\varepsilon$$

$$\frac{\partial(\rho\varepsilon)}{\partial t} + \nabla(\rho\varepsilon U) = \nabla\left[\frac{\mu_t}{\sigma_\varepsilon} grad\ \varepsilon\right] + C_{1\varepsilon}\frac{\varepsilon}{k} 2\mu_t E_{ij}.E_{ij} - C_{2\varepsilon}\rho\frac{\varepsilon^2}{k}$$

The equations contain five adjustable constants C_μ, σ_k, σ_ε, $C_{1\varepsilon}$ and $C_{2\varepsilon}$. They have the following default values in CFD software: $C_\mu = 0{,}09$, $\sigma_k = 1{,}00$, $\sigma_\varepsilon = 1{,}30$, $C_{1\varepsilon} = 1{,}44$ and $C_{2\varepsilon} = 1{,}92$. These default values have been determined from experiments for fundamental turbulent flows. They have been found to work fairly well for a wide range of wall-bounded and free shear flows. Although the default values of the model constants are the standard ones most widely accepted.[31]

Boundary conditions

The k-ε model requires following boundary conditions:

- inlet   distribution of k and ε must be given
- outlet $\partial k/\partial n = 0$ and $\partial\varepsilon/\partial n = 0$
- free stream $k = 0$ and $\varepsilon = 0$
- solid walls   approach depends on Reynolds number

Engineers rarely have measurements of k and ε at their disposal. Progress can be made by entering values of k and ε from the literature and subsequently exploring the sensitivity of the results to these inlet distributions. If no information is available at all, crude approximations for the inlet distributions for k and ε in internal flows can be obtained from the turbulence intensity T_i and a characteristic length L of the equipment (equivalent pipe radius) by means of the following simple assumed forms:[32]

$$k = \frac{3}{2}(U_{ref}T_i)^2 \qquad \varepsilon = C_\mu^{3/4}\frac{k^{3/2}}{l} \qquad l = 0{,}07\ L$$

---

[31] ANSYS 14.5 Help, Fluent, User's Guide, chapter 4.3.1 Standard k-ε Model

[32] Versteeg (1995), p. 72

Universal distributions near a solid wall are based on the work of Launder and Spalding, and have been most widely used in industrial flows.

At high Reynolds number: if y is the coordinate direction normal to a solid wall, the mean velocity at a point y_p with $30 < y_p^* < 500$ satisfies the log law and measurements of turbulent kinetic energy budgets indicate that the rate of turbulence production equals the rate of dissipation.

$$U^* = \frac{U}{u_\tau} = \frac{1}{\kappa}\ln(Ey_p^*) \qquad k = \frac{u_\tau^2}{\sqrt{C_\mu}} \qquad \varepsilon = \frac{u_\tau^3}{\kappa y}$$

where κ is the Karman's constant with 0,41 and E the wall roughness with 9,8 for smooth walls.

For low Reynolds numbers the log law is not valid so the above mentioned boundary conditions cannot be used. Modifications to the k-ε model are required, which includes wall damping to ensure that viscous stresses take over from turbulent Reynolds stresses at low Reynolds numbers and in the viscous sub-layer adjacent to solid walls. The modified equations of the low Reynolds number k-ε model are:

$$\mu_t = \rho C_\mu f_\mu \frac{k^2}{\varepsilon}$$

$$\frac{\partial(\rho k)}{\partial t} + \nabla(\rho kU) = \nabla\left[\left(\mu + \frac{\mu_t}{\sigma_k}\right)grad\, k\right] + 2\mu_t E_{ij}.E_{ij} - \rho\varepsilon$$

$$\frac{\partial(\rho\varepsilon)}{\partial t} + \nabla(\rho\varepsilon U) = \nabla\left[\left(\mu + \frac{\mu_t}{\sigma_\varepsilon}\right)grad\, \varepsilon\right] + C_{1\varepsilon}f_1\frac{\varepsilon}{k}2\mu_t E_{ij}.E_{ij} - C_{2\varepsilon}f_2\rho\frac{\varepsilon^2}{k}$$

The most obvious modification which is made, is to include a viscous contribution in the diffusion terms. C_μ, $C_{1\varepsilon}$ and $C_{2\varepsilon}$ were multiplied by wall damping functions f_μ, f_1 and f_2, which were themselves functions of the turbulence Reynolds numbers (see Lam and Bremhorst (1981) wall damping functions, Versteeg (1995) p.74).[33]

---

[33] Versteeg (1995) p.72ff.

3 THE LIFE OF VIKTOR SCHAUBERGER

Viktor Schauberger (30 June 1885 – 25 September 1958) was born in Holzschlag, Austria. In the course of his life he developed to a remarkable natural scientist, inventor and philosopher. Because of his understanding of water, air and earth he met in his life mostly on resistance. Schauberger was one of the first naturalists, who warned that the development in agriculture, hydraulic engineering and silviculture is fatal and would destroy the nature. Already in the twenties he predicted in written words our current environmental crisis.[34]

3.1 BIOGRAPHY

Figure 6 Viktor Schauberger
(http://www.schauberger.co.uk/)

Viktor Schauberger (Figure 6) originates from a long line of Austrian foresters. After graduating the secondary school he cancelled the civil service carrier and lived for the first one year alone in the forest. While hiking through these forests, he allegedly witnessed phenomena like stones floating to the surface in cold ponds and trout swimming up waterfalls. Schauberger linked these events to cold, dense and whirling water. In 1904 he passed the exam as a forester. Shortly after the birth of his son Walter Schauberger was drafted for military service and was wounded several times.[35] After the First World War he worked for Adolf I, Prince of Schaumburg-Lippe as a forester. In the course of this Schauberger designed and had built several innovative log flumes based on his observations and reduced the carrying costs for wood to a tenth of the previous costs.[36] For his timber flotation channels he used meandering forms and shapes and controlled the water temperature in the channels. In the year 1924 Schauberger became a Public Council consultant for the log flumes for the Austrian State.[37]

As a consultant he was involved in the construction of three large plants in Austria. In this context he also applied his first patent. More log flumes followed in Austria, Yugoslavia, Turkey and other Countries until he ended the construction of log flumes due to ongoing litigation with the academic camp.[38] The log flumes used for timber transport allegedly disregarded the Archimedes' principle, because they were able to carry objects heavier than water by creating a centripetal movement. Professor Forchheimer, an internationally renowned hydrologist, was used to study the log flumes thoroughly. Later the professor published with Schauberger a series of articles in an Austrian Journal of Hydrology. Schauberger himself published his first and only book "Unsere sinnlose Arbeit" in the year 1933.[39]

Afterwards patents in the fields of water engineering and turbine construction were submitted from Schauberger. He tried to artificially generate centripetal movement in various

---

[34] Alexandersson (2008), p.14

[35] www.pks.or.at

[36] Lattacher (2003), p.22

[37] Alexandersson (2008), p.43

[38] Alexandersson (2008), p.48

[39] Alexandersson (2008), p. 44ff

types of machines. One target of him was the creation of spring water from an artificial way.[40] Another idea was the direct generation of electricity from water.[41]

1934 Viktor Schauberger met Adolf Hitler, who was interested in his work.[42] But Schauberger didn't make a secret of his rejection against Hitler. The consequence was observation, confiscation of his equipment and finally almost to an execution.[43]

Many companies were interested on his next invention. He developed his "Repulsine". According to Schauberger it is a machine that can be used as an energy generation plant or as a flight unit. Till this day no successful replica was built.[44] There is no one machine among Schauberger like the "Repulsine" that has created such myths and stories.

In the year 1941 he worked for Messerschmitt on cooling systems for airplanes and two years later he was conscripted in the concentration camp Mauthausen. With other detained engineers Schauberger should build a drivetrain for U-Boots, an evolution of his "Repulsine".[45]

To the end of the war US-American and Soviet troops confiscated his equipment and documents. After some other projects Schauberger received an offer of American representatives to continue his research and projects in Texas. He went with his son Walter to the USA, but after serious misunderstandings he had to sign a disclaimer for his past and future work for his homeward journey. Schauberger returned with his son back to Austria and died five days after his arrival in Linz on September 25, 1958.

Today, the Schauberger family keeps a fragmentary archive of his writings and patent documents along with fractions of some machines. While his concepts regarding water, river regulation and tap water vitalization are being applied successfully, engineers and enthusiasts following his trail are unable to recreate any of his more complex invention. Apparently, Viktor Schauberger built mainly prototypes and often did not bother to develop his inventions to the point of sellable products. The difficulty in understanding his unscientific language and thinking does not make it easier to reproduce his ideas.

However, many of his inventions try to make use of the concentrated force of a medium's natural movement, rather than opposing and forcing it to unnatural movement, where great losses due to resistance and friction occur. As shown by Schauberger and Prof. Pöpel in water flow experiments, the most effective pipe for water transport would probably be a copper pipe in cycloid spiralling form, featuring a stunning loss of resistance. It is obvious that - given the accuracy of such observations - many current technologies could be candidates for basic reassessment and could undergo significant change, along with scientific theory.[46] Exactly this builds the core of the master thesis. The experimental data form the so called Pöpel or Stuttgart experiment has to be understood and reproduced and the spiralling movement should be implemented in superchargers for the automative industry.

The next chapters are describing some of his inventions with the focus of the Pöpel experiment, followed by the idea how the hypothesis from Schauberger and Pöpel could be implemented in automotive compressors.

---

[40] Alexandersson (2008), p. 82ff

[41] Alexandersson (2008), p. 117

[42] Alexandersson (2008), p. 112

[43] Alexandersson (2008), p. 145f

[44] www.implosion-ev.de

[45] Lattacher (2003),, S.103ff

[46] Werdenberg (2006), p. 11

3.2   BASIC IDEAS OF VIKTOR SCHAUBERGER

3.2.1   THE MOVEMENT OF WATER

In nature can be observed that water always finds its way in a meandering, wiggly line and constantly spirals in this movement. According to Schauberger this is the right flow form of water in which it can be recharged and refreshed and energetic is refined. If water is forced to flow in straight pipes rather than in spiral pipes, it loses its support and drags force and becomes stale and dies slowly. Schauberger described the water as "the blood of earth". For him water was an "inorganic body", a "living thing", which is in turn part of a larger organism, the earth. Similarly as in our human body, the blood flows and supports the body with nutrients, so does the water for the body of the earth.

Natural right flowing waters not only move in a meander way, they are also always in the shade. Trees and bushes located on the bank donate the water the vital shade, which it needs to maintain its quality. Water which is subjected to the sun becomes aggressive and destroys the bank.

Shaded water gets cool and approaches the greatest specific gravity of water at +4°C and moves due to the curl in the middle of the axis fastest, while micro organic suspended solids, energy fabric of the highest quality and micronutrients are washed on the bank border and can be deposited there to support the area with new building materials. In particular, the cooling effect, which is caused not only by the shadows, but actually primarily resulting from the spiral movement, had greatest importance for Schauberger. The anomaly point of water at +4 ° C applied to him as the best quality status of water because it has here the highest specific gravity, which leads to the largest suspension and drag force, and thus it is able to transport the sediments, such as sand and gravel which in turn release their micronutrients in the water by the steady mechanical attrition.

3.2.2   LOG FLUMES

With his log flumes Schauberger demonstrated with great success how important the correct form of flow and temperature of water is.

He constructed a series of extraordinary log flumes that went against the conventional knowledge of timber floating at his time. The flumes didn't take the straightest path between two points, but followed the meandering valleys and streams. In these flumes, guide vanes were mounted in the curves, making water twist in a spiral along its axis. This fact, together with a meticulous regulation of water temperature along the flumes and waterways used, made it possible to float timber under what was traditionally regarded as impossible conditions. Schauberger's log flumes needed significantly less water than traditionally ones and with a transport rate which significantly exceeded what was considered normal. It was even reported that timber heavier than water could be floated, timber that would sink to the bottom under normal conditions. Remnants of these flumes and

Figure 7 The Krampen-Neuberg flume
(Johansson et al. (2002), p. 3)

floating arrangements still exist today and can be observed at different locations in Austria. Figure 7 shows one of Schauberger's log flumes, the Krampen-Neuberg flume in Austria in the 1930's. Note the egg formed section and how the flume meanders like a stream.[47]

Static calculations in those years determined that the log flumes had been built twelve times more strongly than it needs to have been. The experts were amazed and asked how Schauberger came to build it in this particular form. He answered very archly that he had obtained the shape from a common chicken's egg. What he had known, but the experts had not, was that when the first inflow of water entered the basin it would swirl across the bottom and around the sides (Figure 8). All the flows would then meet at the centre where it was standing and recoil in the opposite direction, thus creating an opposing surge of water, which would counteract the momentum of the oncoming water and relieve the wall of destructive pressure.[48]
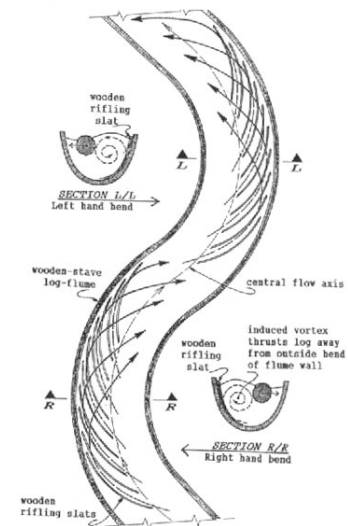

Figure 8 The principle of the log flumes (Coats (2001), p. 153)

3.2.3 LEVITATION ENERGY

In addition to the cooling effect, spiral movement causes another effect that is completely unknown in modern science: levitation. Schauberger defined levitation energy as the life energy. It has the effect that the trees grow up, allows birds to fly and makes it possible that a trout can stands motionless in a raging mountain stream. The levitation energy springs from a particular movement. Every movement causes molecular or atomic vibration changes. Depending on the movement building or degrading forms of energy can be developed. The explanation of levitation leads to chemical and physical areas, but also in the subtle regions beyond our three dimensional perceptual reality.

The levitation results from the implosion. The implosion must be understood as the counterpart to the explosion. It has an astringent and structural development. For example cell formation, and thus the entire growth is based on implosion. The explosion acts expansive and structural resolution. The natural right and building technology must therefore be based on the implosion and not on explosion, how it is treading today's technology with the explosion and fire technology. The core of the levitation energy is therefore the object created by the cycloid spiral curve of the water "the psychic center of the axis". Energies are created in this center of the spiral which could not be mechanistically understood. Schauberger called them as psychic energy forms. Exactly this form of energy, which Schauberger observed by the mentioned standing trout for decades, he finally tried to copy mechanically. He highlighted again and again that this biotechnology is basically very easy to handle if you have once understood the principle. Unfortunately, he didn't make the actual key information public due to patent restrictions and eventually has taken it to the grave.

---

[47] Johansson et al. (2002), p. 2

[48] Coats (2001), p. 150

3.2.4 COPPER DEVICES FOR CULTIVATION

Iron devices deprive the necessary magnetic potential for good growth in the soil. They unload the ground and the water. Schauberger discovered this context when he was invited in the 30's to Bulgaria to investigate the sudden drop in crop yields. He noticed that parts of the country that have been processed with wooden plough were at a higher level of income than in the areas where it was working with the newly introduced iron plows. Schauberger discovered that even slightest admixture of rust prevented any voltage phenomena of water. If there is rust in the bottom, which is caused by the abrasion of the iron plow, the soil and the water loses immediately their power. The water level falls and the soil dries out. It can be observed in the nature that those iron-rich soils are drier than others. With the introduction of fast and deep plows this problem is particularly acute due to the higher attrition. By using a copper plow this disruption of the Earth's magnetism does not occur, because copper is not magnetic. Tests under expert control brought the average yield increase of 17 to 35 %. It also improved the quality of the soil.[49]

Schauberger developed based on his knowledge of the spiral movement the spiral plow (Figure 9), which basically works exactly reverse as a conventional plough. The spiral plow works centripetal, he rotates firstly the earth spirally inward before it is brought into a forward axial movement. In contrast, the conventional plow is first pulled axially straight and then the earth rotates under pressure centrifugally outward away. Schauberger was in the opinion that the spiral curl inward is the life-building principle. The type of movement is extremely important to build the right molecular internal stress. The rotation of the Earth (also of water or air) is therefore crucial. Only in the spiral rolling compaction and qualitative up-valuation of the medium takes place. The spiral plow from Schauberger works about the same way as a bat. As in all things Schauberger tried to copy the nature. Because of the shape of the plow the soil is turned over almost without resistance. There is no friction and no pressure.

Schaubergers plug was actually just before mass production. However, representatives of the national economy as well as the farmers' association began to warn against the use of his copper plow. Using the new plow would cause an overproduction and this leads to significant decrease in the price.

Figure 9 Spiral plow[50]

---

[49]Kokaly, p. 6

[50] http://www.implosion-ev.de/html/goldener_pflug.html

3.2.5 REPULSINE

In a letter to Werner Zimmerman of 21st May 1936, Viktor describes the Repulsine (Figure 10) as follows:

This machine (30 cm wide, 50 cm high) vaporises, purifies and distils water by means of cold processes. At the same time, it will raise water to any desired height, for which almost no power of any kind is needed. My machine is a body which consists of internal and peripheral nozzles, which replace the valves of present machines or supplement them. My machines only require the impulse and manifest the reaction as an expulse, which not merely presses, but simultaneously sucks. This then results in the creation of resistance-less motion, due to the reciprocity which today's resistance makes use of as a "means of propulsion'". The body is merely an antenna, whereas the transmitter is responsible for the phenomenon we call "motion". Motion is a function of temperaments, which within and about themselves are possessed of plus and minus in diverse shapes and sizes. Hence by altering the inner-atomic structure, we can displace the centre of gravity and thereby achieve that which we regard as pure, resistance-free motion. A motion, however, we have for so long not understood, because we ourselves are the resistance, which under the most difficult conditions, has to move itself in order to evolve.[51]

Similar to plants this device operates with simple substances: air, water and carbon dioxide. Additionally some supplements and catalysts were used, which are only partially known. The main catalyst is copper. This biomachine is relatively simple. It contains a centripetal suction inlet and in a special way a centrifuged subsequent part. This second part consists of two profiled wavy copper discs, in which the medium is transported by suction/pressure stages and terminates into nozzle-type devices and the generated repulsive force can be used. The repulsine needs a motor to start. According to written records cooling effects, vacuum and high flow velocities arise inside the repulsine. Thereby also air should have been partially converted into a liquid. This aggregate change leads to enormous suction effects, a kind of implosion, and their force could be used in conventional manner.

According to Schauberger this biomachine uses the energy potential of the surrounding space. Since cooling processes occur, presumably thermal energy is converted into mechanical driving forces. Another possible source of energy are metabolic processes of the biological raw materials C, H and O in interaction with the space, which was mentioned frequently by Schauberger.[52]

The repulsine can be used as a stationary power plant or as an aircraft. A successful reconstruction was not possible until now.

Figure 10 The repulsine[53]

---

[51] Coats (2001), p.279

[52] http://www.implosion-ev.de/html/repulsine_original.html

[53] http://www.implosion-ev.de/html/repulsine_original.html

3.3   THE STUTTGART EXPERIMENT

Viktor Schauberger saw the many processes in life as a part of an indivisible whole, linked by spiral movement. He identified two forms of motion in nature:
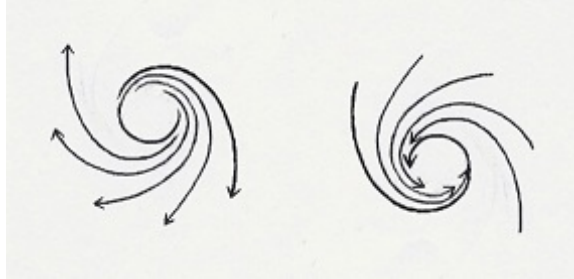

Figure 11 The two forms of motion in nature *(Pangman (2011))*

the outwardly expanding, which is used by nature for breakdown and decomposition and the inwardly spiraling, which is used to build up, to create and to energize.

Generally, Viktor Schauberger viewed inward spiraling vortices as an effective principle in nature, the implosion principle. It emphasizes the importance of form and direction of movement in natural processes.

Vortices are the result of a self-organizing flow where a substance rotates around its own axis with a decreasing radius. The speed of rotation increases toward the center where a sub-pressure forms. Theoretically, the speed at the center of a vortex is infinite, capable of breaking through dimensional boundaries. The vortex is a gateway between levels of energy. From a tornado to the spiralling growth of plants, the vortex is nature's mechanism for increasing the quality of energy from a lower to a higher level. Figure 12 on the left shows a vortex in a draining bottle of water.

Figure 12 Water vortex
(http://en.wikipedia.org/wiki/Vortex)

According to Schauberger, vortices in water are natural implosion energy generators. In 1952, Schauberger conducted several experiments with vortices and pipes at the Technical University of Stuttgart in Germany with Prof. Franz Pöpel. These experiments were co-funded by the German government. Supposedly, Pöpel and the German government were interested in sound scientific experiments to finally discredit Schauberger's theories. Amongst successful particle separation experiments using vortices, flow rates of specially built pipes were tested. Conical, straight, and spiralling pipes were studied; also pipes of different materials. Interestingly enough, these investigations seemed to prove basic implosion theory: Schauberger stated that if water is allowed to flow in a cycloid spiralling way (similar to vortex motion) friction will disappear and the system produces suction energy instead. According to Pöpel's data, this is exactly what happened in these special pipe

forms, which Schauberger had adapted from the horn of a kudu antelope (Figure 13). At certain points the water's velocity seemingly harmonized with the dimension and form of the pipe, and frictional resistance dropped, became inexistent and a slight suction energy surplus was produced. Another interesting result was the more conical and spiralling the pipes became, the more the frictional resistance decreased. Also pipes made from copper demonstrated lower resistance than those made of glass. Under certain circumstances, negative friction was reported. In other words, the water appeared to leave the walls of the pipe. Figure 14 shows the results of the experiment. This resonance could be described as a successful communication of form (pipe) with the direction of the water's natural movement. However, the results of decreasing friction were discussed only marginally in Pöpel's

Figure 13 Kudu antelope
(http://de.wikipedia.org/wiki/Gro%C3%9Fer_Kudu)

final report and the curiosum negative friction wasn't even addressed. Reputedly, these findings were consistent with a Diplomawork by Kullberg in 1982, which is unfortunately only available in Swedish[54]. According to Schauberger's theory, the effect of vortex motion (suction, high rotational speed, cooling and densification of matter and energy) in the presence of suspended matter will also result in colloidal solutions (i.e. highly dissolved substances), chemical reactions, transmutation of chemical elements and immaterial phenomena like charged water vitality and vitalizing energies for the environment.

Figure 14 Results from the Pöpel experiment *(adapted from Alexandersson, p. 128)*

It has to be noted, that the experiment document is a contradiction to the first law of thermodynamics, which states that energy cannot be produced spontaneously.

---

[54] Alexandersson (1997), p. 164

4 NEW APPLICATIONS

4.1 FORCED INDUCTION

Most cars and trucks today are powered by four-stroke piston engines. They are controlled by inlet and outlet valves. A work cycle consists of four strokes during two complete revolutions of the crankshaft.

- Intake (charge changing stroke): The air (Diesel engine or direct injection Otto-engine) or the air-fuel mixture (Otto-engine) will be aspirated through the inlet valve as a result of the piston downward movement.
- Compression (power cycle): The cubic capacity will be compressed by the upward movement of the piston.
- Expansion (power stroke): The combustion of the air-fuel mixture is initiated by an ignition spark in the Otto-engine. In diesel engines, fuel is injected at high pressure and the mixture ignites by itself. The explosion pushes the piston downward.
- Exhaust (charge changing stroke): The piston comes up again and the exhaust gases are pushed out.

There are different approaches available to increase the performance:

- Increasing the cubic capacity
  An increase in the cubic capacity leads to an increase in the performance, because in a larger combustion space more fuel can be burned. The enlargement of the cubic capacity could be achieved by increasing the number of cylinders or by increasing the volume of each cylinder. In general, this results in a larger and heavier engine. Sometimes these changes may not be feasible. Concerning the consumption and pollutant emissions no significant advantages can be achieved.

- Increasing the engine speed
  Another way to increase the power of an engine is to increase the engine speed, which means the number of working cycles per unit time is increased. This form of performance improvement has limits because of mechanical stability. Also with increasing revolution speed the frictional and pumping losses increase exponentially and the engine efficiency drops.

- Forced induction
  In the above described procedures the engine operates as an aspirated engine. The combustion air is sucked in during the intake stroke through an air filter from the environment. Forced induction engines supply the engine with a pre-compressed combustion air. The engine aspirates the same volume of air, but due to the higher pressure more air flows into the cubic capacity. This allows more fuel to be burned, so that the power of the engine increases at the same revolution speed and displacement.

The two commonly used forced-induction compressors can be classified in turbochargers and superchargers. A turbocharger is a centrifugal compressor driven by the flow of exhaust gasses. Superchargers can be found as different types of compressors but all are powered directly by the rotation of the engine, usually through a belt drive. The compressor can be centrifugal or a roots type for positive displacement compression.[55]

4.1.1 SUPERCHARGER

In the mechanical charge the combustion air is pre-compressed by a compressor driven from the engine. The power for the supercharger can be provided mechanically by a belt, gear, shaft, or chain connected to the engine's crankshaft.

There are two main types of superchargers defined according to the method of compression: dynamic compressors and positive displacement. The former deliver a fairly constant level of pressure increase at all engine speeds, whereas the latter deliver increasing pressure with increasing engine speed.

Positive-displacement pumps deliver a nearly fixed volume of air per revolution at all speeds (minus leakage, which is almost constant at all speeds for a given pressure, thus its importance decreases at higher speeds). The device divides the air mechanically into parcels for delivery to the engine, mechanically moving the air into the engine bit by bit. Major types of positive-displacement pumps include: Roots, Lysholm twin-screw, sliding vane and scroll-type supercharger, also known as the G-Lader.

Dynamic compressors rely on accelerating the air to high speed and then exchanging that velocity for pressure by diffusing or slowing it down. Major types of dynamic compressor are: centrifugal, multi-stage axial-flow and pressure wave supercharger.[56]

Picture below shows at the left a dynamic compressor, exactly a centrifugal type supercharger and at the right a Lysholm twin-screw positive displacement supercharger.
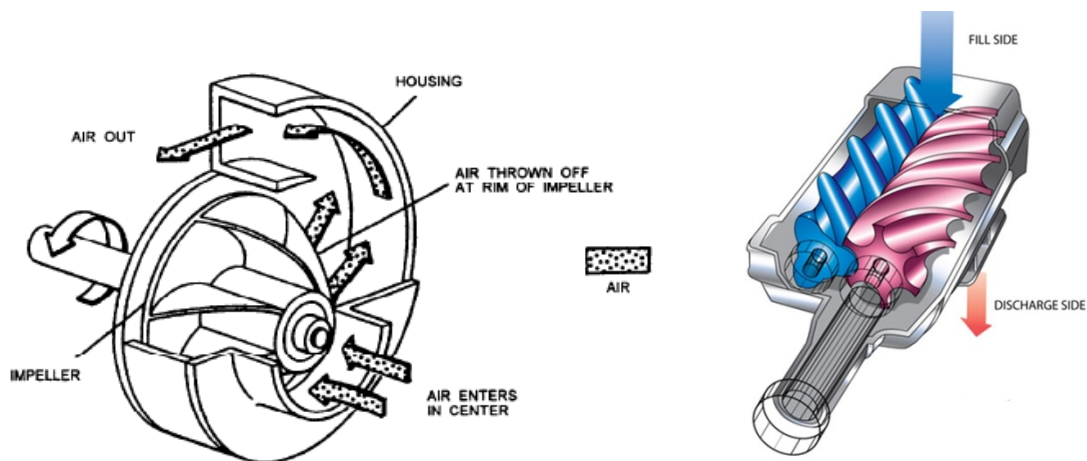
Figure 15 Dynamic compressor and positive displacement[57]

One disadvantage of supercharging is that compressing the air increases its temperature. When a supercharger is used on an internal combustion engine, the temperature of the fuel/air charge becomes a major limiting factor in engine performance. Extreme tempera-

---

[55] https://en.wikipedia.org/wiki/Forced_induction

[56] http://en.wikipedia.org/wiki/Supercharger

[57] http://auto.howstuffworks.com/supercharger3.htm

tures will cause detonation of the fuel-air mixture (spark ignition engines) and damage to the engine. In cars, this can cause a problem when it is a hot day outside, or when an excessive level of boost is reached.

It is possible to estimate the temperature rise across a supercharger by modelling it as an isentropic process:

$$\frac{T_2}{T_1} = \left(\frac{p_2}{p_1}\right)^{\frac{\gamma-1}{\gamma}}$$

where:

T_1 ambient air temperature

T_2 temperature after the compressor

p_1 ambient atmospheric pressure

p_1 pressure after compressor

γ ratio of specific heat capacities ($C_p/C_v = 1,4$ for air)

C_p specific heat at constant pressure

C_v specific heat at constant volume

For example, if a supercharged engine is pushing 0,7 bar (10 psi) of boost at sea level (ambient pressure of 1,013 bar (14,7 psi) and ambient temperature of 24 °C), the temperature of the air after the supercharger will be 71.4 °C. This temperature is known as the compressor discharge temperature (CDT) and highlights why a method for cooling the air after the compressor is so important.

In addition to causing possible detonation and damage, hot intake air decreases power in at least one way. At a given pressure, the hotter the air the lower its density, so the mass of intake air is decreased, reducing the efficiency and boost level of the supercharger.[58]

Also the achieved performance improvement is partly sapped by the high input rating of the compressor. The power consumption of a supercharger is up to 15% of the engine power, which leads to a higher fuel consumption.

4.1.2 TURBOCHARGER

A turbocharger uses some of the lost exhaust gas energy to drive a turbine. A compressor is connected by a common shaft with the turbine and aspirates and compresses the combustion air and feeds the engine with it. A mechanical coupling to the motor doesn't exist.

The typical boost provided by a turbocharger is 0,4 to 0,6 bar (6 to 8 psi). Since normal atmospheric pressure is 1,013 bar at sea level, you can see that you are getting about 50 percent more
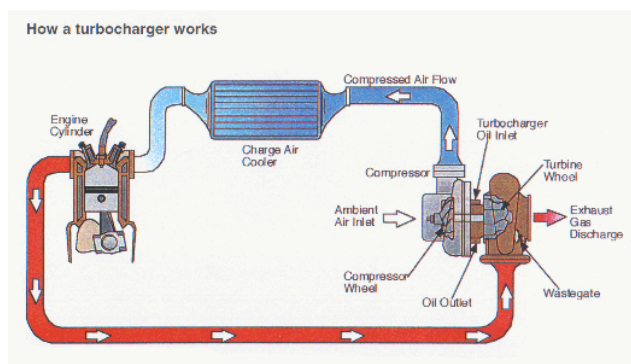
Figure 16 Principle of a turbocharger

(http://www.indiancarsbikes.in/automotive-technology/turbochared-petrol-engines-gasoline-engines-25822/)

---

[58] http://en.wikipedia.org/wiki/Supercharger

air into the engine. Therefore, you would expect to get 50 percent more power. It's not perfectly efficient, so you might get a 30- to 40-percent improvement instead.

One cause of the inefficiency comes from the fact that the power to spin the turbine is not free. Having a turbine in the exhaust flow increases the restriction in the exhaust. This means that on the exhaust stroke, the engine has to push against a higher back-pressure. This subtracts a little bit of power from the cylinders that are firing at the same time.
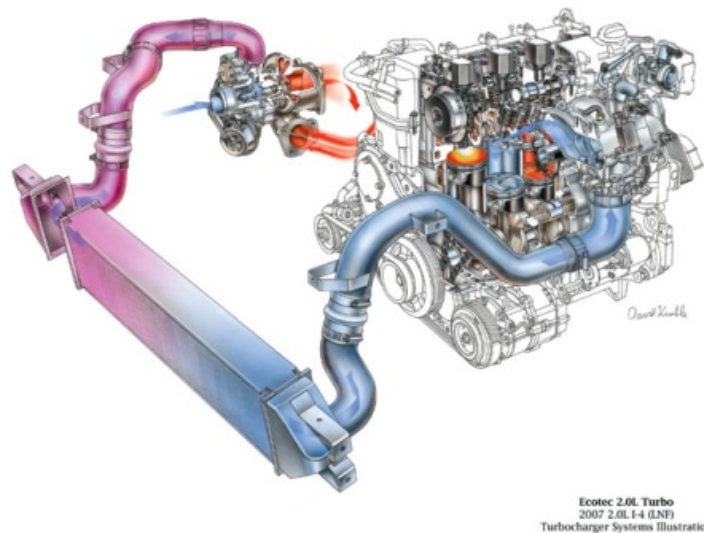
Ecotec 2.0L Turbo
2007 2.0L I-4 (LNF)
Turbocharger Systems Illustration

Figure 17 Turbocharger system illustration[59]

4.1.3 SUPERCHARGER VERSUS TURBOCHARGER

Keeping the air cool that enters the engine is an important part of the design of both superchargers and turbochargers. Compressing air increases its temperature, so it is common to use a small radiator called an intercooler between the pump and the engine to reduce the temperature of the air.

As mentioned above there are three main categories of motor charging for automotive use:

- Centrifugal turbochargers, driven from exhaust gases.
- Centrifugal superchargers, driven directly by the engine via a belt-drive.
- Positive displacement pumps, such as the Roots, Lysholm twin-screw, and TVS (Eaton) blowers.

Roots blowers tend to be 40–50% efficient at high boost levels. Centrifugal superchargers are 70–85% efficient. Lysholm-style blowers can be nearly as efficient as their centrifugal counterparts over a narrow range of load/speed/boost, for which the system must be specifically designed.

Positive-displacement superchargers may absorb as much as a third of the total crankshaft power of the engine, and, in many applications, are less efficient than turbochargers. In applications for which engine response and power are more important than any other consideration, like for drag racing, positive-displacement superchargers are very common.

---

[59] http://rricketts.com/wp-content/uploads/2011/11/turbocharger-system.jpg

The thermal efficiency, or fraction of the fuel/air energy that is converted to output power, is less with a mechanically driven supercharger than with a turbocharger, because turbochargers are using energy from the exhaust gases that would normally be wasted. For this reason, both the economy and the power of a turbocharged engine are usually better than with superchargers.

Turbochargers suffer (to a greater or lesser extent) from so-called turbo-spool (turbo lag; more correctly boost lag), in which initial acceleration from low RPM is limited by the lack of sufficient exhaust gas mass flow (pressure). Once engine speed is sufficient to start the turbine spinning, there is a rapid increase in power, as higher turbo boost causes more exhaust gas production, which spins the turbo yet faster, leading to a belated "surge" of acceleration. This makes the maintenance of smoothly increasing RPM far harder with turbochargers than with engine-driven superchargers, which apply boost in direct proportion to the engine speed. The main advantage of an engine with a mechanically driven supercharger is better throttle response, as well as the ability to reach full-boost pressure instantaneously. With the latest turbocharging technology and direct gasoline injection, throttle response on turbocharged cars is nearly as good as with mechanically powered superchargers, but the existing lag time is still considered a major drawback, especially considering that the vast majority of mechanically driven superchargers are now driven off clutched pulleys, much like an air compressor.

Turbocharging has been more popular than superchargers among auto manufacturers owing to better power and efficiency.[60]

4.2   ADVANCED AUTOMATIVE IDEA

The idea of Mr. Franz Mayr, employee of the company Magna Steyr, was to construct an absolutely new kind of compressor for the automotive industry based on the ideas of Schauberger.

The idea is similar to the concept of a centrifugal supercharger which is driven directly by the engine. It should be a modified compressor. Instead of an impeller a cylinder with a spiral channel (or more) is driven by an electric motor. By rotating the spiral the air gets compressed and supplies the engine or is used as a turbine to drive a generator. Considerations regarding this would be the application in the field of fuel cell. Figure 18 represents the basic concept from Magna Steyr. How the cylinder with the spiral tubes will be made is still open and requires innovative solutions. Casting would be probably too heavy, so individual milled layers are illustrated. Perhaps in the future the manufacturing with a 3d printer would be possible.

According to Schauberger friction reduction should occur by this cycloid spiral movement of the fluid, which therefore should then lead then to significant improvements for chargers. Prerequisite is of course that the assertions of Schauberger as mentioned a chapter before are being proven.

To keep the diploma thesis within manageable limits, the basic geometry of the spiral was specified. Also only the compression effects of the spiral was simulated and not the whole system with the housing of the compressor.

---

[60] http://en.wikipedia.org/wiki/Supercharger
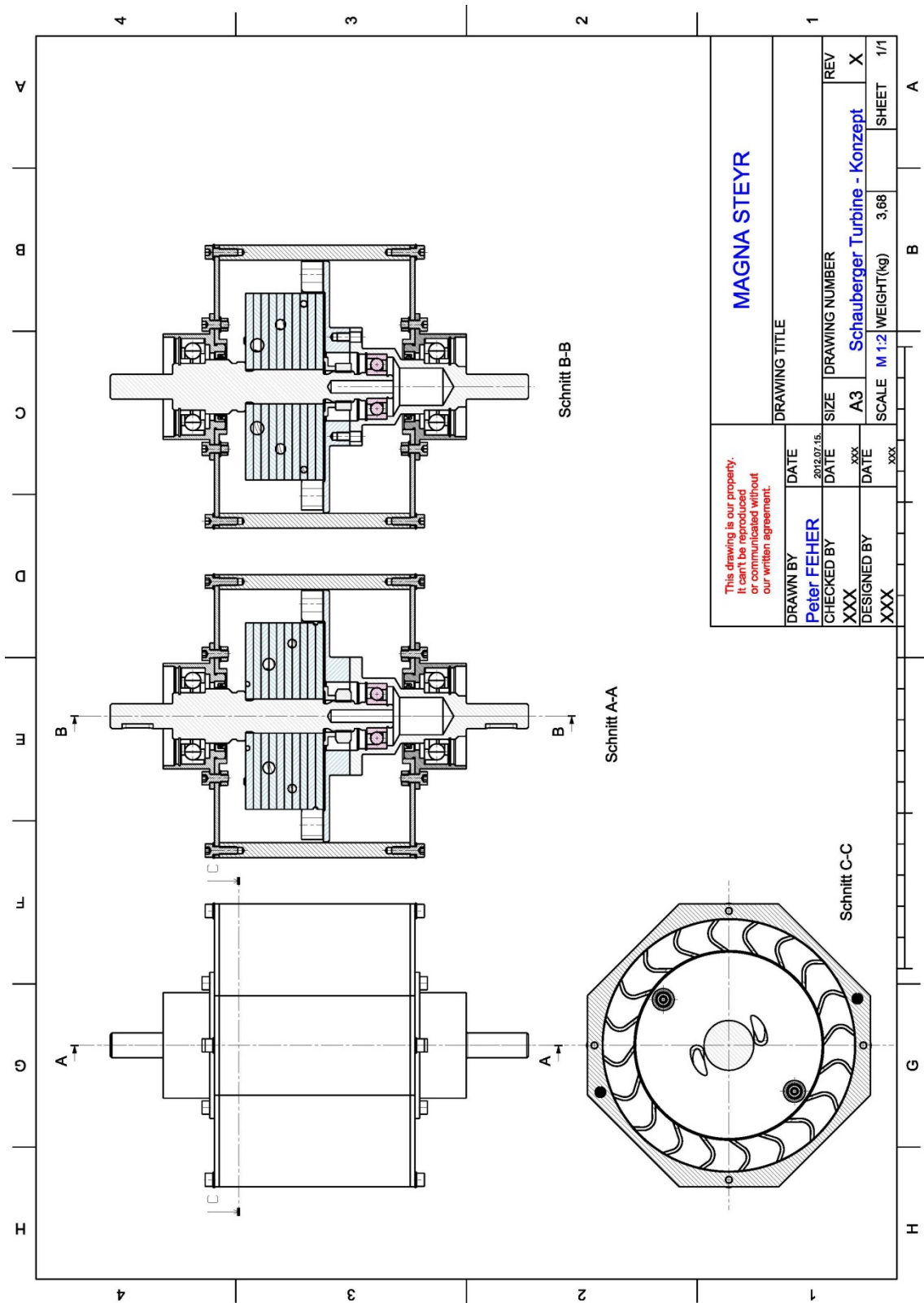
Figure 18 The Schauberger concept for a turbine *(Magna Steyr)*

5 REPRODUCING THE STUTTGART EXPERIMENT

First of all Schauberger's assertion has to be proven. According to him frictional resistance of water flow is dependent on shape and material of a pipe and can become negative if water is allowed to move in natural vortex form. In straight pipes frictional resistance increases with discharge amount of water and copper seems to be a better material for water transport than glass. A cycloid spiralling copper pipe seems to feature resonance points with the discharge amount, where frictional resistance is decreasing, non-existent or even negative, as water flows in suction, inward rolling motion and seemingly loses contact with the pipe walls.

5.1 THE ORIGINAL EXPERIMENT

Schauberger wanted to proof the correctness of his theory about the movement of water by a scientifically recognized institution. Through Schaubergers initiative investigations were carried out by Professor Franz Pöpel at the Stuttgart Institute of Hygiene in 1952. The report was published in 1977 for the first time in the book 3 from the journal "Kosmische Evolution".

The experiment led to observations and measurement results, which apparently impressed Professor Pöpel in such a way that he changed his previously negative opinion and attitude. Pöpel's work was to explain and formulate the observations and experimental results, which should confirm the view of Schauberger.

Professor Pöpel agreed to undertake the investigation using the pipes of various configurations that Schauberger supplied for the experiment. Figure 19 illustrates the different pipes used for the test.
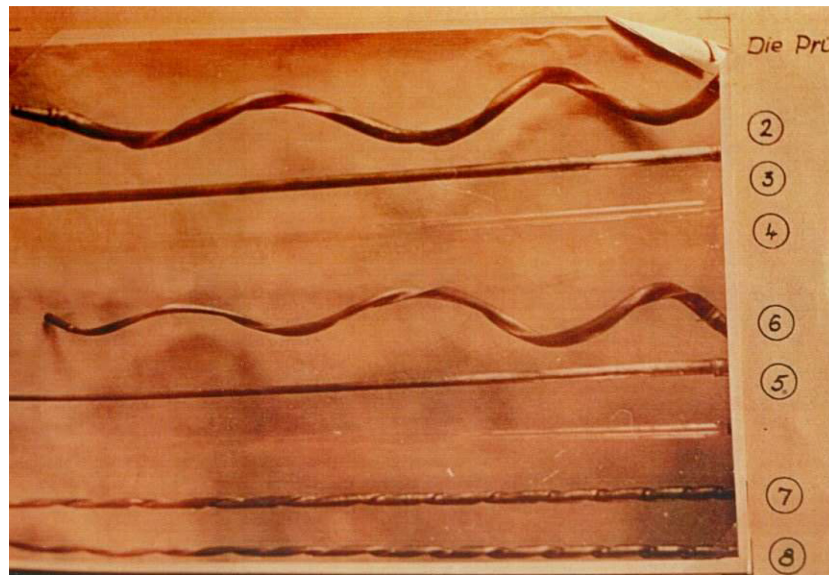
Figure 19 Pipes of various configurations[61]

---

[61] Brödel (2004), p. 15

An accurate description of these various shapes and their respective flows is rather difficult. The most interesting pipes, the rifled and helical copper tubes were extremely difficult and expensive to manufacture, because their unusual shape made any of the normal casting processes almost impossible. They could be construed as "double-rifled" or "spiral helical" pipes or simple mentioned as the kudu horn, because Schauberger adapted the shape of the pipe from the African kudu antelope. Table 1 lists again the various pipe configurations.

Pipe 1	no pipe, only a simple tube connection for using it as a comparative measurement; it is the experiment without a test pipe
Pipe 2	double rifled or spiral helical pipe: 5,05 cm^2 cross section area in form of an indented egg, consistently over the length, 1,45 m long
Pipe 3	straight copper pipe with circular cross section, 2,54 cm in diameter and 1,45 m long
Pipe 4	similar to pipe 3 but made of glass, 2,54 cm in diameter and 1,45 m long
Pipe 5	light conical copper tube, similar as pipe 3 but with itself conically narrowing cross section area, 1,45 m long
Pipe 6	conical double rifled or conical spiral helical pipe, such as pipe 2 but with narrowing cross section, 1,45 m long
Pipe 7	straight conical rifled copper pipe 1,45 m long
Pipe 8	narrow, straight conical rifled copper pipe, 1,45 m long

Table 1 The various pipe configurations

The concept of the experimental set up is shown in Figure 20. Water enters the pipe from a levelling vessel, which supplies a constant head of water. The water then passes through the test pipe and into the outlet chamber, subsequently flowing to waste. Adjacent to the outlet, three small, calibrated vertical glass tubes are arranged. The left-hand tube measures the available head of water and is directly connected to the levelling vessel. The middle tube is connected into the system immediately at the end of the test pipe and the right-hand tube at a point just below the outlet at the top of the expanding cone. The middle and right-hand tubes measure the drop or rise in pressure. The higher the indicated water-levels, the less the loss of head and friction. By lowering the whole of the right-hand side of the arrangement, the flow can be increased due to the steepening of the gradient and the effect of gravity.[62]

---

[62] Coats (2001), p. 183
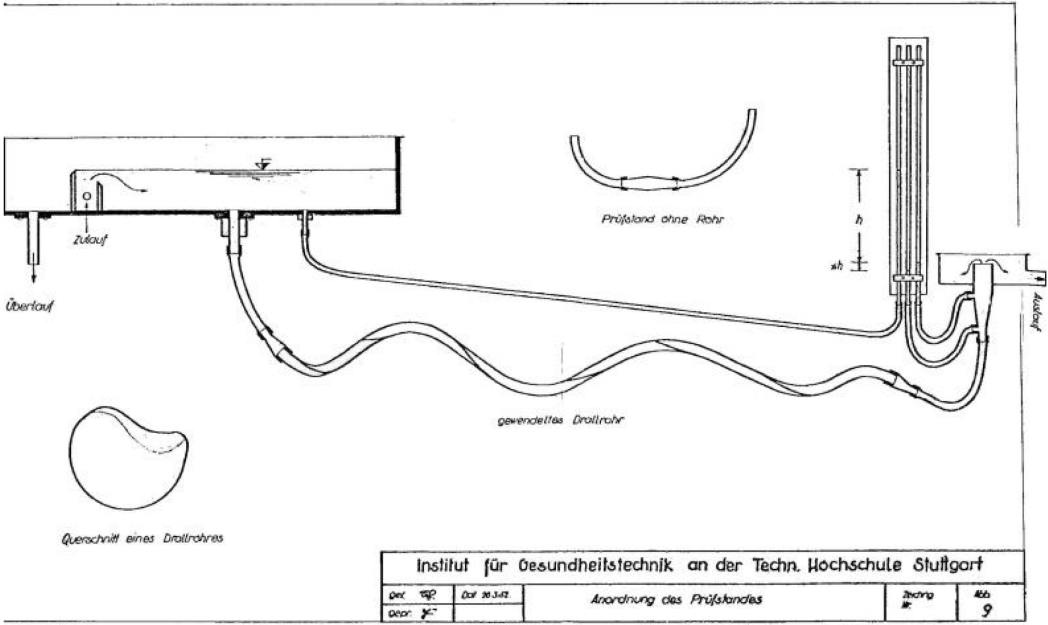
Figure 20 Prof. Pöpel's experiment[63]

Figure 21 is an original photograph from the Stuttgart test in the year 1952
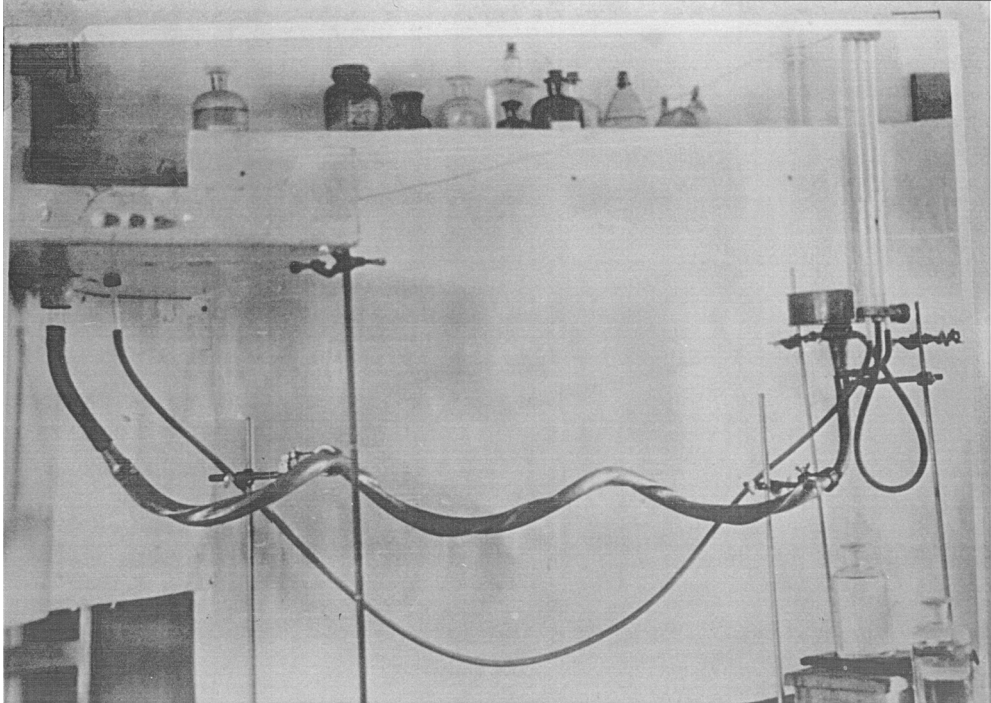
Figure 21 Original photograph of the Pöpel experiment[64]

---

[63] Brödel (2004), p. 45
[64] Association for Implosion

The measured water level difference were applied and interpolated in a double logarithmic coordinate system as a function of the measured flow rate.
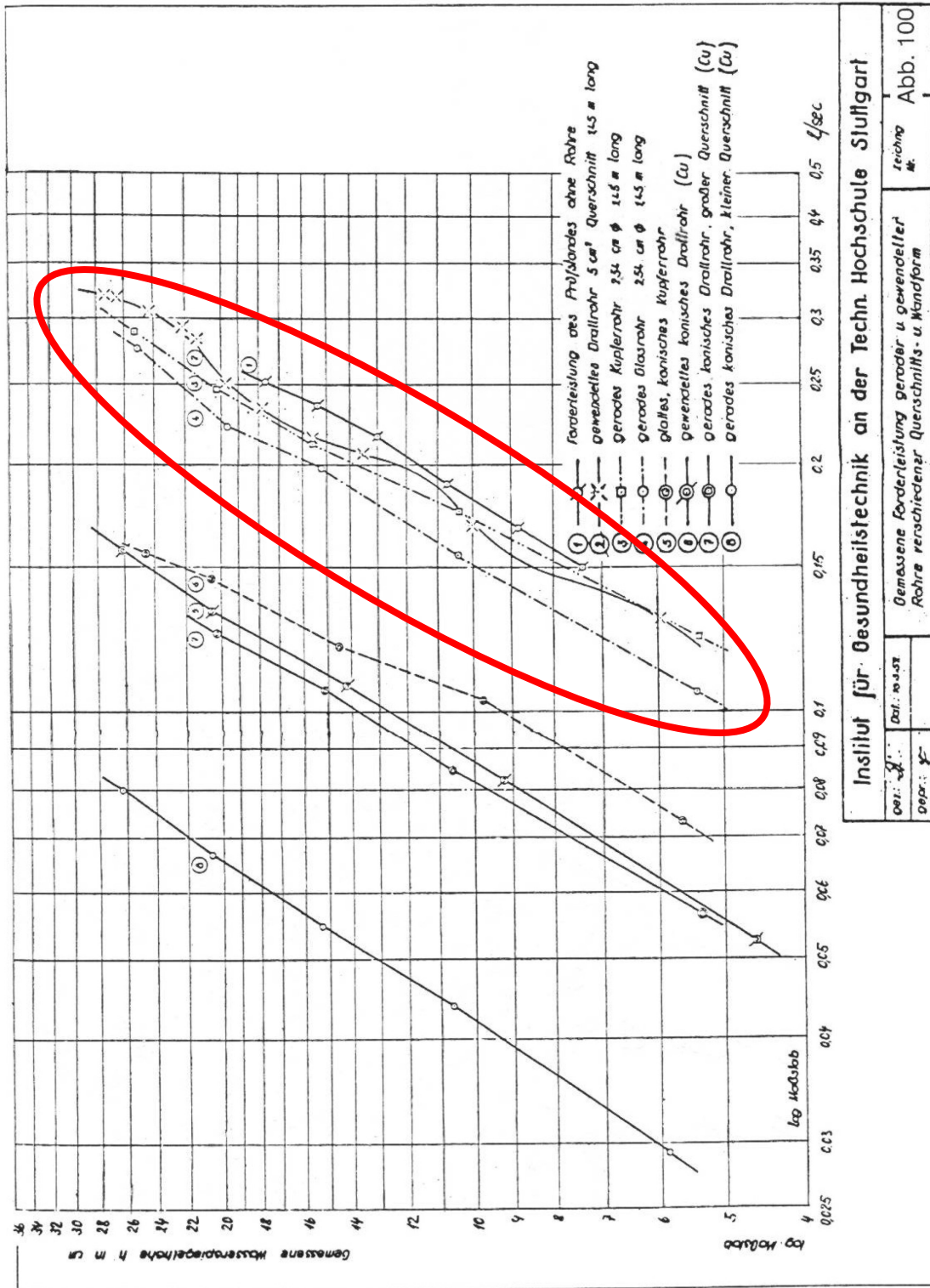
Figure 22 The results from the Stuttgart experiment[65]

---

[65] Brödel (2004), p. 48

Seen as marked with red in Figure 22 a comparison of the pipes makes only sense for pipe number 2 (kudu horn), 3 (straight copper pipe) and 4 (straight glass pipe). That's the reason why Schauberger and Pöpel were mainly focused on those. By reducing their measured water level differences with the still existing pressure head at the outlet, they came to further results listed below. The water level differences were equated as friction losses. Data in bold are representing extrapolated values.

	friction losses		
flow rate	kudu horn	straight copper pipe	straight glass pipe
l/s	cm	cm	cm
0,12	**0,10**	0,05	1,85
0,13	0,19	0,05	2,07
0,14	0,00	0,23	2,20
0,15	0,40	0,33	2,48
0,16	0,95	0,45	2,85
0,17	0,95	0,70	3,25
0,18	0,65	1,20	3,75
0,19	0,45	1,85	4,25
0,20	0,95	2,25	4,65
0,21	2,05	2,55	5,05
0,22	2,50	2,85	5,30
0,23	2,45	2,95	5,45
0,24	2,10	3,10	5,60
0,25	1,70	3,24	5,79
0,26	1,25	3,35	6,00
0,27	0,80	3,50	6,20
0,28	0,35	3,75	**6,65**
0,29	0,00	4,00	**7,00**
0,30	0,00	**4,30**	**7,30**
0,31	0,10		
0,32	0,80	**4,90**	**7,30**
0,34	**3,50**	**4,90**	
0,36	**4,60**	**4,90**	
0,38	**3,70**	**5,05**	
0,40	**2,50**	**5,38**	
0,42	**1,60**	**5,80**	
0,44	**0,70**	**6,50**	

Table 2 The results from the Stuttgart experiment

Those "friction losses" are also plotted in a diagram as a function of the flow rate seen on the next page. The upward portions of the curve indicate that friction is being generated or pressure is increasing and the downward sections where these are reducing. The glass pipe (No. 4) was actually found to be the least suitable for water transfer, having a higher frictional coefficient than a similar copper pipe, in which friction begins to take effect only at higher flow volumes. Both straight glass and straight copper (No. 3) pipes exhibit a certain fluctuation in values but, in the main, friction is constantly on the increase. Fluctuation in frictional values becomes more evident in the straight rifled pipes, but it can be seen that

the spiral-helical pipe (No. 2) produces a markedly different profile to those of the other test-pipes. On two areas, it dips below the line of zero friction at the bottom of the graph. Caused by the configuration of the pipe-walls, water seems to be directed away from the walls, thus reducing the friction.[66]
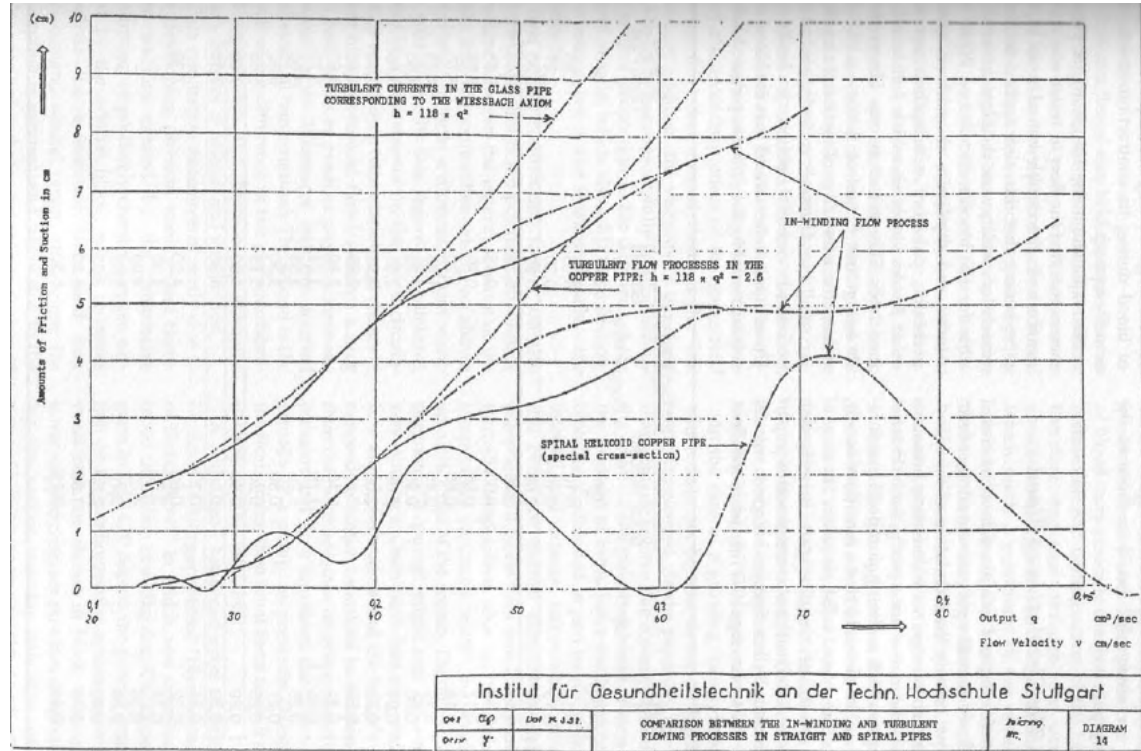
Figure 23 Results of the Stuttgart experiment[67]

Unfortunately, the report is partly incomplete and leaves some open questions relating to the experimental setup and interpretation of their results.

5.2 THE ASSOCIATION FOR IMPLOSION

However, the Association for Implosion in Germany has tackled the task to repeat and reproduce the Stuttgart experiment. In January 1994 rifled- and spiral helical pipes were examined. The experimental setup was largely based on the original test from 1952. Unfortunately also a detailed report about their test is missing, but they also couldn't repeat the results of Stuttgart. Be it, that the evaluation from Pöpel and Schauberger was faulty or that the original pipes couldn't be reproduced well enough. The undefined condition is no satisfying in any case.

Figure 24 The experimental setup from the Association for Implosion

---

[66] Coats (2001), p. 186
[67] Coats (2001), p. 187

5.3 A FURTHER ATTEMPT TO REPRODUCE THE TEST

After a request to the association they were willing to provide all information and recent results they currently have about the Stuttgart test. The information included also some results from reproducing the experiment in 2009 by Mr. Reiche.

The experimental set up was mainly based on the original. Unlike the Stuttgart experiment where only up to a maximum difference of 26 cm water column was investigated, an area of 10 to 96 cm was analyzed. A straight copper pipe with 25,4 mm internal diameter and cross-sectional area of 5,07 cm^2, a rifled copper pipe and the spiral helical both with also a cross-sectional area of about 5-5,1 cm^2 were examined. All tested pipes did have a length of 1450 mm.

Figure 25 The rifled tube and the kudu horn *(Association for Implosion)*

The upper inlet box was at a height of approximately 2 m, about 1 m long, 80 cm wide and 15 cm high. The inlet in the pipe was located at the bottom in a small funnel with 3 cm radius of curvature.
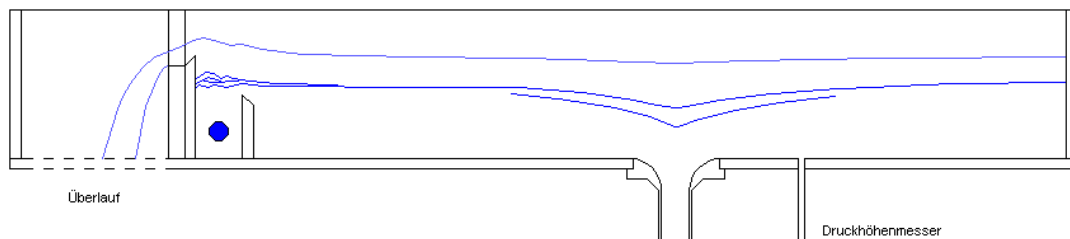
Figure 26 The inlet box[68]

The pressure drop was created by the acceleration of gravity from the water, but the inlet chamber was filled by two pumps. An Overflow ensures a uniform surface. The pressure levels in the inlet and outlet box were measured at equal intervals to the pipe. Tubes and transition pieces, which have similar inner diameter with a maximum deviation of 3 mm radius of the pipe under test, were used in order to keep the energy losses and flow obstacles low. Unlike the original experiment, where additional extensions and contractions were incorporated (which can cause secondary flow and pressure losses), the transition tubes between the hose and the pipe was designed to have nearly seamless transitions. To ensure a round cross-sectional area, hoses with stable spiral insertions were used.
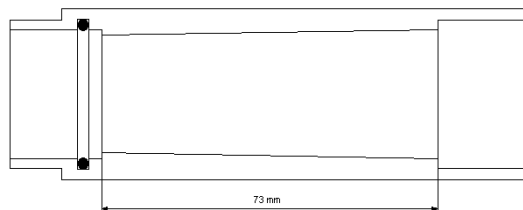
Figure 27 Transition piece

(Association for Implosion)

---

[68] Association of Implosion

Only mean values of at least 5 measurements were incorporated as values in the evaluation. With increasing the pressure head the water level in the test hose at the outlet fluctuated up to 1 cm. So averages of these variations were used. 22 measurement points of different vertical height were simulated. The phenomena observed and calculated by Prof. Pöpel could not be confirmed. The shape of curves follows the traditional doctrine. The tubes with the lower surface and thus with the lower wall friction have always the highest flow rate. The only one amplitude in the curve of the straight pipe is due to inaccuracies in reading the pressure levels.
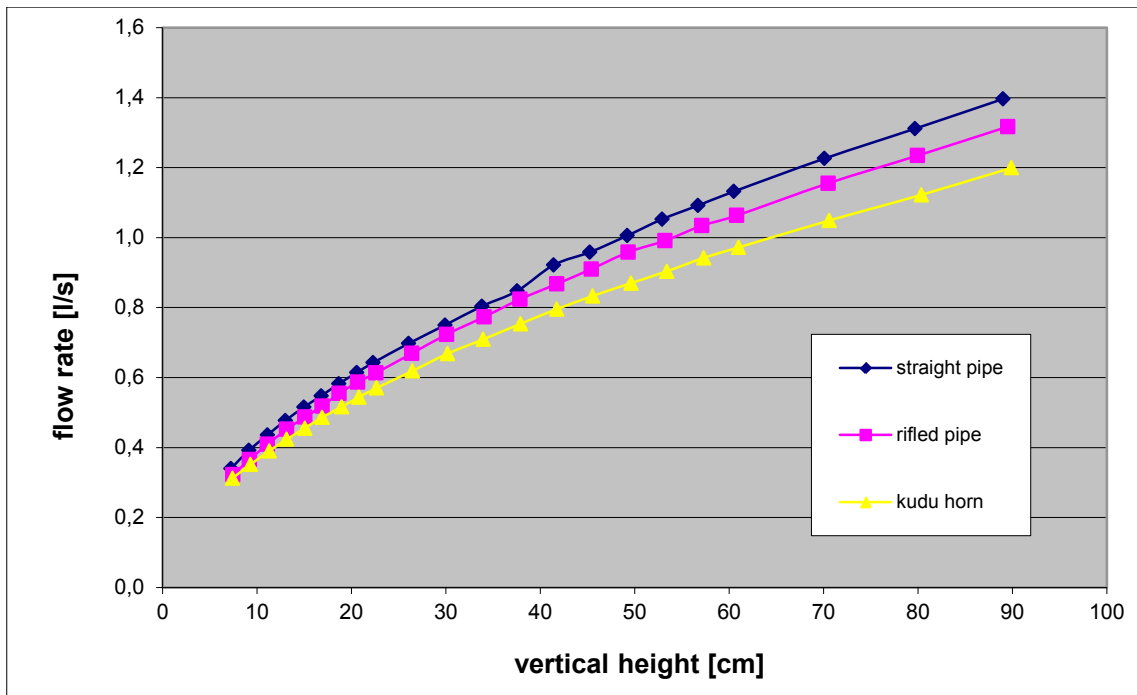
Figure 28 Results from Reiche[69]

---

[69] Association of Implosion

5.4   SIMULATING THE EXPERIMENT

Despite the questionable set up of the test and the unexpected results from the original, this mysteries about the "kudu horn" should be unravelled by using Computational Fluid Dynamics.

The target of the flow simulation is to reproduce Figure 29. The difference of glass and copper was neglected, so only a straight pipe, a rifled pipe and the "kudu horn" with equal cross-section area were examined.

To further minimize the number of simulations only three different flow rates were select-ed. 0,3 l/s (litres per second), 0,35 l/s and 0,45 l/s are indicating significant points of the results marked with the red lines in the following diagram. Finally nine simulations have to be done (for each pipe type three different flow rates).
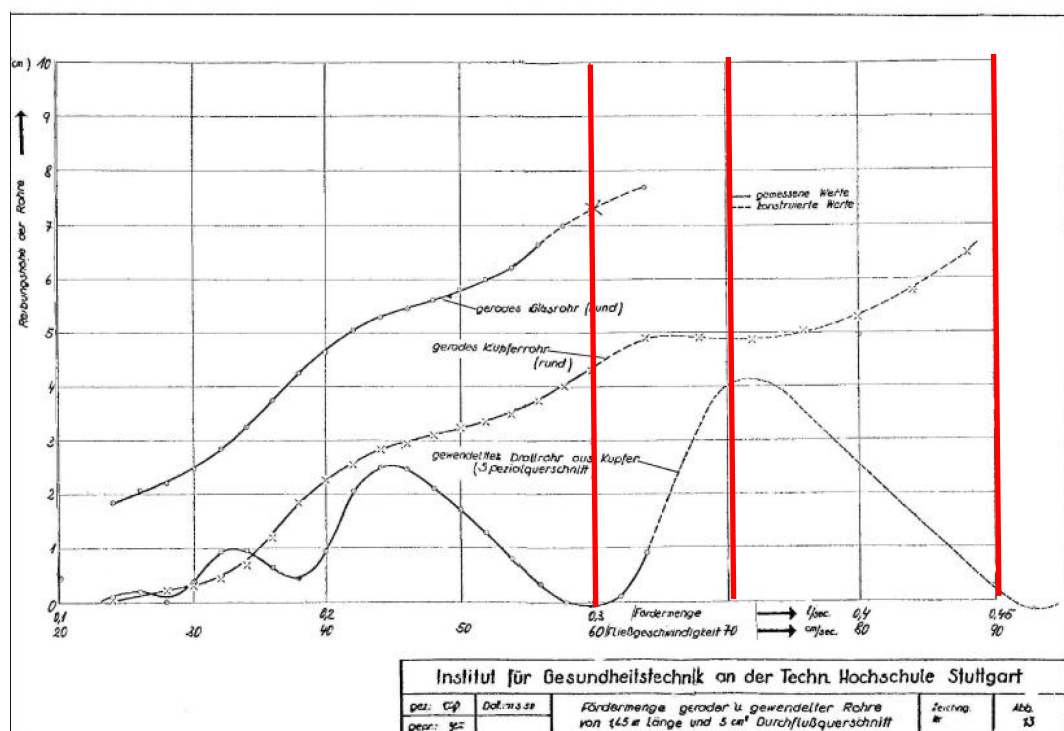
Figure 29 The results of the Stuttgart experiment[70]

---

[70] Pöpel (1952)

5.4.1 MODELING THE PIPES

All geometries for the diploma thesis were created with the software Rhinoceros [v4.0]. The software is simple to handle and the functions can be learned easily. The main reason for using this program was that all kinds of spirals can be easily constructed. Another big advantage of the program is its ability to export data in numerous file formats. So it was easy to read them with the simulation software.

STRAIGHT PIPE

The picture below shows the model of the straight pipe.
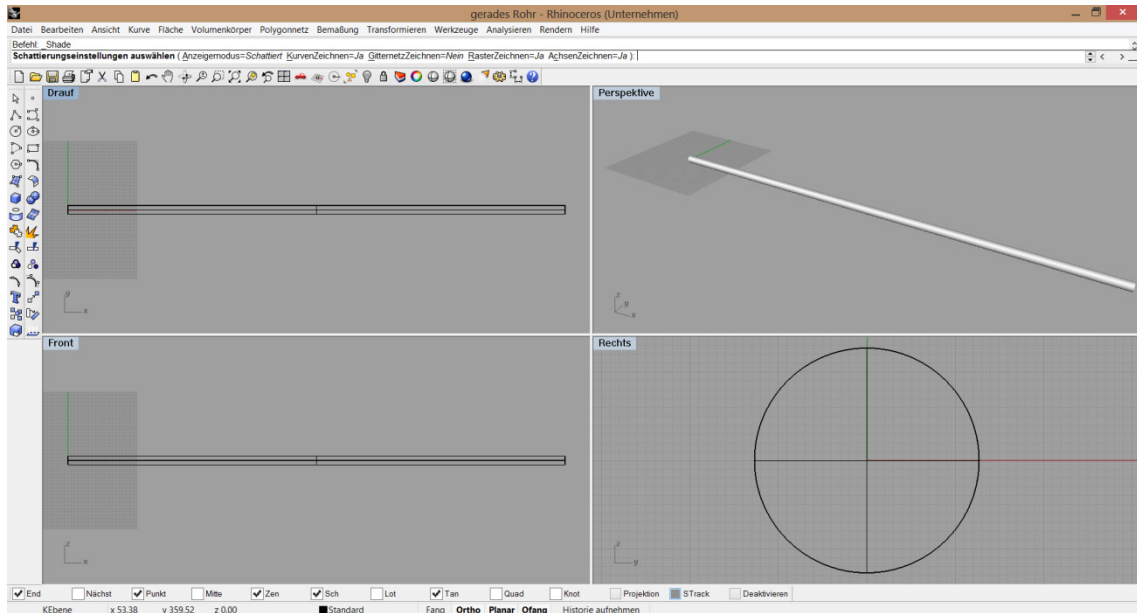
Figure 30 The construction of the straight pipe

According to the report from Pöpel the geometry of the straight pipe for the experiment was as follows:

- length   1.45 m
- diameter   2.54 cm
- cross-section area   5.07 cm^2

SPIRALLING PIPE

The modelling of the spiralling pipe is represented by the next two pictures.
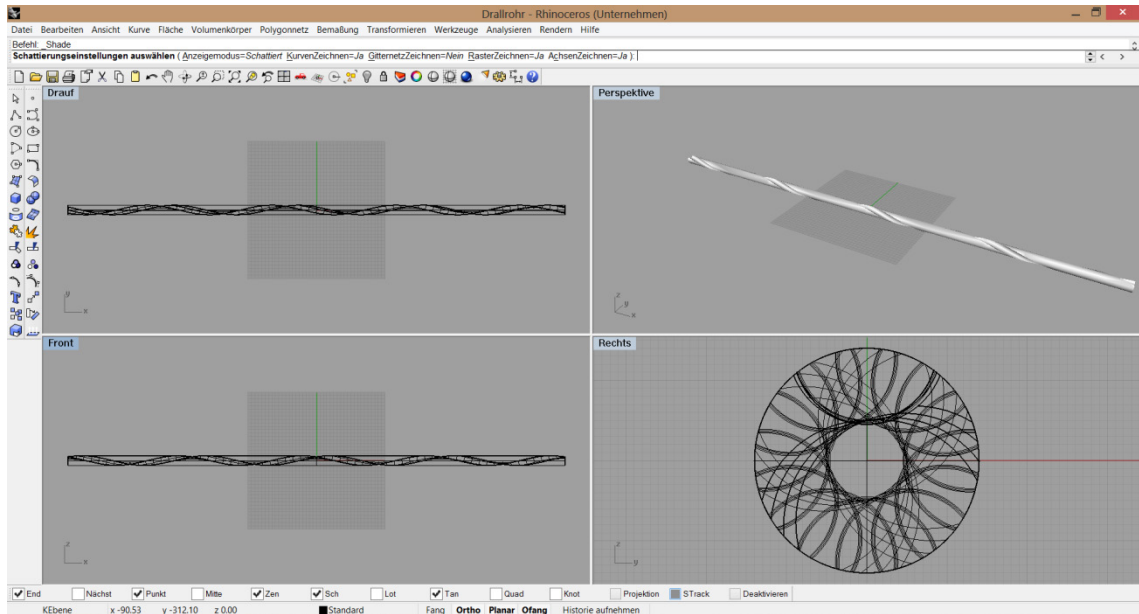
Figure 31 The spiralling pipe in rhino
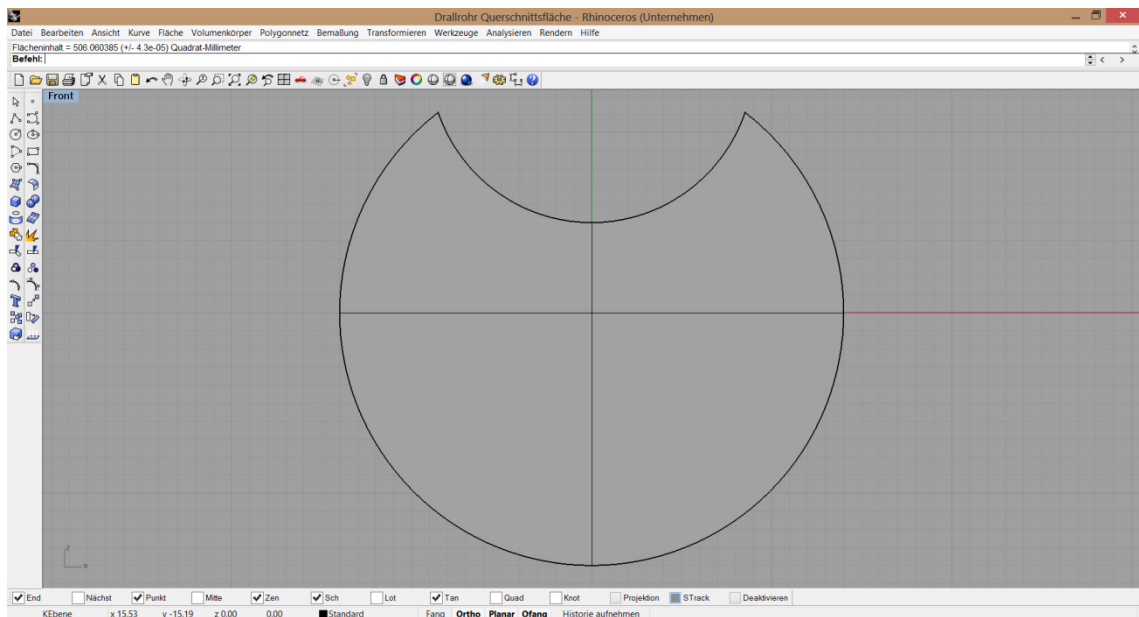
Figure 32 The cross-sectional area of the spiralling pipe

For the spiralling pipe only the length and the value of the cross-sectional area could be discovered from the reports. All tested pipes had a length of 1.45 m. To compare the pipes the equally cross-sectional area of 5.07 cm^2 is very important. Based on the original rifled pipe a similar cross-sectional area was achieved by constructing a pipe with a diameter of 2.8 cm less a groove of 1.8 cm in diameter. This form of the cross section was also used for the kudu horn.

KUDU HORN

Based on the original (Figure 21) a similar pipe was tried to be modelled. The result can be seen below.
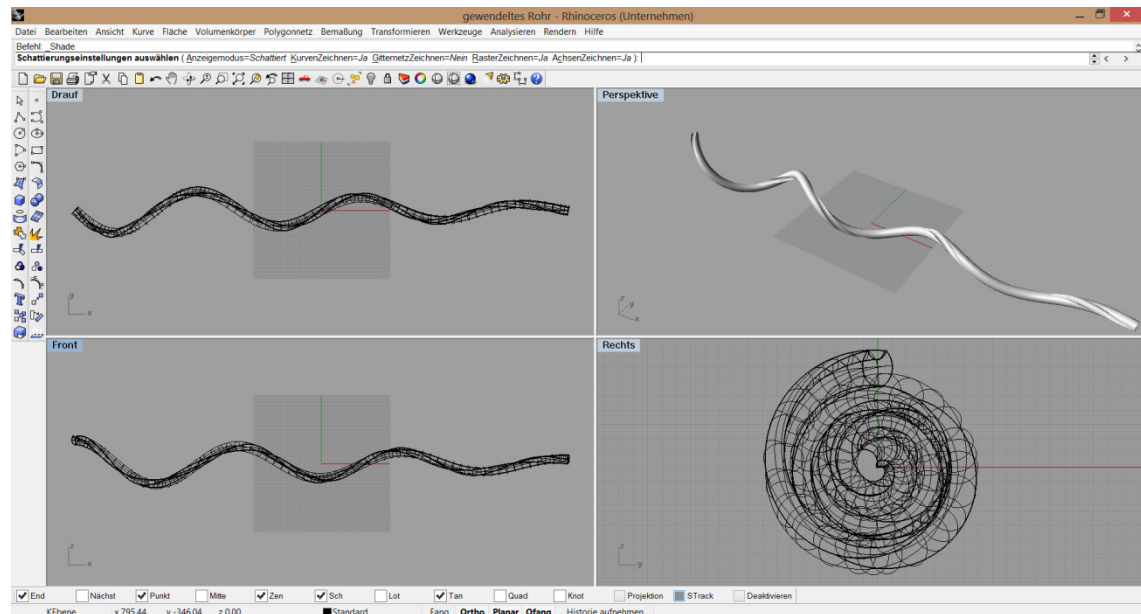
Figure 33 Modelling the "kudu horn"
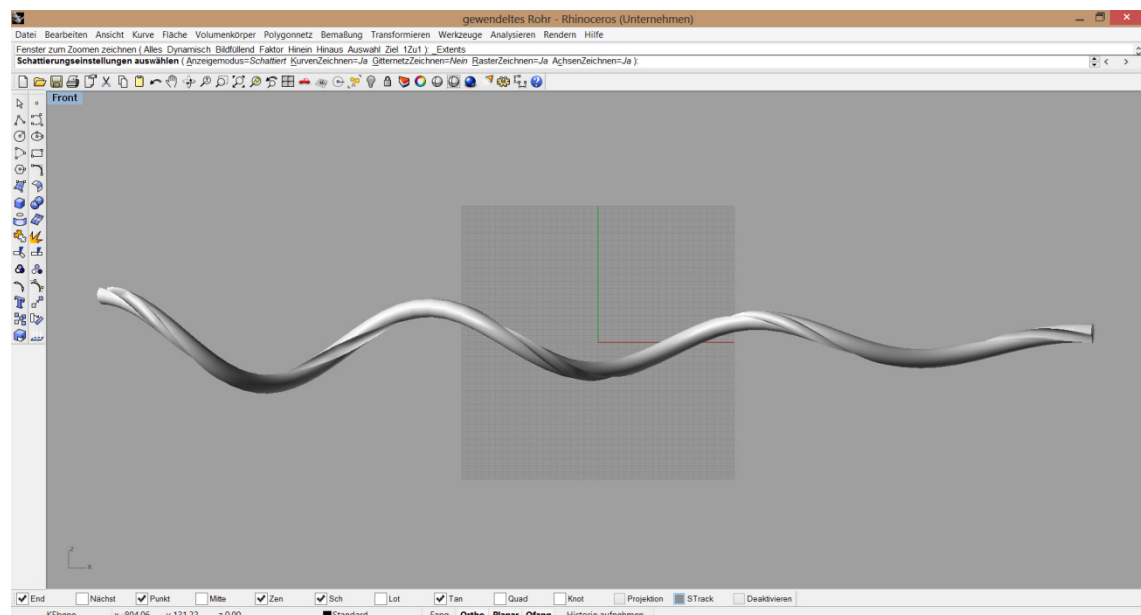
Figure 34 The "kudu horn"

The flow of water in a cycloid spiralling way, similar to vortex motion, was the ideal form for Schauberger. According to him, this is exactly what happens in these special pipe forms, which were adapted from the horn of a kudu antelope. Note, if water flows from the left to the right, the centripetal force is the driving force because the water flows more and more to the center of the axis.

5.4.2 SIMULATION

As an example how the simulation is set up and run, the "kudu horn" is used for demonstrating all important steps. For more detailed explanations, please refer to the ANSYS 14.5 User Manual, especially the chapter 12.5. Setting Up the k- ε Model.

CFD as mentioned already in the first chapter stands for Computational Fluid Dynamics. It is a way of modelling complex fluid flow by breaking down geometry into cells that comprise a mesh. At each cell an algorithm is applied to compute the fluid flow for the individual cell.

To reproduce the "Stuttgart experiment" the pipes were created with computer software as already seen and a water flow from one end of the pipe to the other should be simulated. If some effects were friction decreases or becomes negative, also some pressure changes should be seen. Also the inlet tube, the transition tubes and the diffusor at the outlet is not necessary, which anyway would only falsify the flow behaviour. Therefore the simulation was kept as simple as possible. A predetermined quantity of water flows from one side of the test pipe to the other side, without any height difference. The pressure difference between the outlet and inlet is then evaluated and should lead to a similar diagram according to Pöpel and Schauberger.

CREATING THE MESH

Explaining how the simulations were made with the Fluid Flow Modelling Software FLU-ENT from ANSYS cannot be done without discussing GAMBIT first. GAMBIT is used as a tool to build a model or import existing geometries from various CAD applications. With a surface geometry in place a computational mesh can be generated allowing it to be used for the computational fluid dynamics.

Because of the complex geometries resulting from the spirals, all geometries were constructed with the CAD Software Rhino and were imported in GAMBIT as ACIS files, which is a standard geometric modelling file format.

Further the complex geometries like the "kudu horn" or the spirals needed for the Magna Steyr experiment turned out to be difficult for creating the meshes. To examine the quality of the grid there are two main factors that can be evaluated in GAMBIT. The first is the so called EquiAngle Skew which should not be higher than 0,7. This factor expresses the skewness of the cells. Good results are achieved if most of the cells are below 0,5. The second quality factor is the Aspect Ratio which should be less than 100. It is a measure how the cells are stretched. To satisfy the limits the spiral pipes had to be divided into very small volumes (Figure 35), leading to more effort.
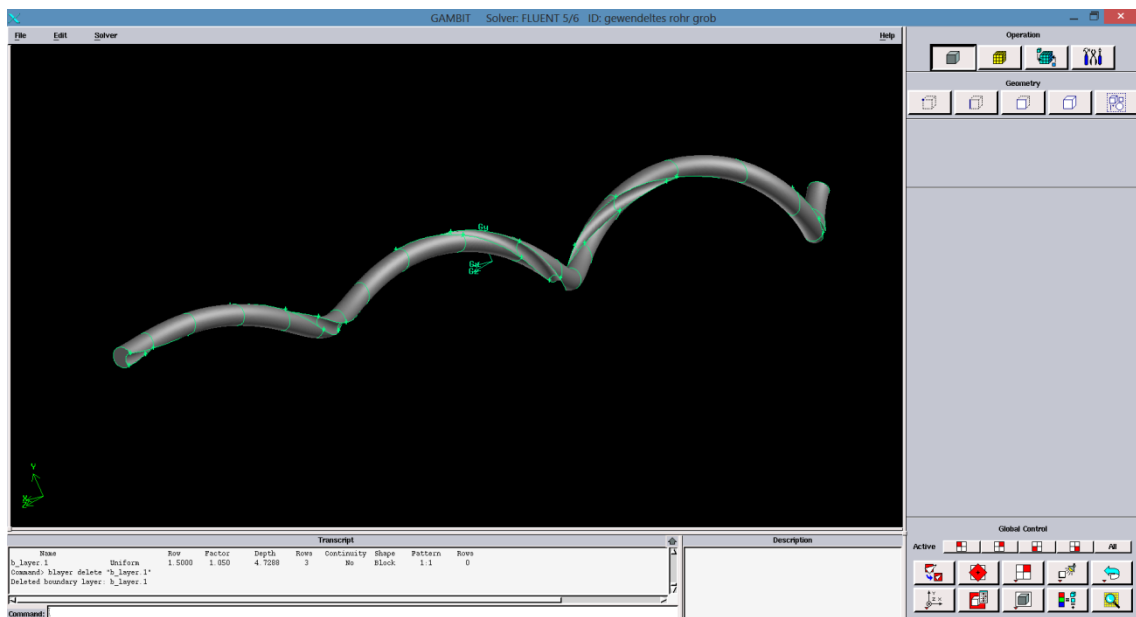
Figure 35 The "kudu horn" in Gambit

BOUNDARY LAYER

As already mentioned in the theoretical fundamentals numerous experiments have shown that the near-wall region can be largely subdivided into three layers. In the innermost layer, called the "viscous sublayer", the flow is almost laminar, and the viscosity plays a dominant role in momentum and heat or mass transfer. In the outer layer, called the fully-turbulent layer, turbulence plays a major role. Finally, there is an interim region between the viscous sublayer and the fully turbulent layer where the effects of molecular viscosity and turbulence are equally important.

FLUENT offers two approaches to modelling the near-wall region. In one approach, the viscosity-affected inner region (viscous sublayer and buffer layer) is not resolved. Instead, semi-empirical formulas called "wall functions" are used to bridge the viscosity-affected region between the wall and the fully-turbulent region.

In another approach, the turbulence models are modified to enable the viscosity-affected region to be resolved with a mesh all the way to the wall, including the viscous sublayer. This will be termed the "near-wall modelling" approach, but this method was not used for these tests.[71]

But before the near-wall region can be modelled, first of all the boundary layer has to be defined in GAMBIT followed by creating the full mesh. The boundary layer defines the spacing of mesh node rows in regions immediately adjacent to edges and/or faces. They are used primarily to control mesh density and, thereby, to control the amount of information available from the computational model in specific regions of interest.

As an example of a boundary layer application, consider a computational model of a pipe, where a viscous fluid flows through it. Under normal circumstances, it is likely that the velocity gradients are large in the region immediately adjacent to the pipe wall and small near the center of the pipe. By attaching a boundary layer to the face that represents the pipe wall, you can increase the mesh density near the wall and decrease the density near the center of the cylinder, thereby obtaining sufficient information to characterise the gradients in both regions while minimizing the total number of mesh nodes in the model.

To define a boundary layer, the following information must be specified:

- Boundary layer algorithm
- Height of the first row of mesh elements
- Growth factor – which specifies the height of each succeeding row of elements
- Total number of rows – which defines the depth of the boundary layer
- Edge or face to which the boundary layer is attached
- Face or volume that defines the direction of the boundary layer[72]

---

[71] ANSYS 14.5 Help, Fluent, User's Guide, chapter 4.13.1.1 Wall Functions vs. Near-Wall Treatments
[72] GAMBIT 2.4 Modeling Guide, chapter 3 Meshing the Model

Figure 36 demonstrates how the boundary layer and in further steps the full mesh was created for the "kudu horn". The white cells are illustrating the boundary layer near the wall. It was very hard to reach a homogenous, useable mesh, because of the special form of the pipe.
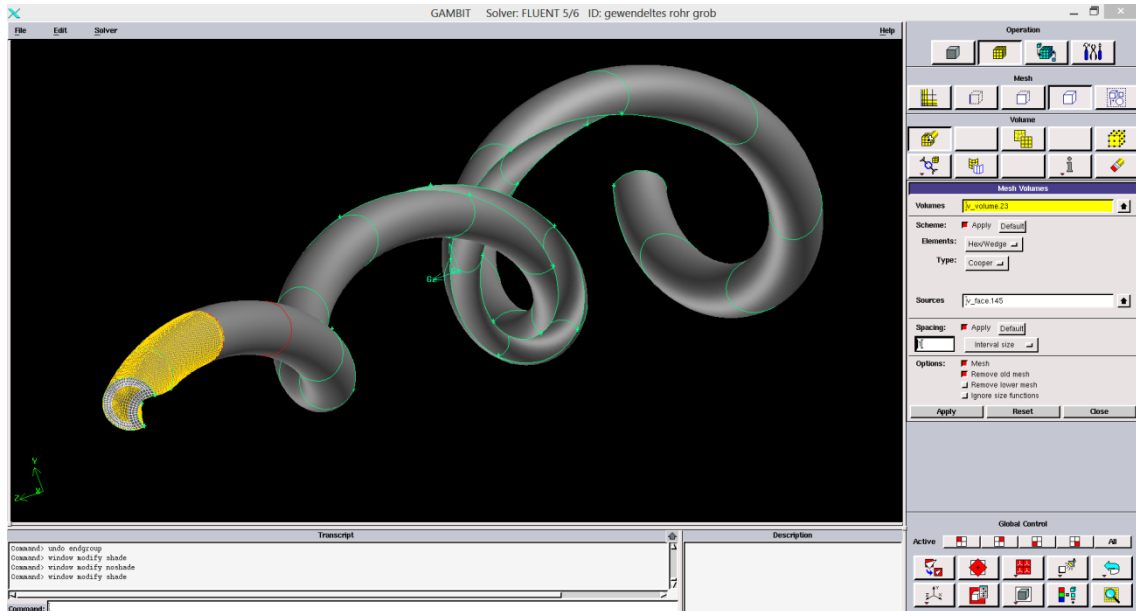
Figure 36 Creating the mesh

FLUENT offers four to five choices of wall-function approaches depending on the choice of turbulent model. To check the fluid flow simulation near the wall the y+ value (explained in chapter 2.7) can be evaluated in Fluent. Depending on the used near wall function the y+ must occur in a given range and must not exceed certain values, otherwise the simulation results near the wall is inaccurate and the grid needs to be revised. It turned out to be effective to simulate a coarse grid first and refine it later. The finer the grid the better the quality of it, but the number of cells determines the computational effort, which was unacceptable with reaching more than a few million cells.

After defining the surface types of the inlet and outlet of the pipe as mass-flow inlet and pressure outlet and the outer surfaces as wall, the mesh was exported to Fluent. By the subdivision of the tube into many smaller volumes also many intermediate faces were generated. Those faces were defined as surface type "interior" and are very helpful for the analysis in FLUENT.

SETTING UP THE SIMULATION

If a useable mesh was achieved, it can be exported to the simulation software FLUENT. The first step by setting up the whole model is to scale the mesh in the right units (Figure 37). Also another quality check of the mesh can be done in Fluent.
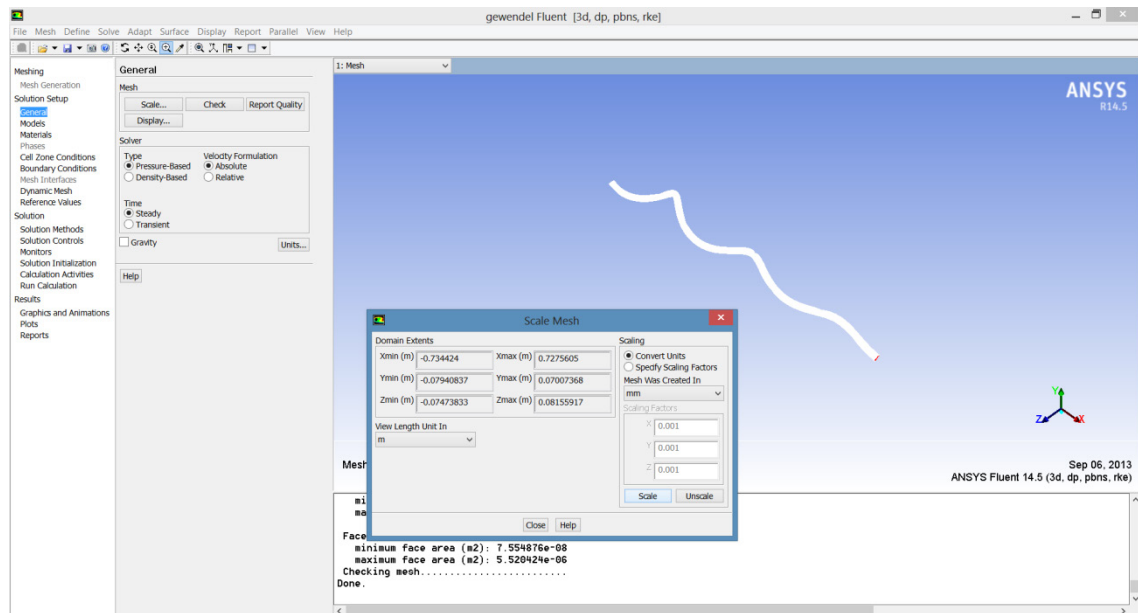
Figure 37 First settings of the Fluid Model

The first settings are some definitions about the Solver. For the simulation a pressure based Navier-Stokes algorithm with the use of the absolute velocity formulation is solved. Further the flow is defined as time independent. Also the gravity acceleration was neglected because no real height difference exists in this test.

The effects of turbulence have been taken into account using the k-ε model (chapter 2.7 Turbulence and its modelling). Due to recommendations the realizable- and not the standard k-ε model was selected, as explained in chapter 2.7 Turbulence and its modelling (Figure 38). The realizable model shows substantial improvements over the standard k-ε model where the flow features include strong streamline curvature, vortices and rotation.

The realizable k – ε model differs from the standard k – ε model in two important ways:

- The realizable k – ε model contains an alternative formulation for the turbulent viscosity.
- A modified transport equation for the dissipation rate ε has been derived from an exact equation for the transport of the mean-square vorticity fluctuation.

The term "realizable" means that the model satisfies certain mathematical constraints on the Reynolds stresses, consistent with the physics of turbulent flows. Neither the standard- nor the RNG k-ε model is realizable. The equations can be seen in ANSYS 14.5 Help, Fluent, User's Guide, chapter 4.3.3 Realizable k-ε Model.

For the tasks of the diploma thesis to simulate spirals also the k-ω and the Reynolds Stress model would be of interest and probably with using this models better results can be achieved, but this would exceed the scope of the work.
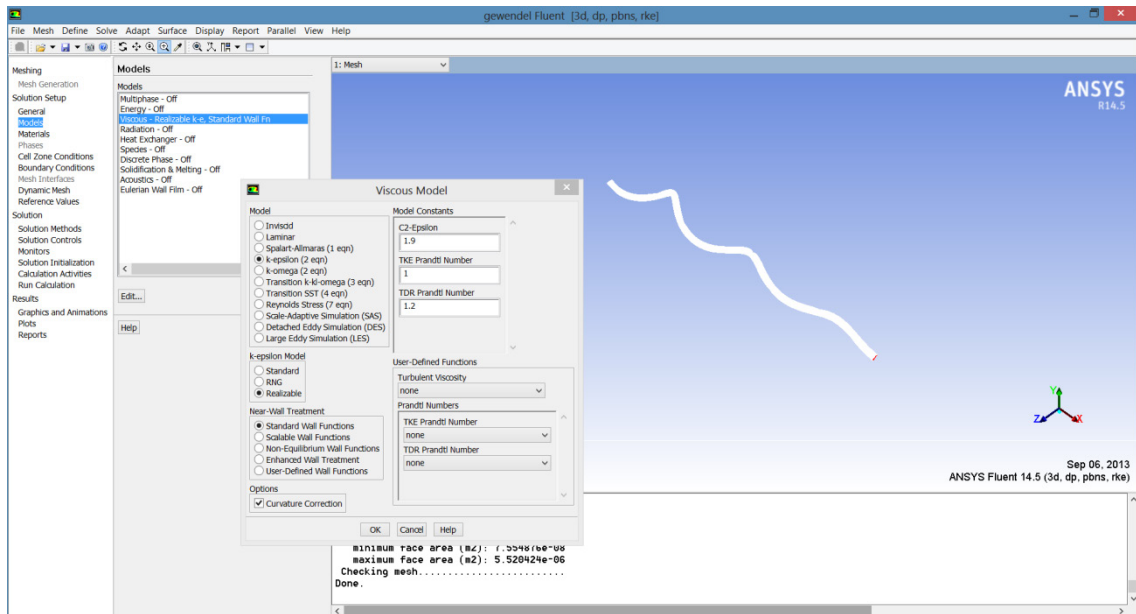
Figure 38 Viscous Model settings

It is also possible to modify the Model Constants, but this is not necessary for most applications and was therefore not done.

Further no heat transfer takes place on the compressor wall, so therefore no solution of the energy equation is needed.

As mentioned, for the k-ε Model FLUENT allows choosing between five Near-Wall Treatment functions. At first the Standard function was tried, which is based on the work of Launder and Spalding, and have been most widely used in industrial flows. The law of the wall for mean velocity yields:

$$U^* = \frac{1}{\kappa}\ln(Ey^*)$$

where

$$U^* \stackrel{\text{def}}{=} \frac{U_P C_\mu^{1/4} k_P^{1/2}}{\tau_W/\rho} \qquad y^* \stackrel{\text{def}}{=} \frac{\rho C_\mu^{1/4} k_P^{1/2} y_P}{\mu}$$

is the dimensionless velocity. y^* is the dimensionless distance from the wall and

κ	=	von Kármán constant (0,4187)
E	=	empirical constant (9,793)
U_P	=	mean velocity of the fluid at the near-wall node P
k_P	=	turbulence kinetic energy at the near-wall node P
y_P	=	distance from point P to the wall
μ	=	dynamic viscosity of the fluid

The range of y^* values for which wall functions are suitable depend on the overall Reynolds number of the flow. The lower limit always lies in the order of $y^* \sim 15$. Below this limit, wall functions will typically deteriorate and the accuracy of the solutions cannot be maintained. The upper limit depends strongly on the Reynolds number. For very high Reynolds numbers, the logarithmic layer can extend to values as high as several thousand, whereas for low Reynolds number flows the upper limit can be as small as 100.[73]

For values below 15 the Scalable Wall function can be used. It avoids the deterioration of standard wall functions under grid refinement below $y^* < 11$. For grids which are coarser than $y^* > 11$, the Standard wall functions are identical. The best way would be to solve the near wall functions with Enhanced Wall Treatment, but therefore the grid has to be fine enough. For that values of $y^* <= 4$ would be perfect.

The creation of a useful grid resulting to reasonable y^* values is one of the most important but also one of the most time-intensive tasks. In general the Standard function was used for the simulation runs, trying to generate a mesh which keeps the y^* values above 20.

---

[73] ANSYS 14.5 Help, Fluent, User's Guide, chapter 4.13.2. Standard Wall Function

As mentioned in chapter 2.7.2 Turbulence models, a k-ɛ model requires some boundary conditions. An often used approximation for the inlet distributions for k and ɛ can be obtained from the turbulence intensity and the characteristic length, which is equivalent to the pipe radius.[74] For turbulence intensity a proven value would be 7 percent.

Figure 39 and Figure 40 are showing the used settings for the inlet and outlet. In this case 0,3 kg/s water enters the pipe (blue arrow) and flows through it.
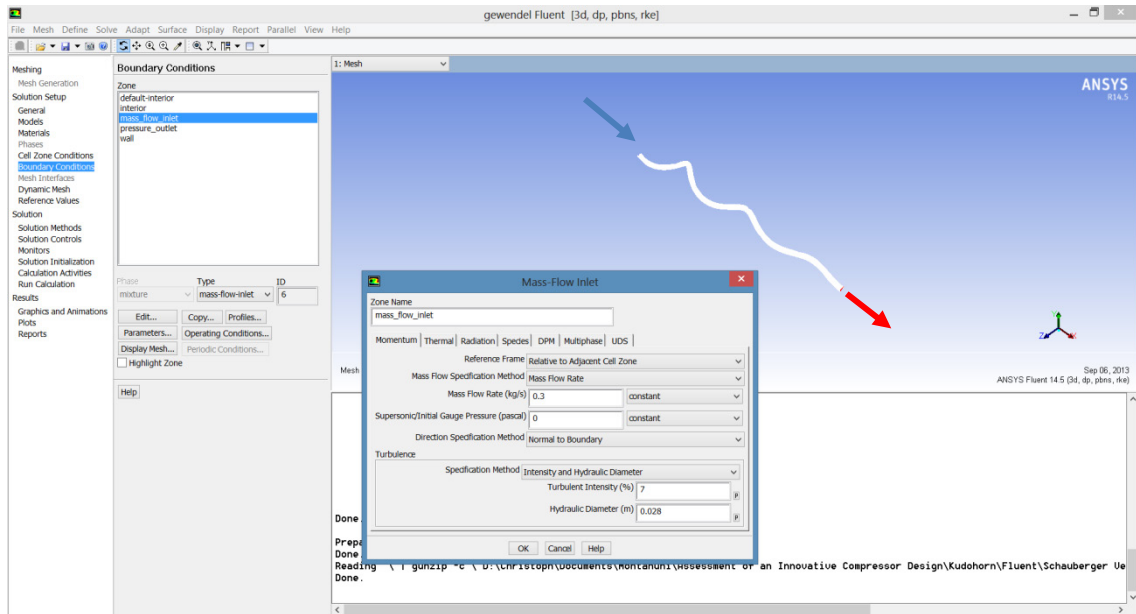
Figure 39 Inlet boundary conditions

At the outlet the 0,3 kg/s water should flow completely out of the pipe, which can be achieved by defining the target flow rate. Also distributions for k and ɛ are defined at the outlet by the 7 percent of intensity and the pipe diameter.
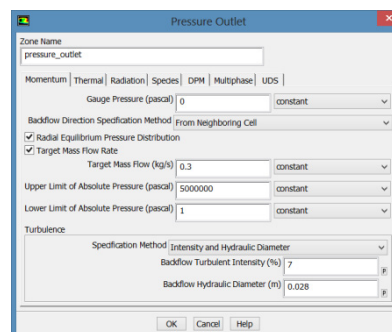
Figure 40 Outlet boundary conditions

---

[74] Versteeg (1995), p. 72

So after setting all relevant data for the model, the iterative solution approach has to be chosen. The pressure-based solver allows solving the flow problem in either a segregated or coupled manner. SIMPLE is a segregated solution algorithm. It is one of the most popular procedures and therefore was used most of the time for this work, but sometimes also the algorithm Coupled was used. For this part the work was strongly counted on the experience of the employees from the ICE Strömungs GmbH, also by adjusting the procedures to achieve useable results. How the settings look in detail is not discussed here, because they varied for each simulation case.

The SIMPLE algorithm uses a relationship between velocity and pressure corrections to enforce mass conservation and to obtain the pressure field.

Using the coupled approach offers some advantages over the non-coupled or segregated approach. The coupled scheme obtains a robust and efficient single phase implementation for steady-state flows, with superior performance compared to the segregated solution schemes. This pressure-based coupled algorithm offers an alternative to the density-based and pressure-based segregated algorithm with SIMPLE-type pressure-velocity coupling. For transient flows, using the coupled algorithm is necessary when the quality of the mesh is poor, or if large time steps are used.[75]

For more details how the algorithms work see please ANSYS 14.5 Help, Fluent, User's Guide, chapter 20.4.3 Pressure-Velocity Coupling.

In the introduction of CFD it was mentioned that for determining the success of the simulation (algorithm) the mathematical concept convergence can be used. In this case the solution is converged after 248 iterations. By running the simulation, the focus was also on converging the given flow rate at the inlet, the target flow rate at the outlet and the resulting pressures with time. In principle it can be said that all simulation results finally converged quite well.
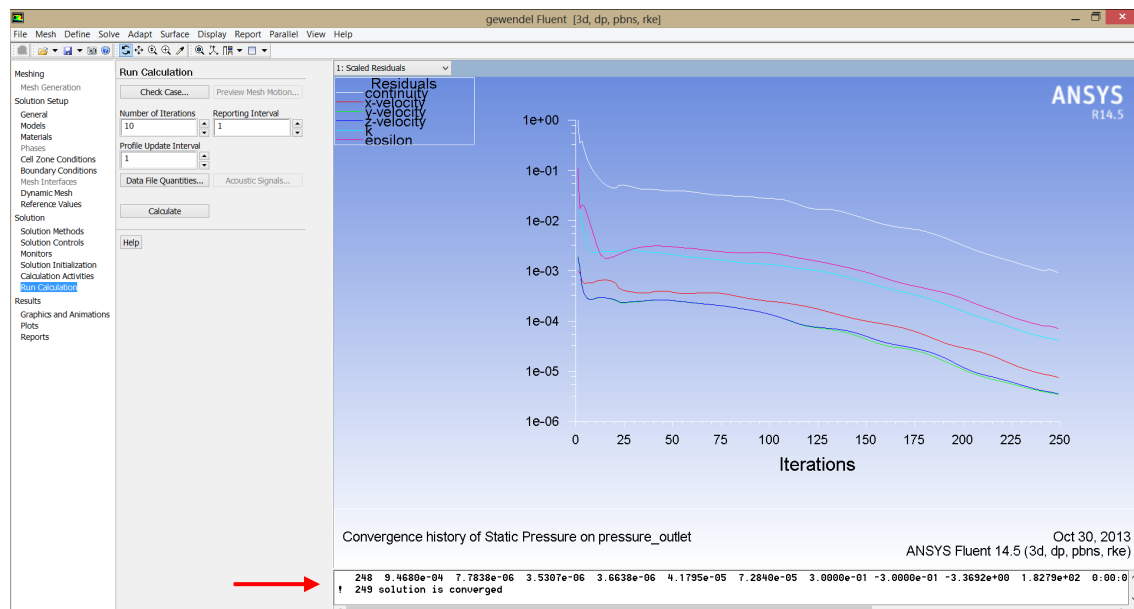
Figure 41 Convergence history on the outlet

---

[75] ANSYS 14.5 Help, Fluent, User's Guide, chapter 20.4.3. Pressure-Velocity Coupling

ANSYS FLUENT offers a lot of different methods to analyse the results of the simulation. One these techniques showing the results are illustrated the figure below in form of pathlines. Pathlines are used to visualize the flow of massless particles in the problem domain. The particles are released from the inlet (blue arrow) of the kudu horn flowing through the pipe.[76] As can be seen, no special flow behaviour, as Schauberger claimed, can be obtained.
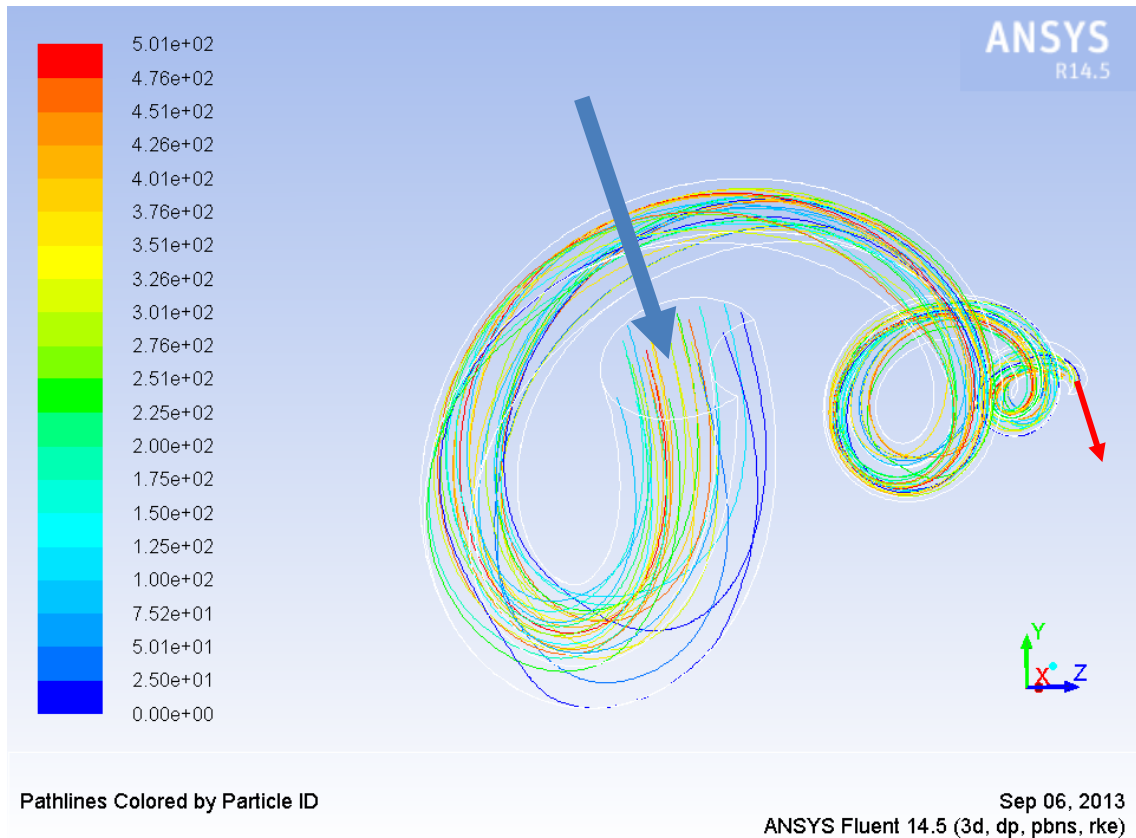
Figure 42 Visualisation of pathlines in the "kudu horn"

5.5   RESULTS

The results of the different simulation runs were evaluated in Fluent and Microsoft Excel. Table 3 below lists the resulting inlet and outlet pressures for the three different cases for each pipe type. If effects would exist where frictional resistance gets smaller, or even negative, then also the pressure difference gets changed. Unfortunately and according to our knowledge about the fluid mechanics this was not the case. All three pipes show a linear behaviour relating to the flow rate and therefore refute the Pöpel and Schaubergers experiment (Figure 43).

	flow rate [l/s]	Static pressure difference [Pa]	Total pressure difference [Pa]
straight pipe	0,30	285	281
	0,35	374	368
	0,45	584	574
rifled pipe	0,30	385	367
	0,35	505	482
	0,45	789	750
kudu horn	0,30	486	477
	0,35	637	625
	0,45	993	973

Table 3 The simulation results of the Stuttgart experiment
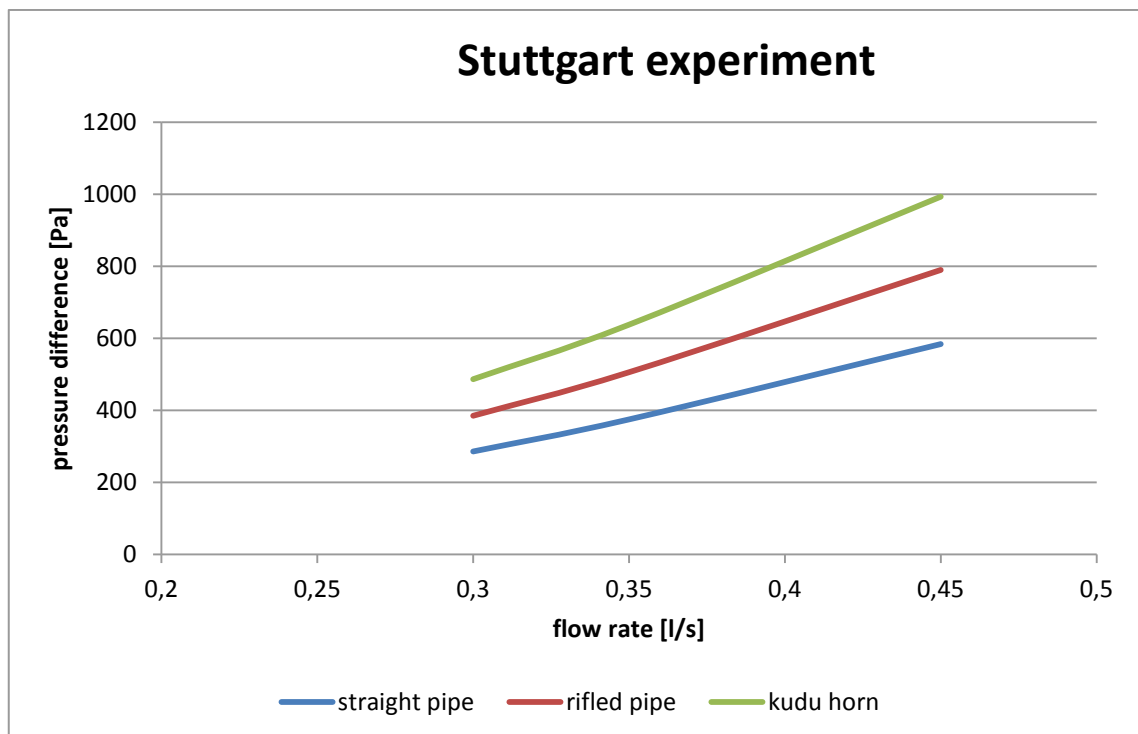
Figure 43 The simulation results of the Stuttgart experiment

5.5.1 INTERPRETATION OF THE RESULTS

The simulations could not confirm the results of the Pöpel experiment and thus the theory of Schauberger. According to the expectations the simulation resulted to a linear relationship between flow rate and flow losses. The pipes with the smallest wall surfaces and thus with the lower friction areas are having the highest flow rate. Therefore the kudu pipe with the largest surface shows the lowest efficiency.

Unfortunately Pöpel's report completely misses an error analysis and accurate evaluation of the experimental setup with its individual elements, which makes it difficult to reproduce their data. The uncommon results can perhaps be explained by some of the following reasons.

"The hypothetical conclusions from the flow experiments were confirmed by measurements of the friction losses and flow rates with 7 straight and spiralled pipes of various cross-sectional shapes and different walls." This quote from Pöpel in the original report is not true. The friction was determined only by calculations and was not explicitly measured. The deduction of the height difference from the inlet and outlet in the calculation of the original experiment does not represent the experimental run without friction. The energy loss due to friction is composed by various components which were used by the experiment. These include the inlet, the transition tubes with the constriction and expansion of the experimental setup, the tube pieces which when bent tend to assume an oval cross section and of course the diffuser at the outlet. To compensate the influence of these components with the installation of a diffuser at the outlet is impossible.

In the area of the diffuser large variations in the cross-sectional widening occur. Why a diffusor was chosen in the Stuttgart experiment set-up is unclear. This sector alone represents already great potential for errors. Depending on the flow velocity a detachment of the flow field from the diffuser wall can occur, and at these locations the pressure drops. In addition previously initiated fluctuations are getting increased. The measurement points, which were set by Pöpel briefly at the beginning and at the end of the diffuser, should not be elected this way to expect reliable measurement results. The cross section is suddenly expanded where it gets detached from the wall depending on the flow rate. This of course causes internal irregularities in the flow field. Depending on how far the measuring point is from the extension of the diffusor, some repulsion effects can occur to the lower measurement point, where then of course a lower pressure to the corresponding representative pressure would be measured. With this used experiment set-up no reliable data can be obtained. If these values then are used for the pressure measurements and are compared with the values in the entry box, the phenomena of "negative friction" can be achieved.

Furthermore, the reading on the scale also represents a source of error. Unfortunately nothing was documented as how large the variation of the error reading could have been.

The best to prevent potential factors or to register them in the same order of magnitude at multiple measuring points is to have exactly the same conditions at the measurement points. This can be achieved if the flow pattern at the inlet and at the outlet would be the same. The pressure level at the measuring point of the inlet in the original experiment is measured with the dynamic component. To minimize such dynamic effects the water level at the inlet box should be large enough and the inlet from the pump into the box should be constructed in a way that the movement caused by the pump not or only slightly influences the inlet of the test pipe.

Friction occurs wherever media moves. This leads to a change in temperature of the medium and / or the medium bounding materials. Such a precision temperature measurement

to deduce the existence of friction is much less prone to errors, as to calculate friction over the various energy states at certain measurement points.

Fact is that the inlet, the transition tubes and the diffuser have a significant influence on the flow behaviour, but this was ignored entirely in their investigations.

Also the daring to extrapolate from the measured results, which are only of small scale, is unscientific in the highest degree.

Perhaps it would have been better to give the job to a Fluid Dynamics institution.

6 MAGNA STEYR INVESTIGATION

Figure 18 in the chapter 4.2 Advanced Automotive Idea shows the basic concept of the "kudu or spiral compressor". For the simulation only the compression effects of the spiral are investigated and not the whole system with the housing. The final geometry of the spiral channel was a working process, by changing several times the dimensions. At the beginning the cylinder in which the spiral channel should be manufactured was defined with a diameter of 200 mm and a height of 100 mm. The diameter of the inlet and outlet were given with 15 and 7,5 mm. The figure shows the first concept of the new automotive compressor.
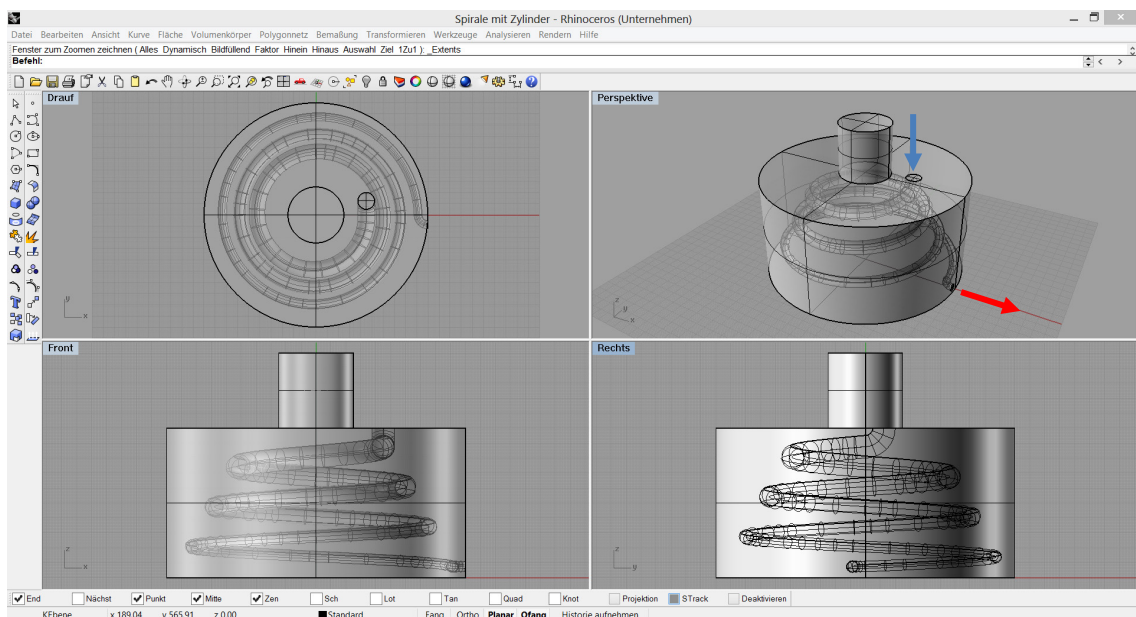
Figure 44 Constructing the first concept of the spiral

The problem with this concept was the handling of the boundary conditions at the inlet and outlet. Turbulences were caused already by the wrinkle at the inlet and outlet, which is according to Schauberger necessary in order to achieve certain effects, but with rotating the spiral (turbochargers are rotating up to 150.000 rpm and more) suction effects occur which prevents a nice flow field at the entrance. Also suction effects outweigh at the outlet and make an interpretation of the results impossible.

Therefore pipes were attached to handle the boundary conditions at the two ends of the spiral (Figure 45). Unfortunately this increased the number of cells significantly which led to unfeasible times of the simulations.
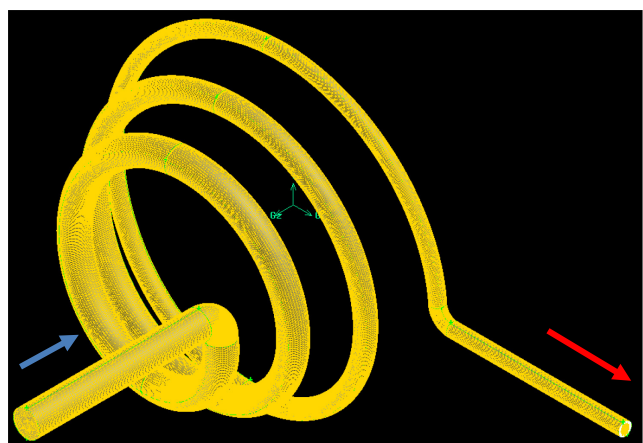
Figure 45 Pipes attached to the inlet and outlet

According to Schauberger the natural water movement is the inwardly spiralling (like a vortices), which should be used to create and to energize. If water is allowed to flow in this cycloid spiralling way friction will disappear. Therefore another concept of the spiral was constructed and simulated, because the reconstruction of the Stuttgart experiment and the design of the new concept were done at the same time. Figure 46 shows an inwardly spiral (see the difference from Figure 45). Regrettably simulation results showed no improvement in terms of the pressure increase and so this concept was also not further investigated.
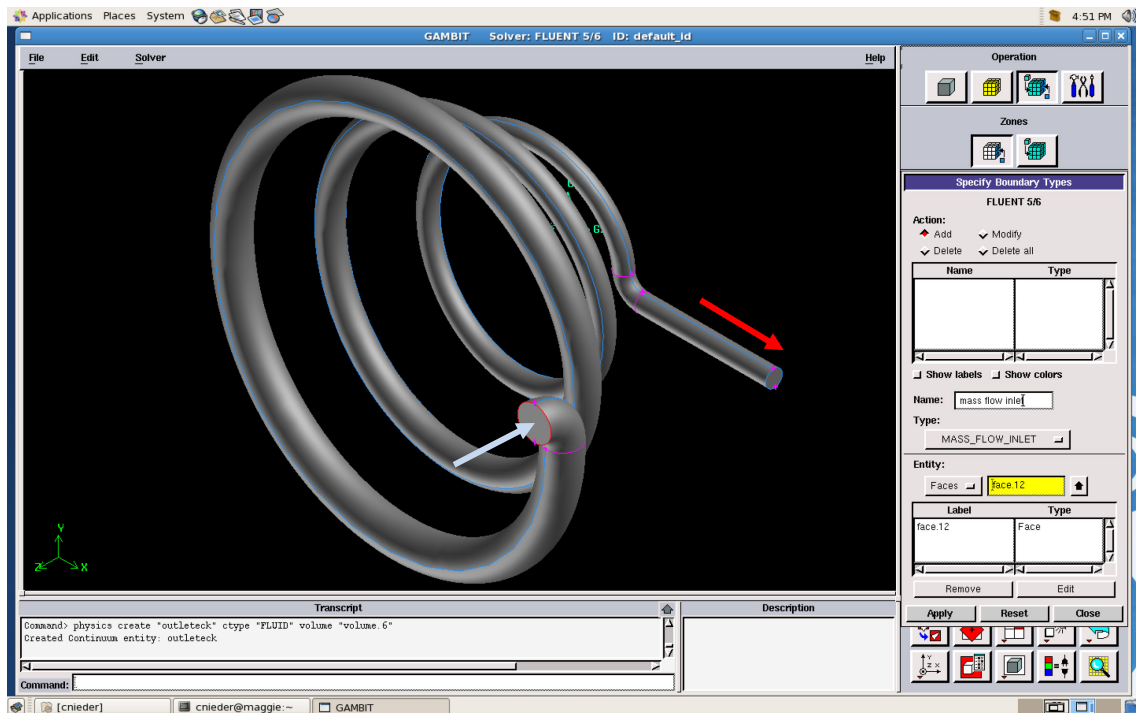
Figure 46 A inwardly spiral

Finally to keep the diploma thesis within manageable limits, the basic geometry of the spiral was revised and specified. The spiral itself was defined with one and a half turns and the ratio between the inlet diameter and outlet diameter was specified with 3:1. By defining the boundary conditions it was tried to simplify the whole investigation and was therefore designed in a simple tangential way. The following subchapters are showing the different simulation cases.

In order to understand and check the results of the simulation for their correctness, stationary simulation runs were made with varying the inlet velocity and therefore the flow rate. As medium water and air was studied. The basic geometry is the simple spiral (next chapter 6.1 Simple Spiral). The inverse spiral was constructed to see if a bigger inlet than outlet has more effect in terms of compression. A special spiral, adapted from the kudu horn, is also included in the experiment. The following subchapters are showing the various geometries and the table below lists all simulation cases.
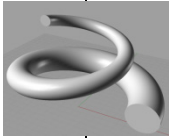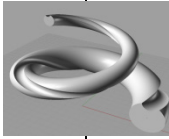
		Inlet velocity in [m/s]	revolutions per minute
SIMPLE SPIRAL	WATER	1	0
		3	0
		5	0
		1	1000
		1	3000
		1	5000
	AIR	10	75000
		10	100000
		10	150000
INVERSE SPIRAL	WATER	1	0
		3	0
		5	0
		1	1000
		1	3000
		1	5000
	AIR	10	75000
		10	100000
		10	150000
KUDU SPIRAL	WATER	1	0
		3	0
		5	0
		1	1000
		1	3000
		1	5000
	AIR	10	75000
		10	100000
		10	150000

Table 4 The various simulation cases

6.1   SIMPLE SPIRAL

Compared to the first concepts the whole spiral was increased. The Inlet was defined with a diameter of 15 mm and the outlet has a diameter of 45 mm. The height of the spiral is about 110 mm. The number of turns of the spiral was set to one and a half.
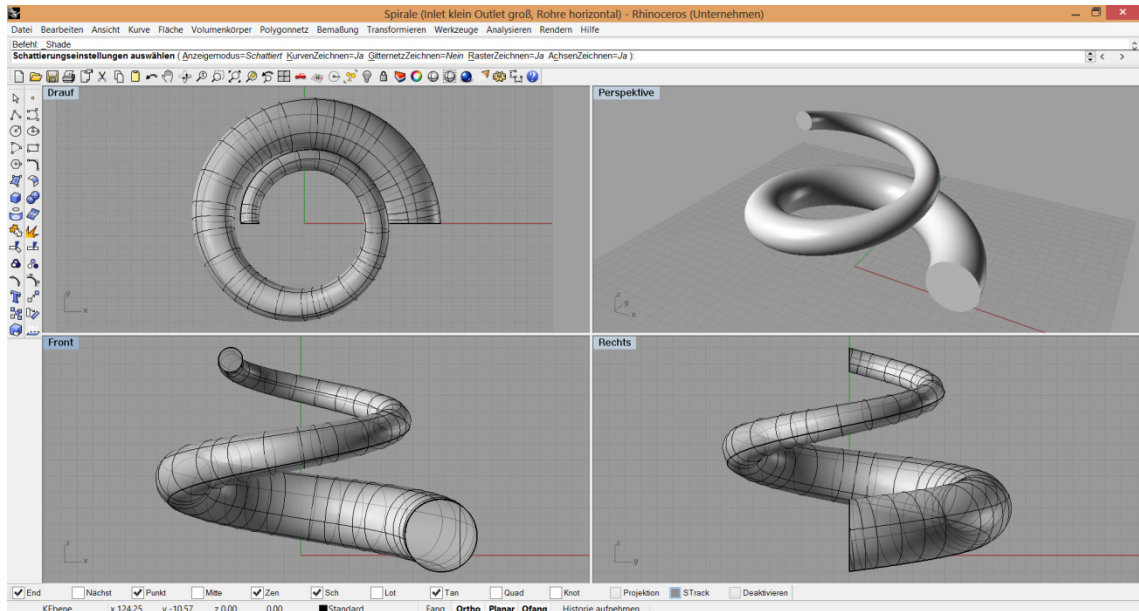
Figure 47 Constructing the simple spiral
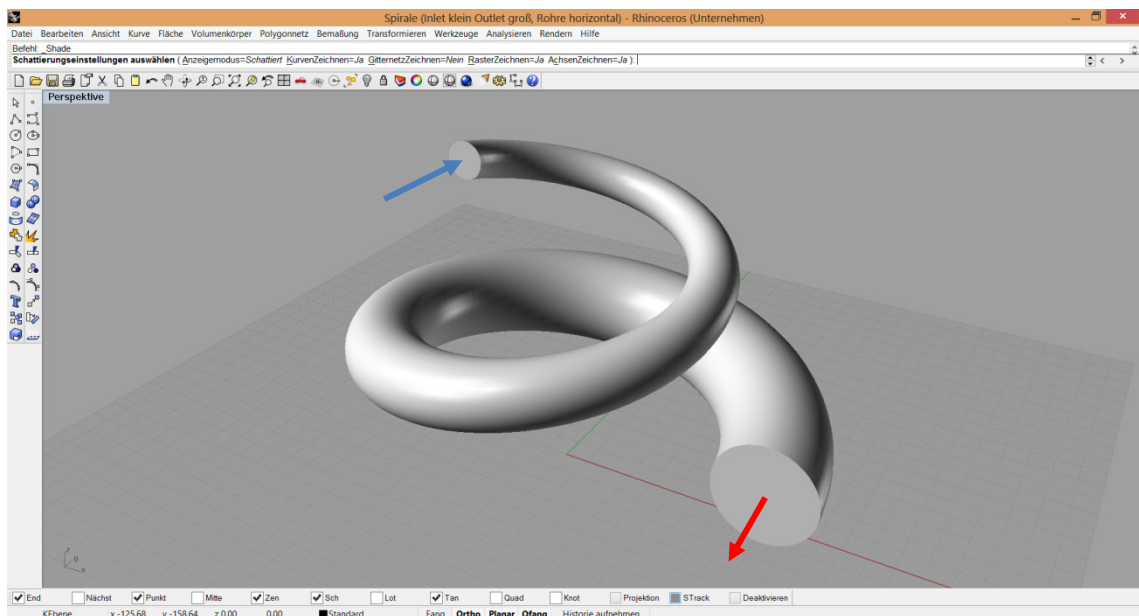
Figure 48 The simple spiral

6.2   INVERSE SPIRAL
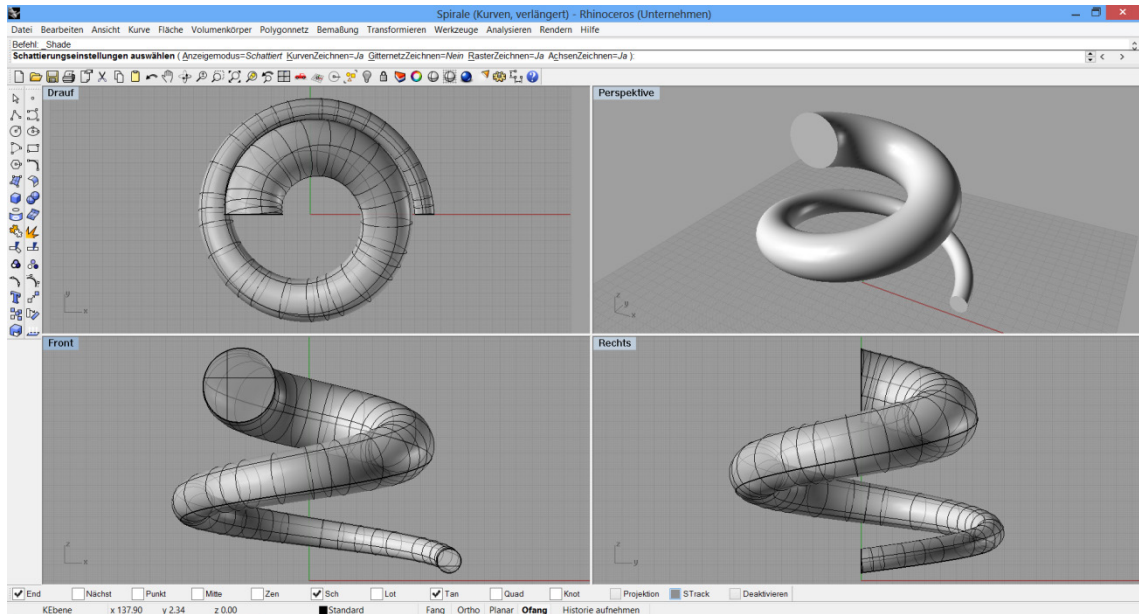
Figure 49 Constructing the inverse simple spiral
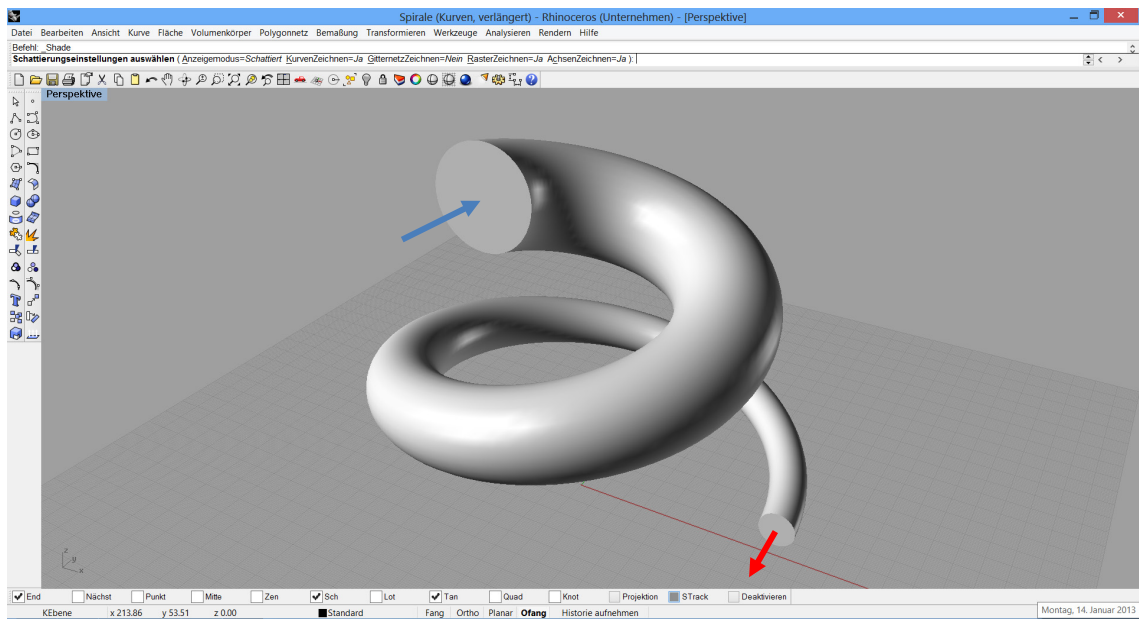
Figure 50 The inverse simple spiral

6.3 KUDU SPIRAL
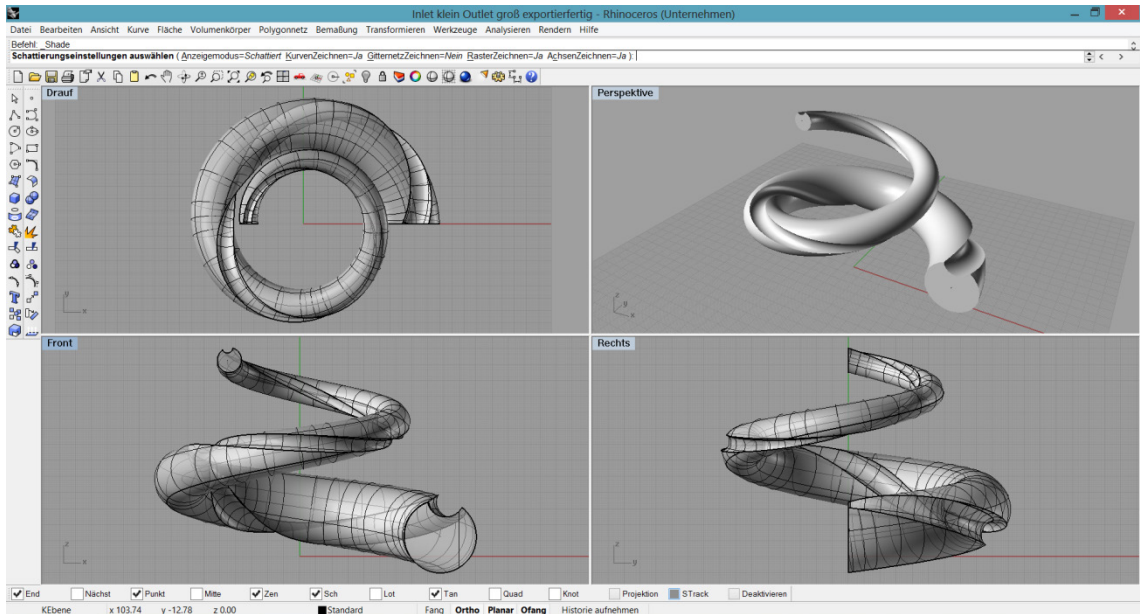
Figure 51 Constructing the kudu spiral
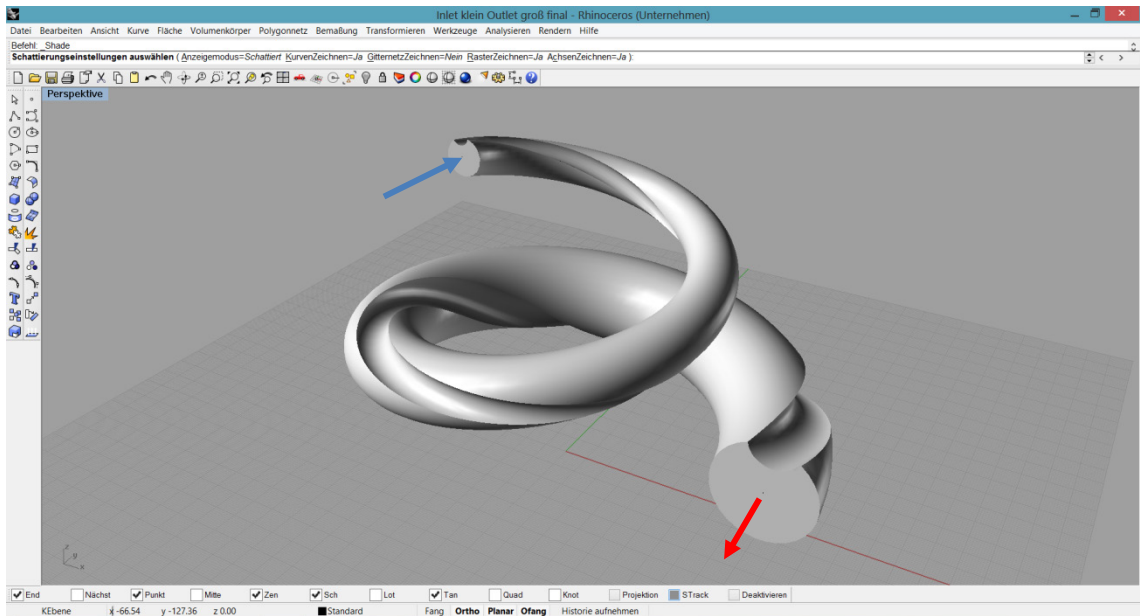
Figure 52 The kudu spiral

6.4   RESULTS

Basically the simulation set up is similar to the settings as it was seen in the Pöpel experiment. Solely only the settings for rotating the spiral had to be added. The rotations per minute must be converted to radiant per seconds. It turned out that the direction of rotation clockwise made no sense. Therefore all rotations were simulated counterclockwise. Figure 53 shows the settings to rotate the spiral in the simulation.
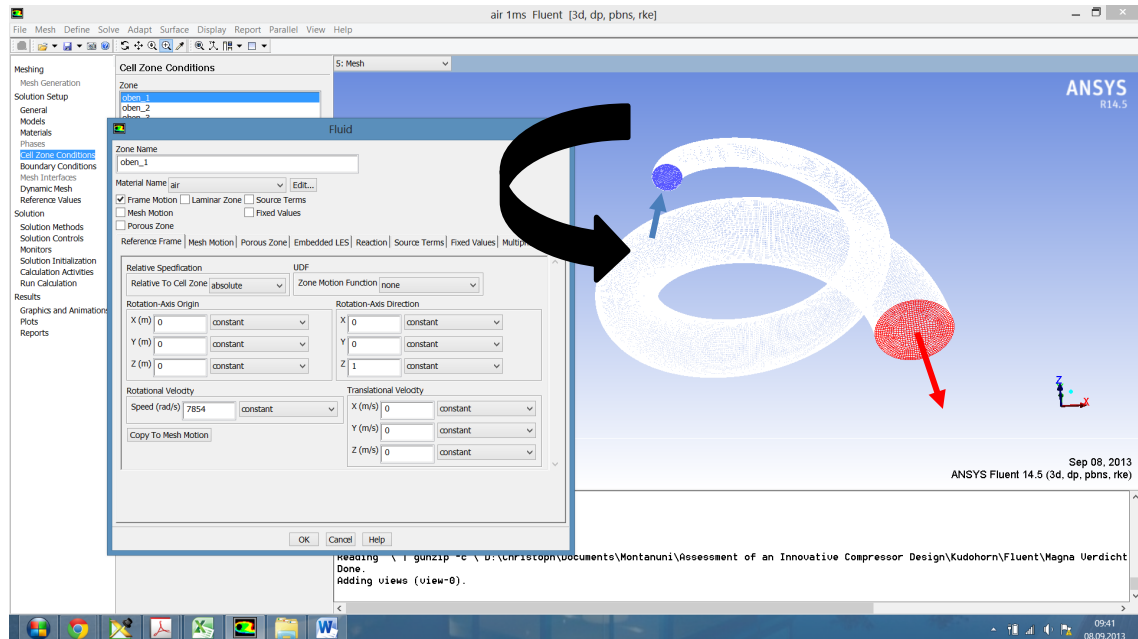
Figure 53 The settings to rotate the spiral in the simulation

All results from the many simulation runs are also evaluated graphically and can be seen on the attached appendix CD. For illustrating some results of the simulation, two cases are shown on the next pages. The first is the case where air flows through the simple spiral by a counterclockwise rotation of 75.000 rpm. To compare, the second who is shown is the kudu horn with the same values.

The first picture displays the y+ values in the full range. Because one mesh was used for all geometries and cases, some issues resulted to y+ values below 20 by using the standard wall function. One of such example can be seen on the second picture, where only y+ values below 20 are illustrated. As it can be seen, the number of cells which are not in the desired y+ range is minor and can be tolerated.

Then the next illustrations are presenting the pressure conditions in the spiral, followed by the turbulence factors kinetic energy, intensity and dissipation rate. The shear stress at the wall ends the graphically evaluation.

For evaluating the results a surface along the spiral was generated. Due to the complex geometry, this was not possible for the kudu horn.

6.4.1 SIMPLE SPIRAL
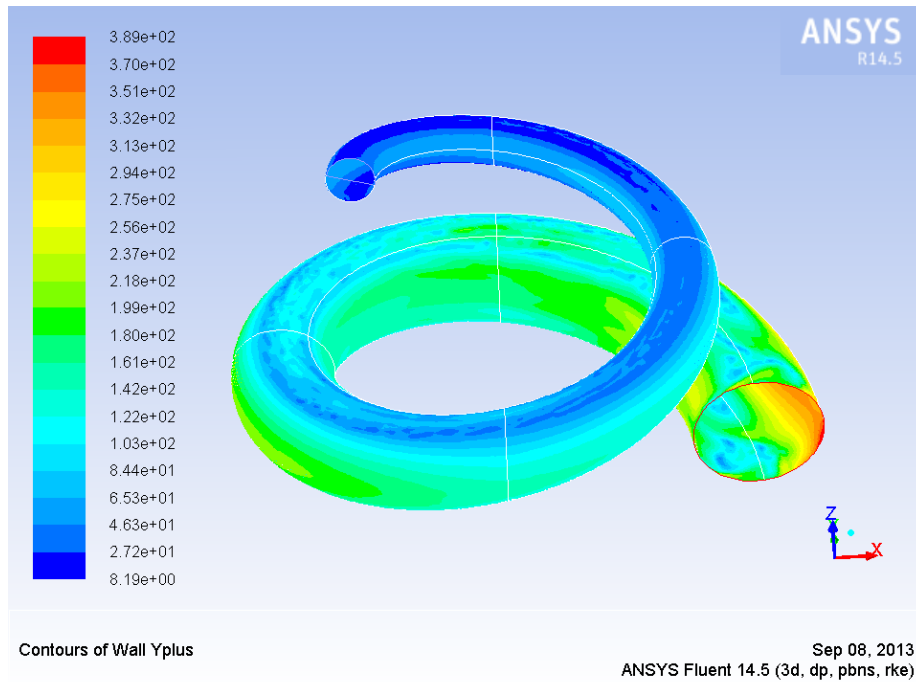
Figure 54 y* values - simple spiral, air, 10 m/s, 75000 rpm, counterclockwise
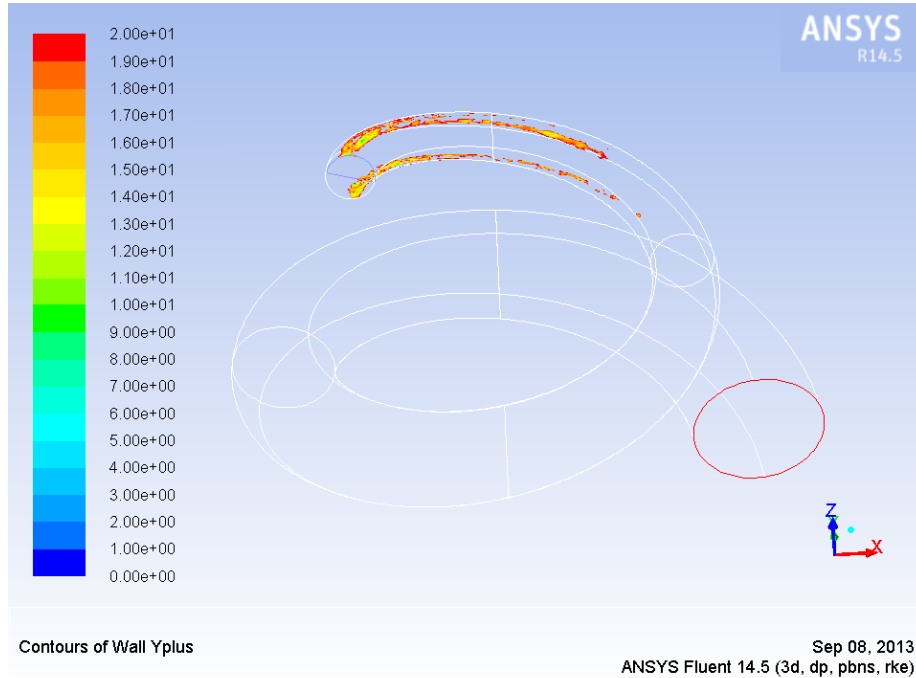
Figure 55 y* values under 20 - simple spiral, air, 10 m/s, 75000 rpm, counterclockwise
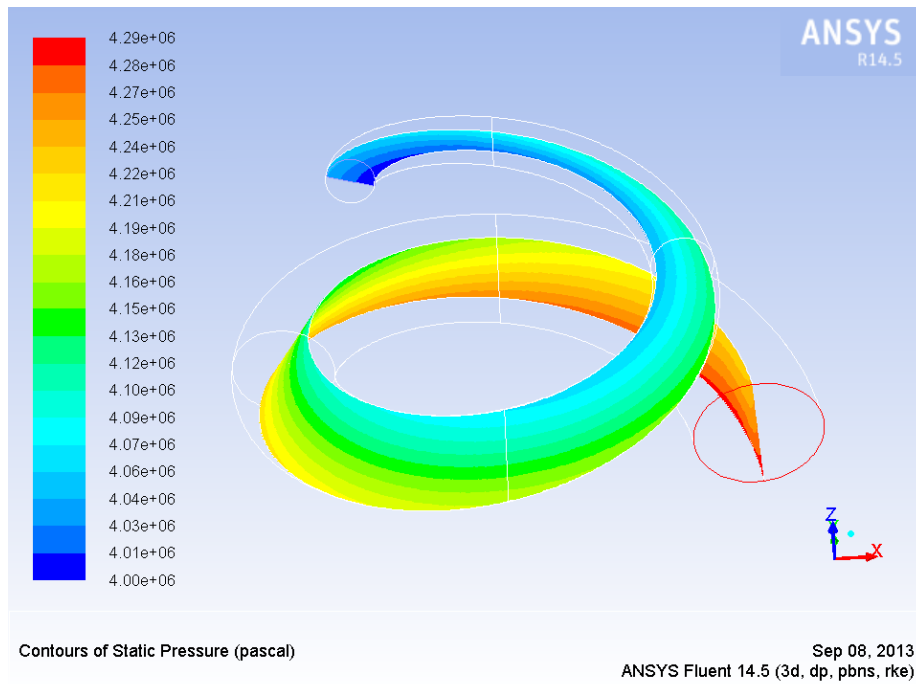
Figure 56 static pressure - simple spiral, air, 10 m/s, 75000 rpm, counterclockwise
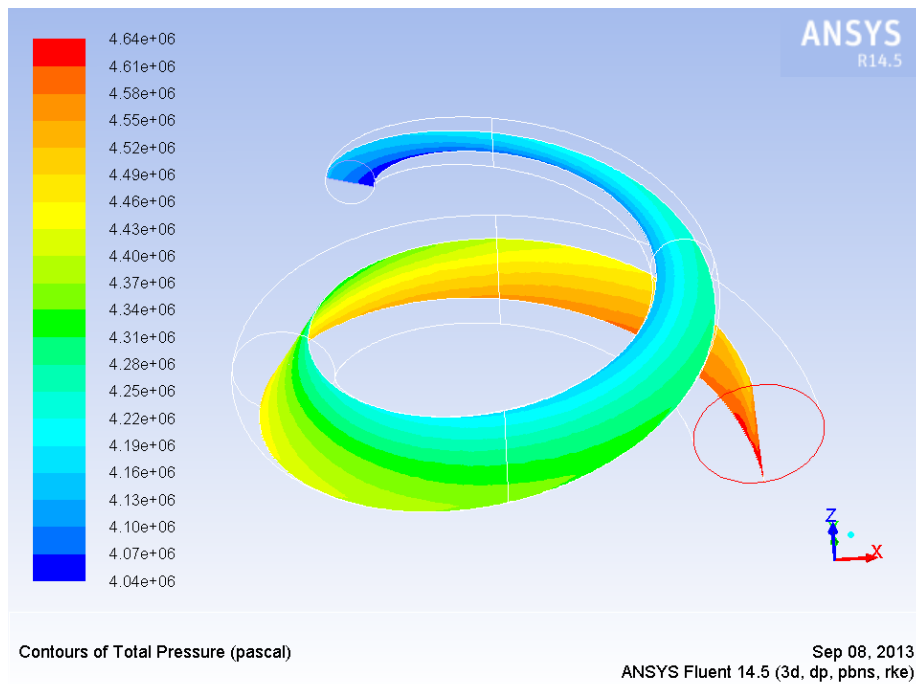
Figure 57 total pressure - simple spiral, air, 10 m/s, 75000 rpm, counterclockwise
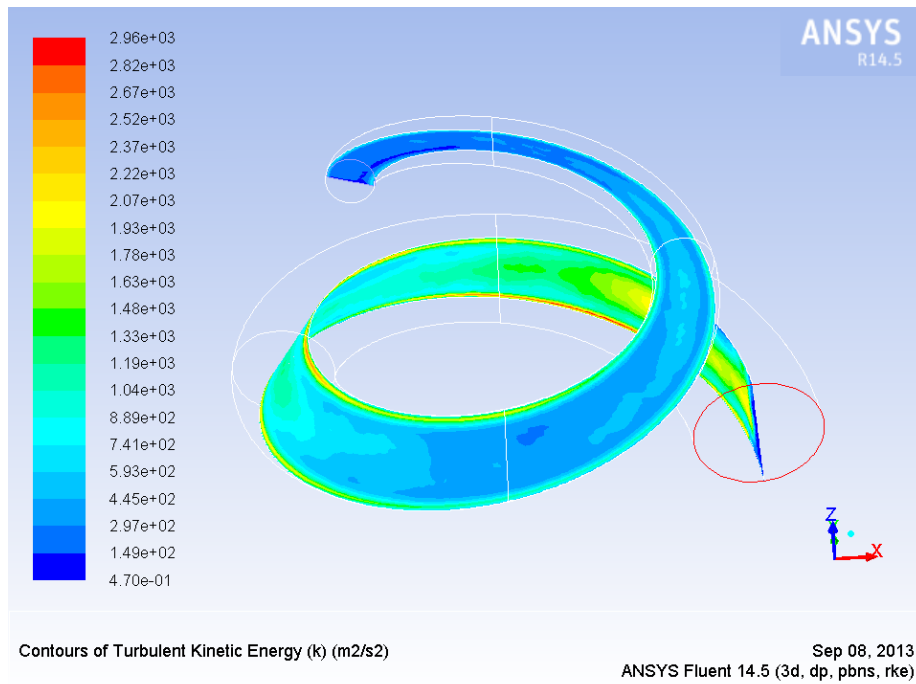
Figure 58 kinetic energy - simple spiral, air, 10 m/s, 75000 rpm, counterclockwise
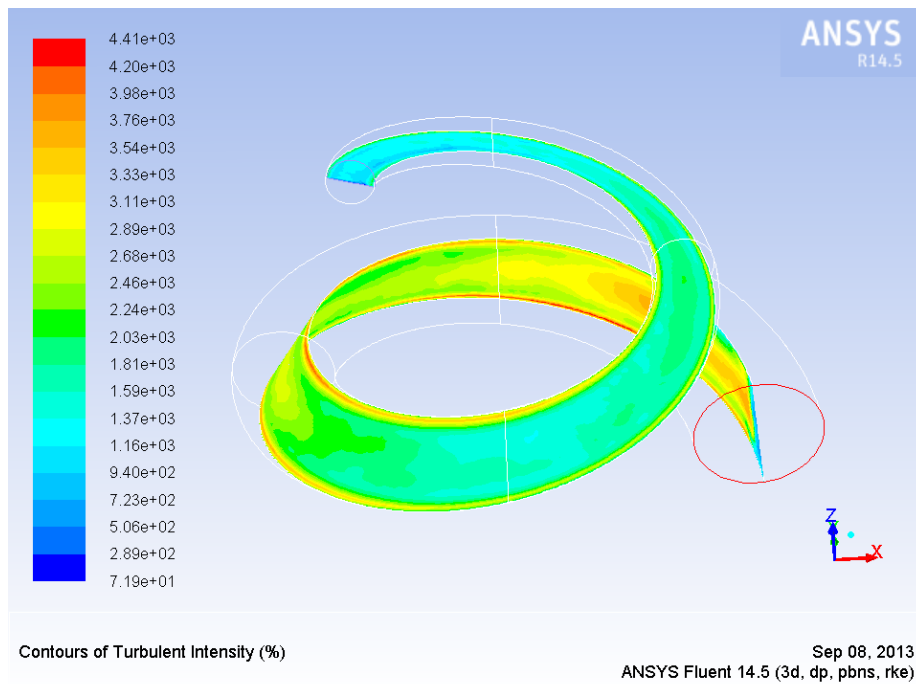
Figure 59 intensity - simple spiral, air, 10 m/s, 75000 rpm, counterclockwise
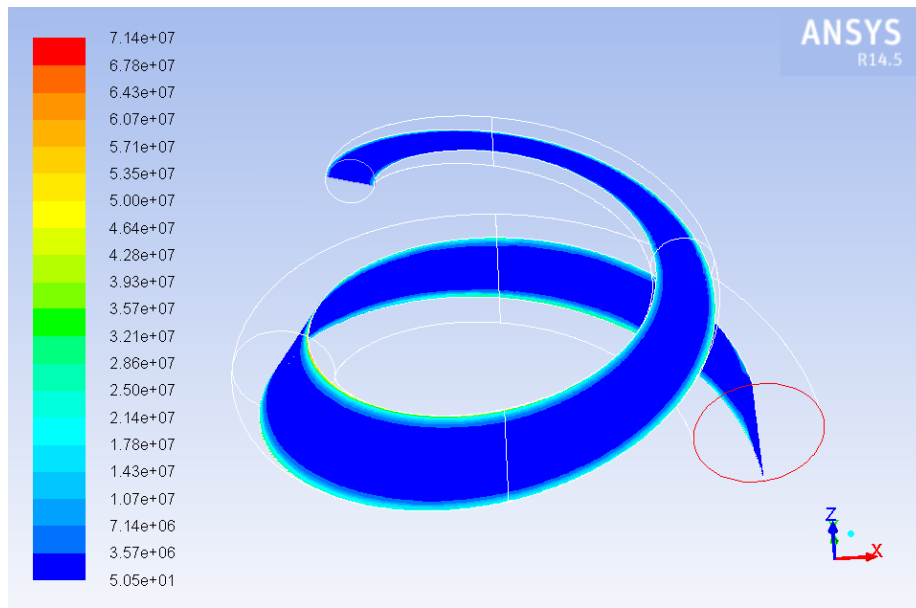
Figure 60 dissipation rate - simple spiral, air, 10 m/s, 75000 rpm, counterclockwise
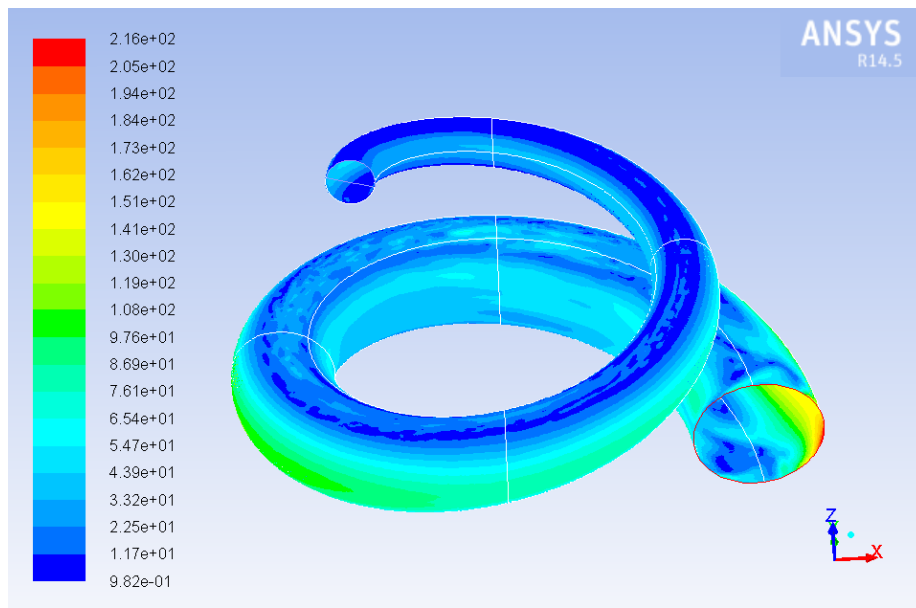
Figure 61 wall shear stress - simple spiral, air, 10 m/s, 75000 rpm, counterclockwise

6.4.2 KUDU HORN
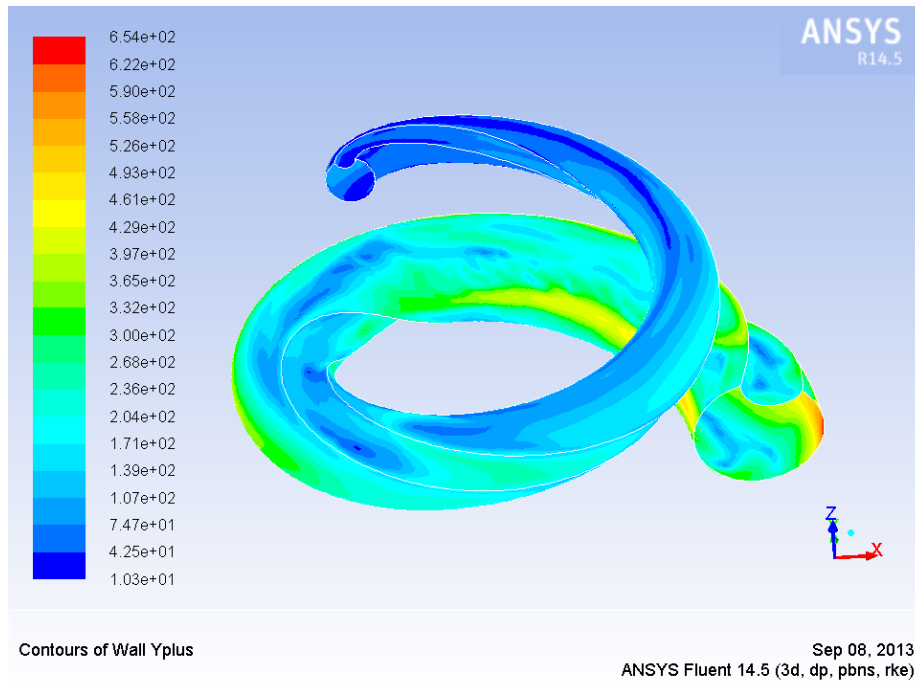
Figure 62 y* values – kudu horn, air, 10 m/s, 75000 rpm, counterclockwise
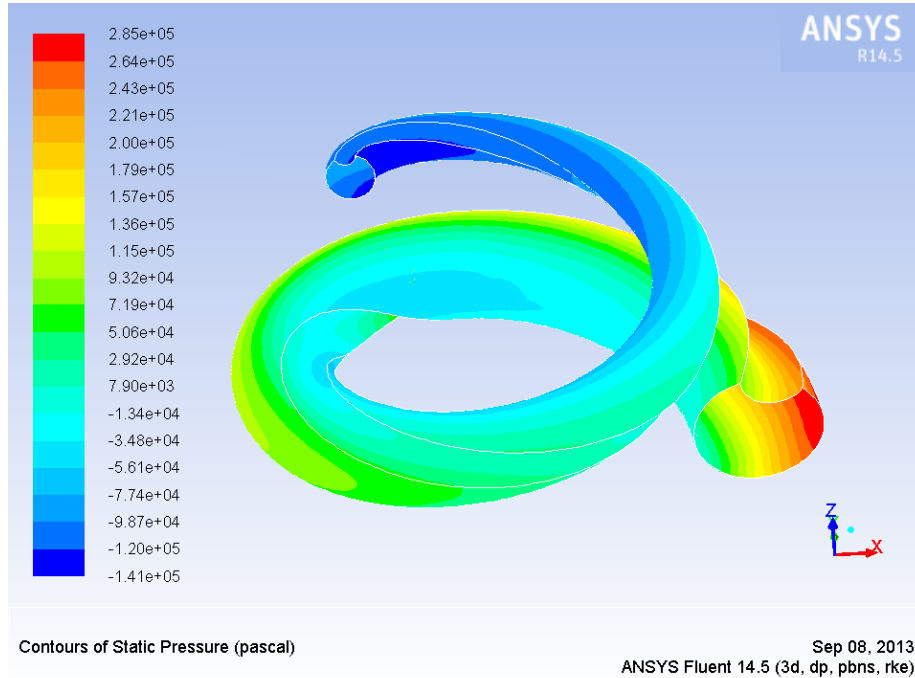
Figure 63 static pressure – kudu horn, air, 10 m/s, 75000 rpm, counterclockwise
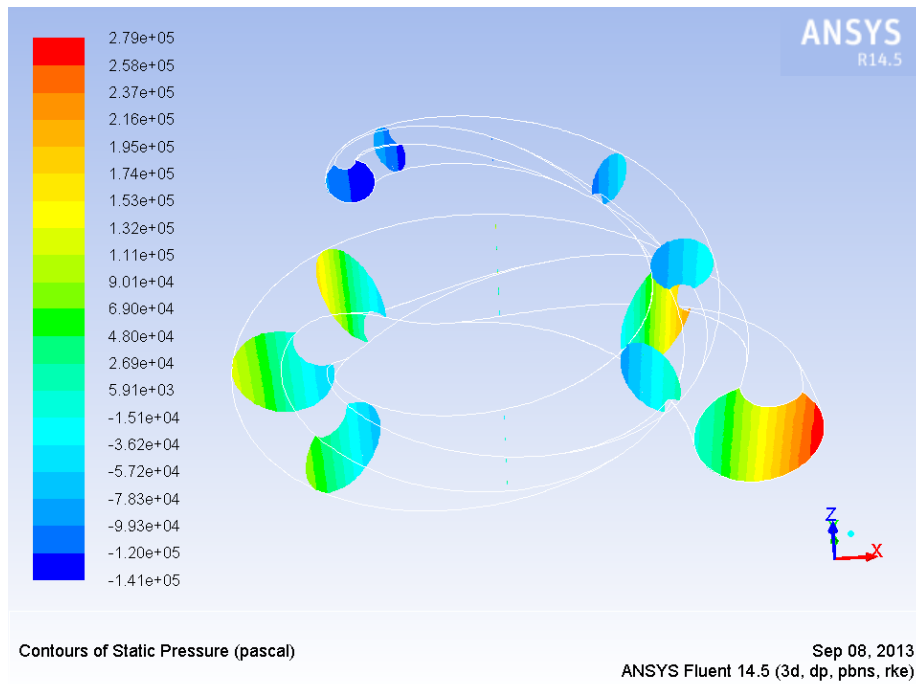
Figure 64 static pressure – kudu horn, air, 10 m/s, 75000 rpm, counterclockwise
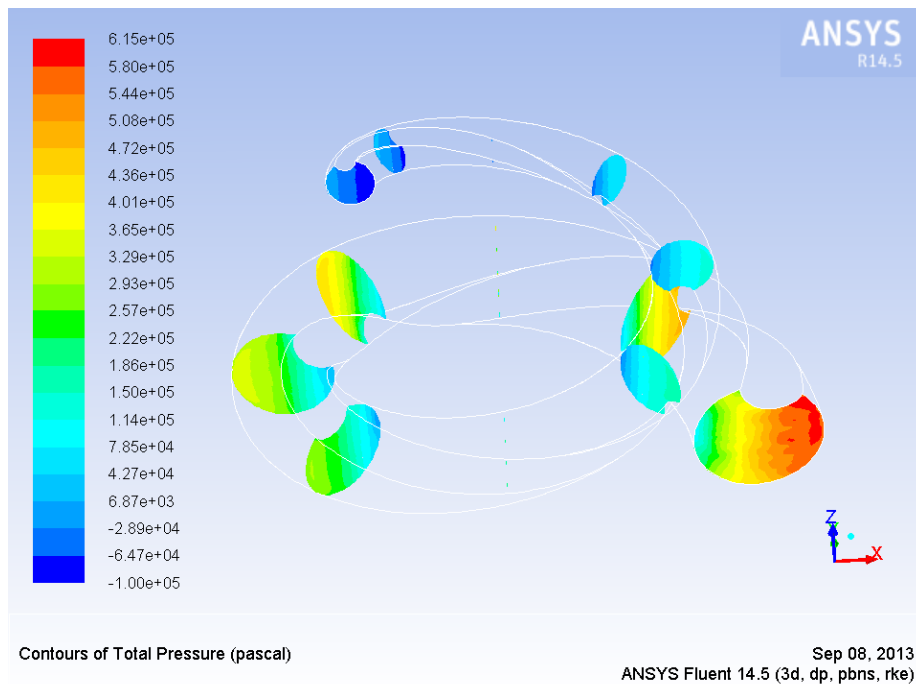
Figure 65 total pressure – kudu horn, air, 10 m/s, 75000 rpm, counterclockwise
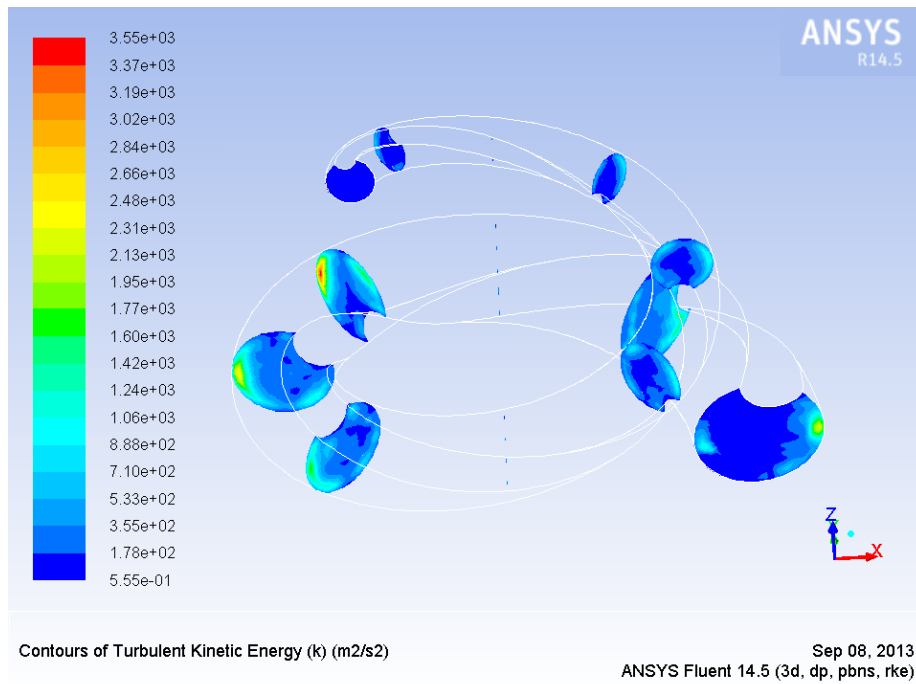
Figure 66 kinetic energy – kudu horn, air, 10 m/s, 75000 rpm, counterclockwise
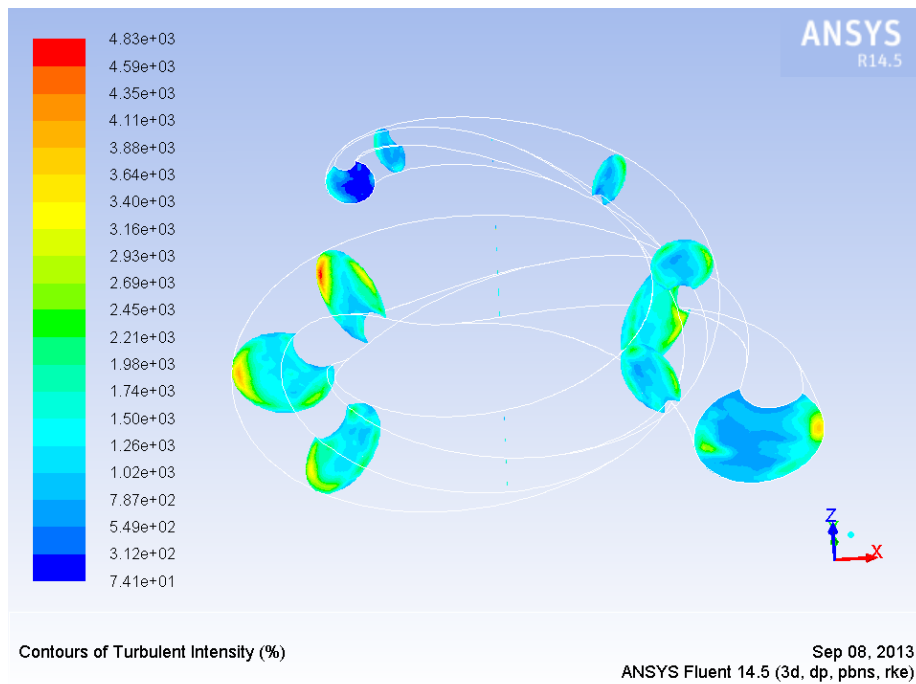
Figure 67 intensity – kudu horn, air, 10 m/s, 75000 rpm, counterclockwise
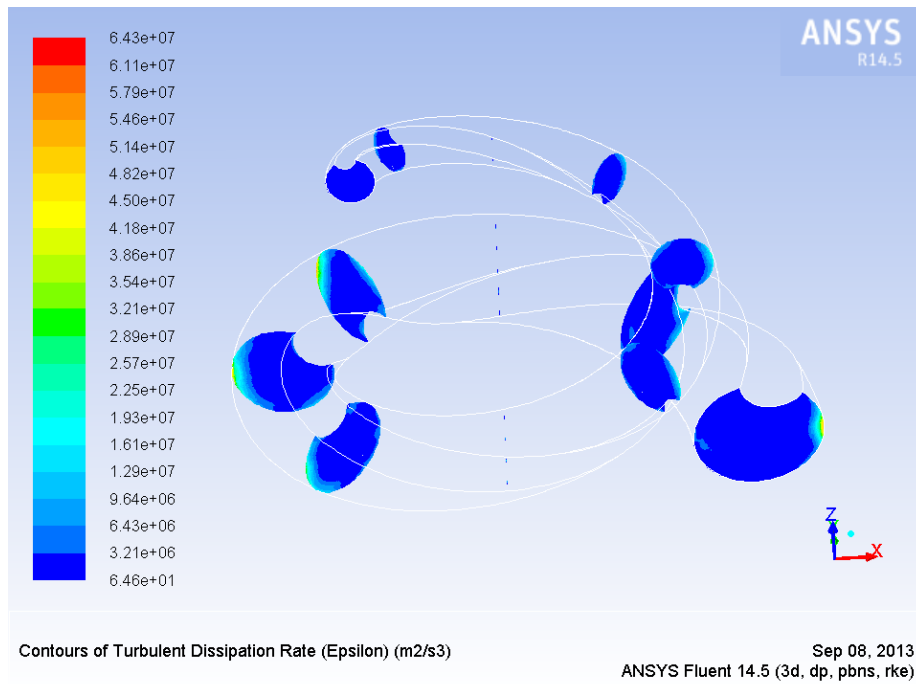
Figure 68 dissipation rate – kudu horn, air, 10 m/s, 75000 rpm, counterclockwise
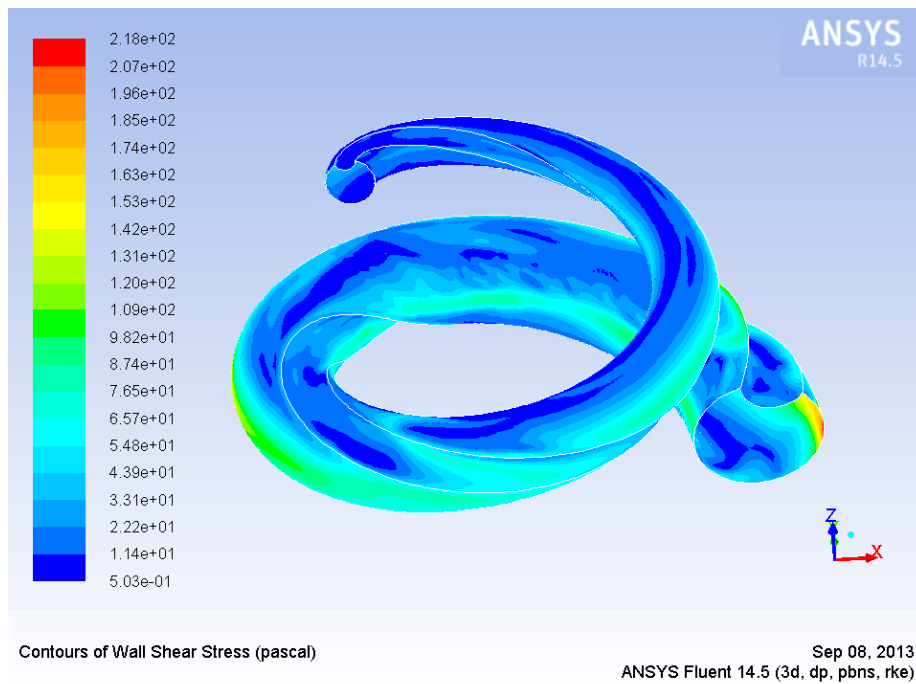
Figure 69 wall shear stress – kudu horn, air, 10 m/s, 75000 rpm, counterclockwise

6.4.3 COMPARING ALL GEOMETRIES

The pressure difference is evaluated once from the outlet, the red face in the figure below, to the inlet (the blue face), and the second is from the green one to the inlet. The reason is that suction effects occur due to the high rotational speed and influences the last part of the spiral. Therefore the second method (comparing from the green interior face to the inlet) is more meaningful.
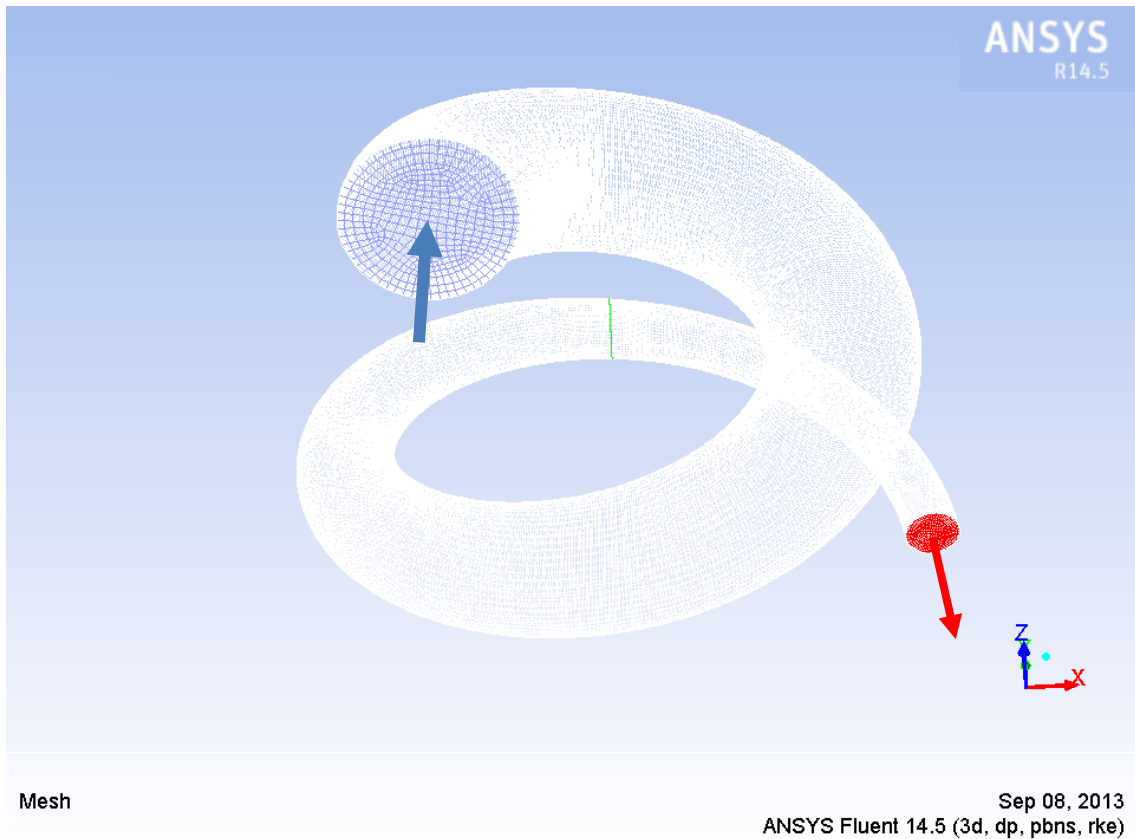
Figure 70 Evaluating the simple spiral

The next tables are presenting the resulting static and total pressure values of the simulations. The difference pressure is converted in bar. Generally a trend is difficult to see. What can be said is that the spiral in principle compresses very well. As expected, air is compressed more than water. The highest difference is achieved with 16 bar. For compression the inverse spiral is not better than the simple spiral. Although the inverse spiral has a smaller outlet and so a higher compression would be suspected, but due to the rotation the dynamic share of the pressure in the simple spiral is much higher and leads to a higher total pressure as the inverse spiral.

		[rpm]	STATIC PRESSURE DIFFERENCE [bar]
SIMPLE SPIRAL	WATER	1000	0,3
		3000	1,0
		5000	5,1
	AIR	75000	2,0
		100000	3,7
		150000	9,0
KUDU SPIRAL	WATER	1000	0,3
		3000	2,5
		5000	7,0
	AIR	75000	1,9
		100000	3,5
		150000	7,8
INVERSE SPIRAL	WATER	1000	0,3
		3000	2,7
		5000	7,4
	AIR	75000	2,1
		100000	3,4
		150000	7,7

Table 5 Static pressure results of the various spirals

		[rpm]	TOTAL PRESSURE DIFFERENCE [bar]
SIIMPLE SPIRAL	WATER	1000	0,6
		3000	3,9
		5000	11,7
	AIR	75000	3,7
		100000	6,8
		150000	16,0
KUDU SPIRAL	WATER	1000	0,6
		3000	4,9
		5000	13,4
	AIR	75000	3,7
		100000	6,6
		150000	14,7
INVERSE SPIRAL	WATER	1000	0,5
		3000	4,7
		5000	13,3
	AIR	75000	3,7
		100000	6,4
		150000	14,4

Table 6 Total pressure results of the various spirals

6.5   REFERENCE COMPRESSOR

6.5.1   GT1544

The main task of this work was to investigate if the concept from Mr. Franz Mayr makes sense and further investigations are meaningful. Therefore the turbocharger GT1544 from GARRETT by Honeywell was chosen as a reference compressor.

Figure 71 GT1544 from Garrett[77]

It's a turbocharger, featuring a Journal bearing and is oil cooled. The turbine housing design consists of a three bolt inlet, and an internal wastegate including actuator. The specifications of the GT1544 are:

Compressor Wheel		Turbine Wheel	
Inducer Diameter	32,9 mm	Diameter	42,2 mm
Exducer Diameter	43,9 mm	Trim	58
Trim	56	A/R	0,34 or 0,35
A/R	0,33		

A/R describes a geometric characteristic of compressor and turbine housings. It is defined as the inlet cross-sectional area divided by the radius from the turbo centreline to the centroid of that area.[78]

Figure 72 A/R ratio[79]

---

[77] http://www.bar-tek-tuning.de/garrett+gt1544+turbo+turbolader.htm
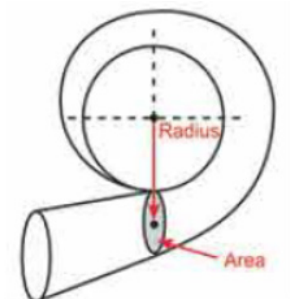
[78] Garrett - TurbochargerGuide Volume 5, p. 7

[79] Garrett - TurbochargerGuide Volume 5, p. 7

Trim is an area ratio to describe both turbine and compressor wheels. Trim is calculated using the inducer and exducer diameters. As trim is increased, the wheel can support more air/gas flow.

$$Trim = \frac{Inducer^2}{Exducer^2} * 100$$
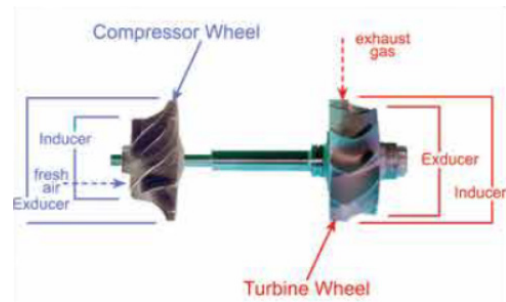
Figure 73 Trim[80]

Figure below identifies aspects of the compressor map from the GT1544. The compressor map is a graph that describes a particular compressor's performance characteristics, including efficiency, mass flow range, boost pressure capability and turbo speed.

The pressure ratio is defined as the absolute outlet pressure divided by the absolute inlet pressure. Remember that absolute pressure at sea level is 1,013 bar or 101.325 Pa. This is referred to as standard atmospheric pressure at standard conditions. [81]
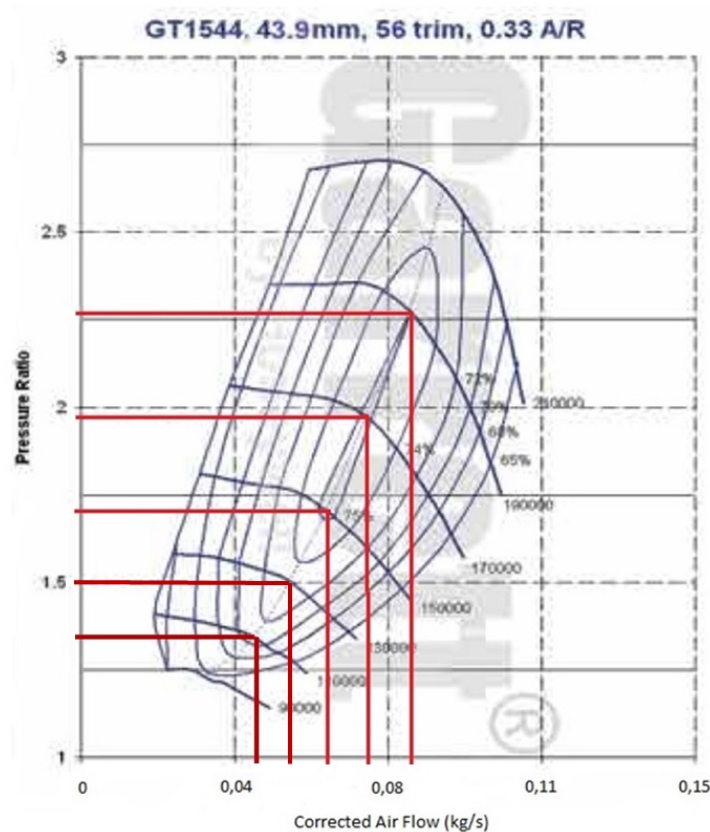
Figure 74 Compressor map of the GT1544[82]

---

[80] Garrett - TurbochargerGuide Volume 5, p. 7

[81] Garrett - TurbochargerGuide Volume 5, p. 9

[82] Garrett - TurbochargerGuide Volume 5, p. 24

Five points in the compressor map were elected for comparing the spiral concept with the GT1544 (marked with red in the compressor map). The values for these points are listed in the next table.

rpm	Air flow [kg/s]	Pressure ratio
100.000	0,05	1,3
130.000	0,055	1,5
150.000	0,06	1,7
170.000	0,07	1,95
190.000	0,09	2,26

Table 7 The reference points of the GT1544

Looking at the compressor map of the reference turbocharger (Figure 74) or at the table above (Table 7) it can be seen that the GARRETT GT1544 achieves higher pressure ratios by increasing the revolutions per minute and the air flow.

As already mentioned the new car compressor would not only have one spiral. It would have several. Seen in chapter 4.2 ADVANCED AUTOMATIVE IDEA the compressor consists of two spiral channels. In production more than one or two spirals would make sense and is already planned, so for comparison it was defined to simulate a compressor made of 6 (concept 1) and 12 spiral channels (concept 2). Hence this resulted in total to 15 simulation cases. The table below lists the input values of the various simulation runs:

rpm	Number of spirals	Air flow [kg/s]
100.000	1	0,05000
	6	0,00833
	12	0,00417
130.000	1	0,05500
	6	0,00917
	12	0,00458
150.000	1	0,06000
	6	0,01000
	12	0,00500
170.000	1	0,07000
	6	0,01167
	12	0,00583
190.000	1	0,09000
	6	0,01500
	12	0,00750

Table 8 Various cases to compare with the GT1544

The simulations were done in the same principle as already explained. By analysing the results of the various simulations the Magna Steyr design showed exactly the opposite behaviour as the reference turbocharger. The resulted pressure ratios were decreasing with increasing the flow rate and the rotational speed. Furthermore it made no significant difference whether the concept consists of one spiral channel, 6 or 12 at these high revolutions. Also it turned out that 130.000 rpm's is the limit of this concept. Above, the pressure ratios of the reference compressor couldn't be achieved by far. Below the 130.000 revolutions per minute better results as the GARRETT GT1544 were reached.

The fifteen resulting pressure ratios from the simulations were compared to the reference GT1544 in Table 9. Except the range below 130.000 rpm's the pressure ratio of the concept with one spiral, six or twelve is pretty the same. It's generally difficult by rotating this concept at such high speeds to see some differences, because by doing so, large suction effects occur at the outlet and also at the inlet of the spiral due to the rotation. With lower rotations per minute also the suction effects are lower.

rpm	Air flow [kg/s]	pressure ratio			
		GT1544	one spiral	concept 1	concept 2
100.000	0,050	1,300	2,559	2,377	2,324
130.000	0,055	1,500	1,445	1,443	1,423
150.000	0,060	1,700	1,207	1,163	1,163
170.000	0,070	1,950	1,053	1,037	1,031
190.000	0,090	2,260	0,955	0,969	0,960

Table 9 Comparing to the GT1544

Figure 75 below illustrates the results of the simulation cases and the values of the reference turbocharger in a compressor map. The opposite behaviour of the concept can be clearly seen on the left area of the plot. The right area indicates the reference compressor were the pressure ratio increases with increasing the revolutions per minute.

For a better comparison all respective cases from the concept and the reference are plotted in the same colour.

The results of the concept are always lower as the reference, except in the issue with 100.000 rpm's were significant better pressure ratios were achieved. This can be seen in the high difference of the two red lines. The red line from the spiral concept is significant higher as the red line of the GT1544.

The yellow line on the left shows the concept values for 130.000 rpm's and the right the reference values for the same case. By looking at them it can be seen that they are more or less at the same high or in other words the new compressor concept and the GT1544 achieve pretty the same pressure ratios in the case of 130.000 revolutions per minute. This indicates a kind of limit for the concept. All other lines from the Magna Steyr concept are lower as their respective reference lines.
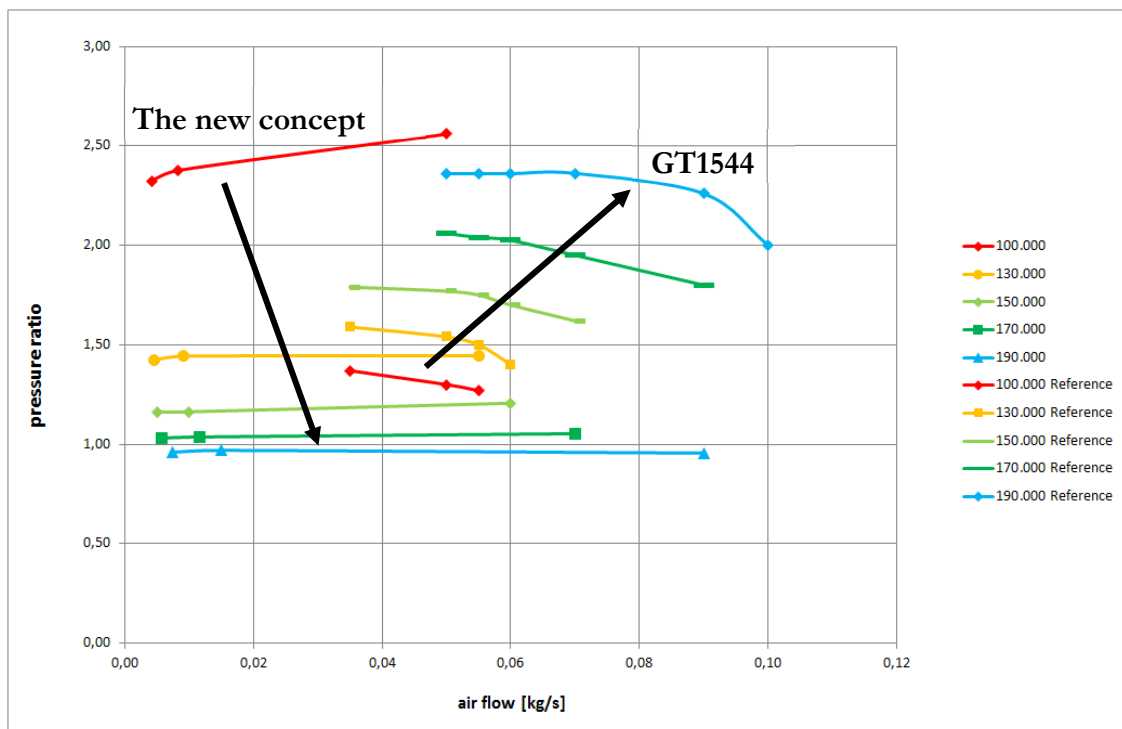
Figure 75 Comparing the new concept with the GT1544 in a compressor map

The concept has shown that it defeats the reference turbocharger at 100.000 rpm's. So it would be of interest how the concept behaves at rotational speeds less than 100.000. Therefore two further cases were investigated. Simulations with 10.000 and 50.000 rpm's were done with the same air flow as the issue with 100.000 rpm's, because no values were available for the GT1544 at those cases.

RPM	Air flow [kg/s]	pressure ratio			
		GT1544	one spiral	concept 1	concept 2
10.000	0,050		0,905	1,026	1,032
50.000	0,050		1,995	2,659	2,755
100.000	0,050	1,300	2,559	2,377	2,324
130.000	0,055	1,500	1,445	1,443	1,423
150.000	0,060	1,700	1,207	1,163	1,163
170.000	0,070	1,950	1,053	1,037	1,031
190.000	0,090	2,260	0,955	0,969	0,960

Table 10 Final results compared to the GT1544

Interesting at the results is that the pressure ratio of the concept increases with rpm, reaches the maximum at 50.000 rpm's, begins decreasing but achieves nevertheless better results as the reference compressor till the limit at 130.000 Rpm's is passed. The values in a more visible way:
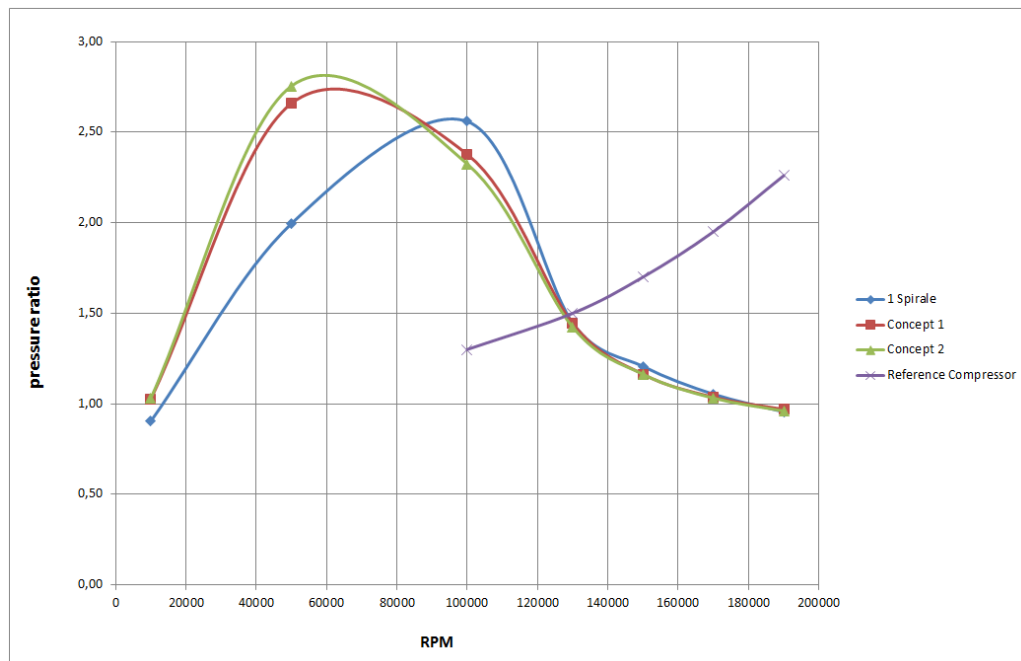
Figure 76 Final results compared to the GT1544

The curve can be described by the definition of the total pressure. The total pressure refers to the sum of static pressure p, dynamic pressure q, and gravitational head, as expressed by Bernoulli's principle:

$$p_0 = p + q + \rho g z$$

were ρ is the fluid density in kg/m³, g the local acceleration due to gravity in m/s², and z is the height above a datum in m.[83] The height above datum is in our case so small that it can be ignored. The dynamic pressure is the kinetic energy per unit volume of a fluid particle and is defined by:[84]

$$q = \frac{1}{2}\rho v^2$$

As it can be imagined the dynamic pressure gets dominated with v = ω*r or a = ω²*r by increasing the rotational speed till a maximum is reached. This happens at round 50.000 rpm's were suction effects are working against a pressure build up and the total pressure begins to decreasing.

Because no big difference can be seen between concept 1 and 2, the following pages are illustrating the results visually from the concept 1 with 6 spiral channels at 10.000 to 150.000 revolutions per minute. Due to the fact that the resulted pressure ratios at 170.000 and 190.000 are far below of those from the reference turbocharger, it makes also no sense to show the plots of the results from these cases.

Note: The respective diagrams of the different cases are shown in the same scale.

---

[83] http://en.wikipedia.org/wiki/Total_pressure
[84] http://en.wikipedia.org/wiki/Dynamic_pressure

CONCEPT 1 - 10.000 RPM
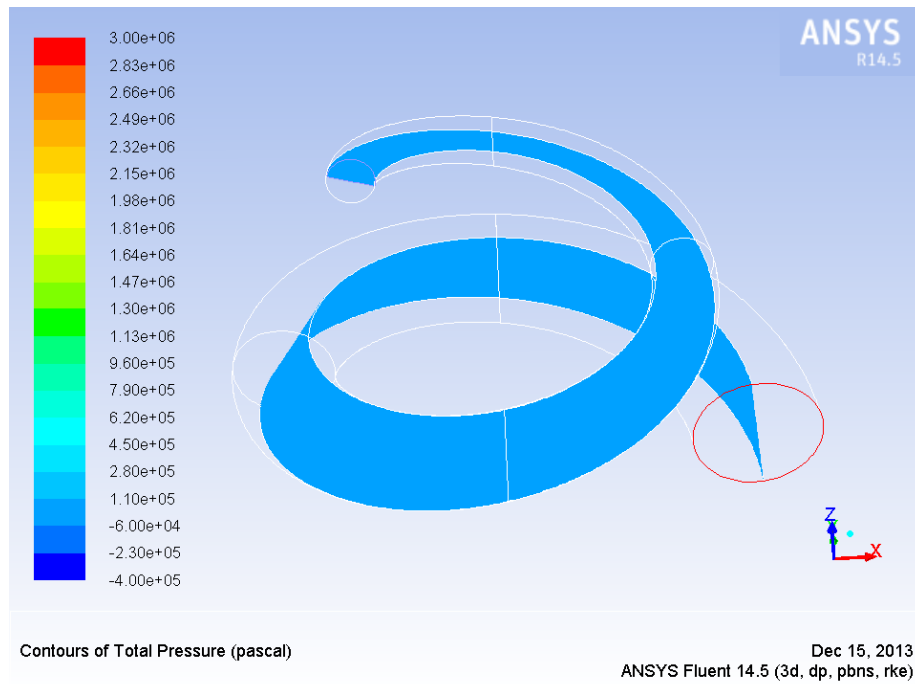
Figure 77 Concept 1, 10.000 rpm, Total pressure
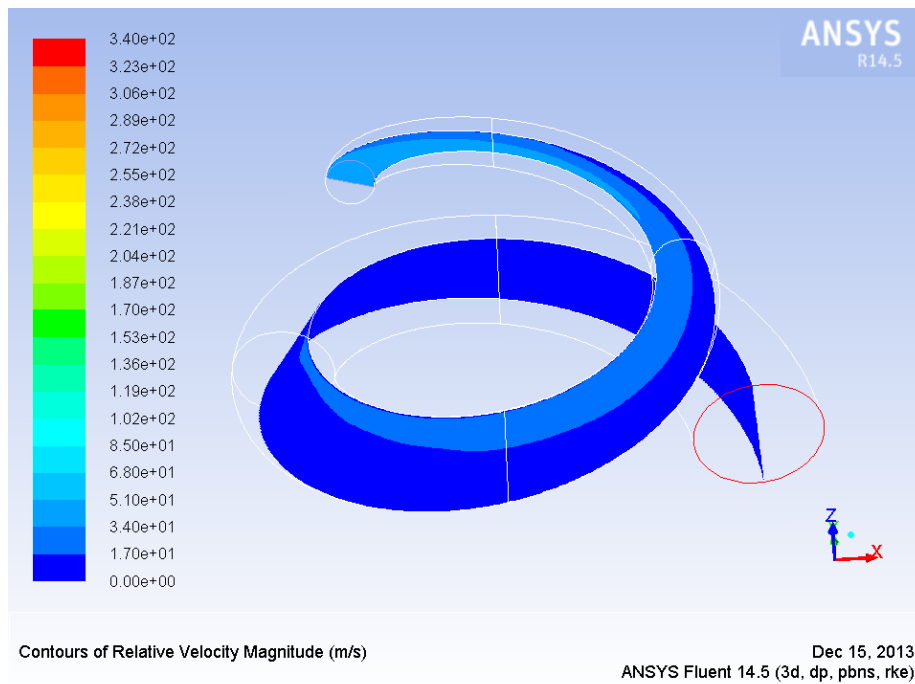
Figure 78 Concept 1, 10.000 rpm, Relative velocity
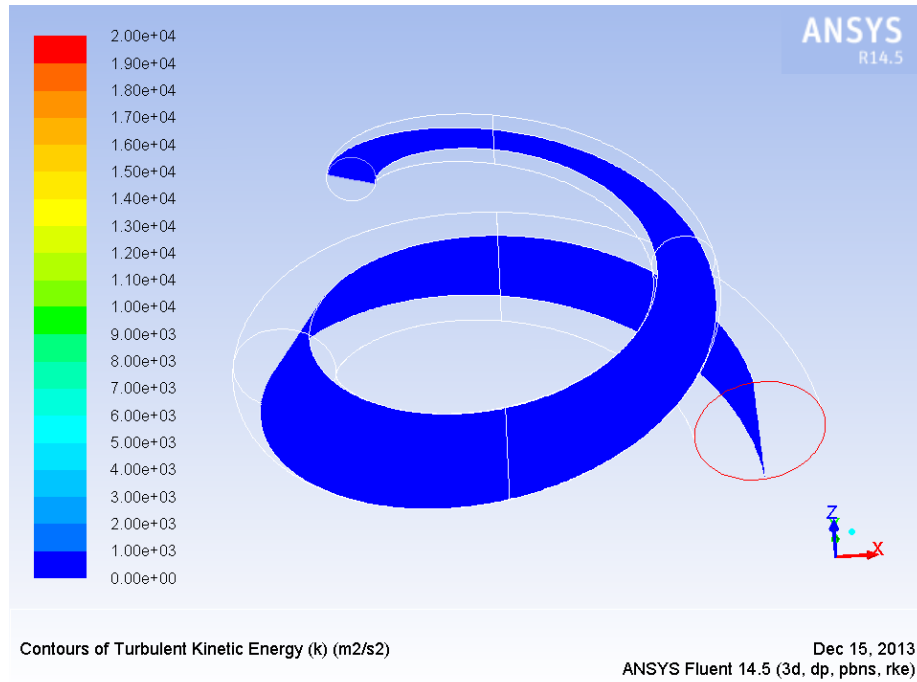
Figure 79 Concept 1, 10.000 rpm, Turbulent kinetic energy
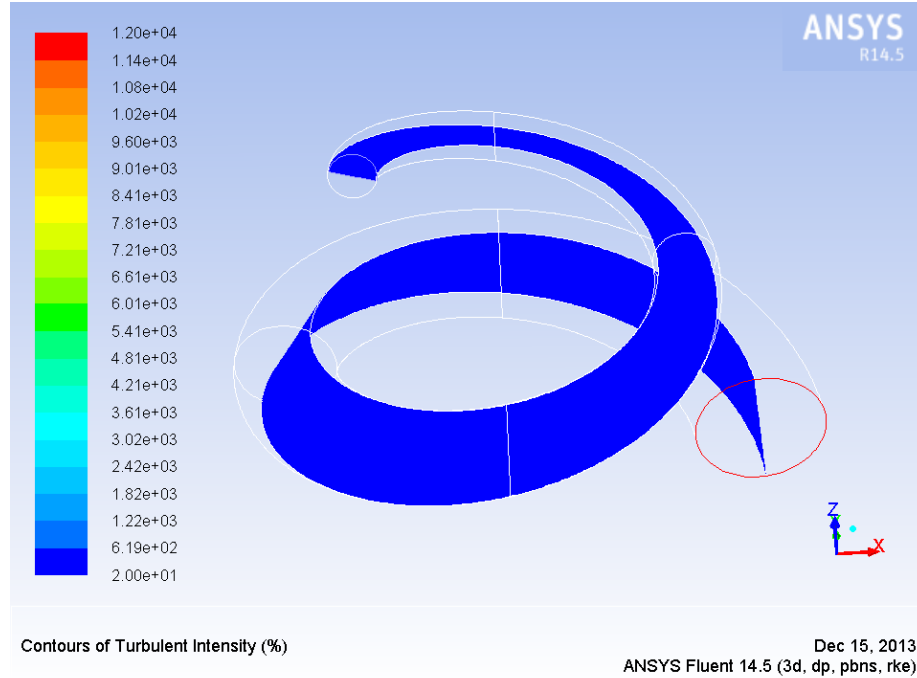
Figure 80 Concept 1, 10.000 rpm, Turbulent intensity
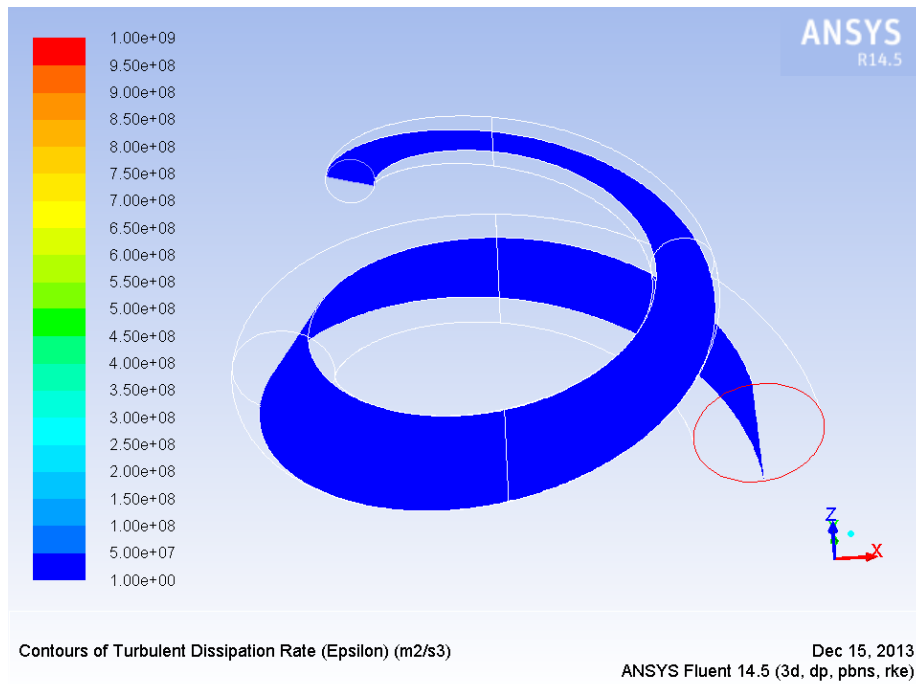
Figure 81 Concept 1, 10.000 rpm, Dissipation rate
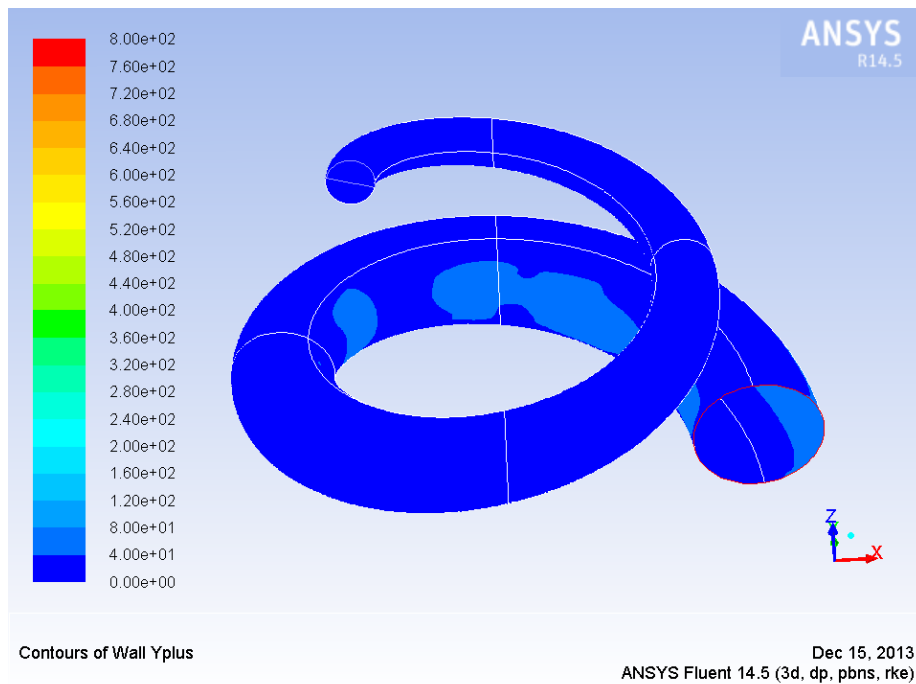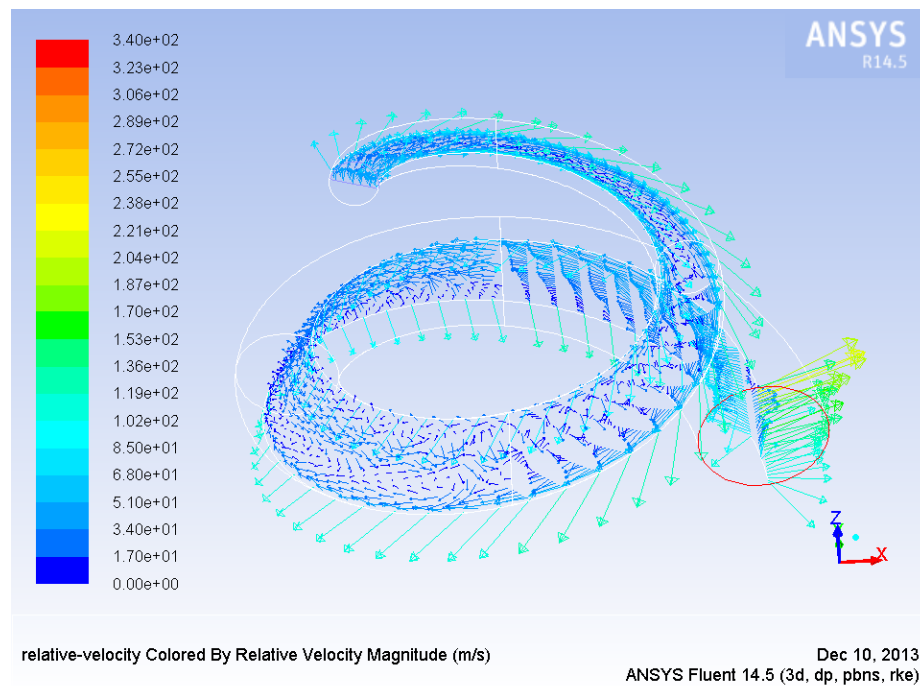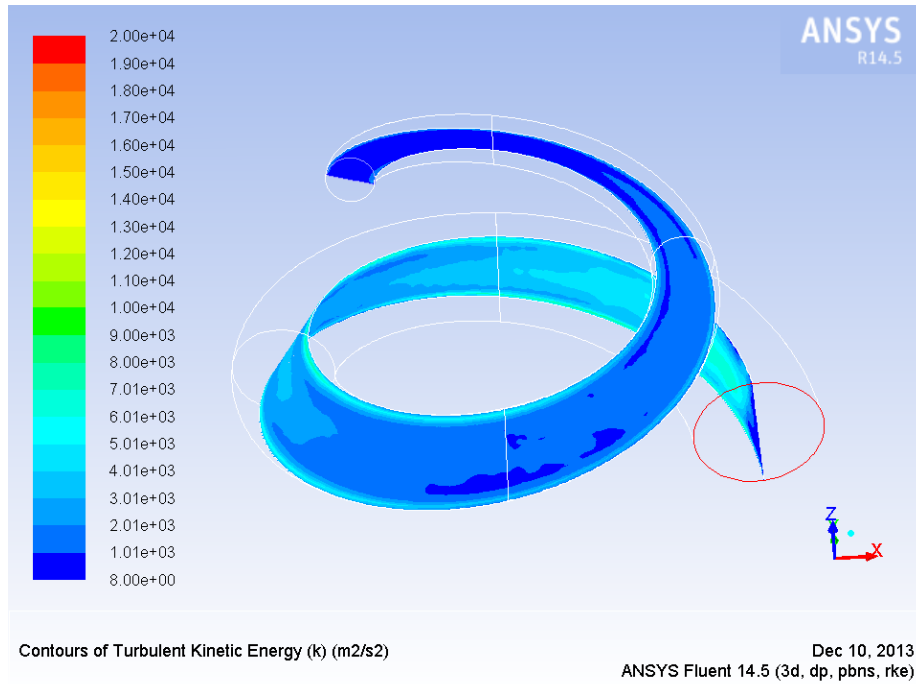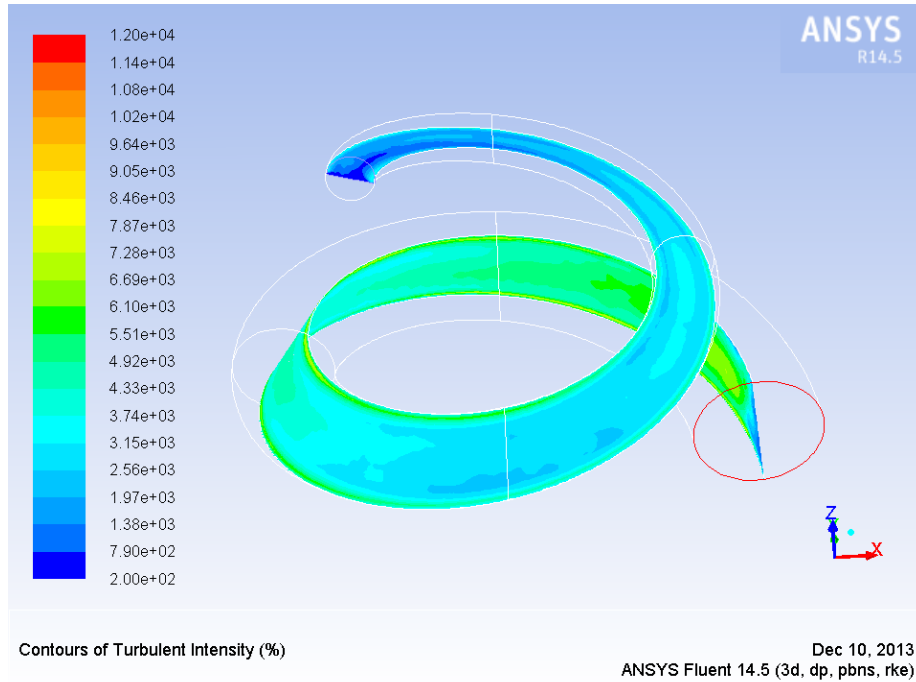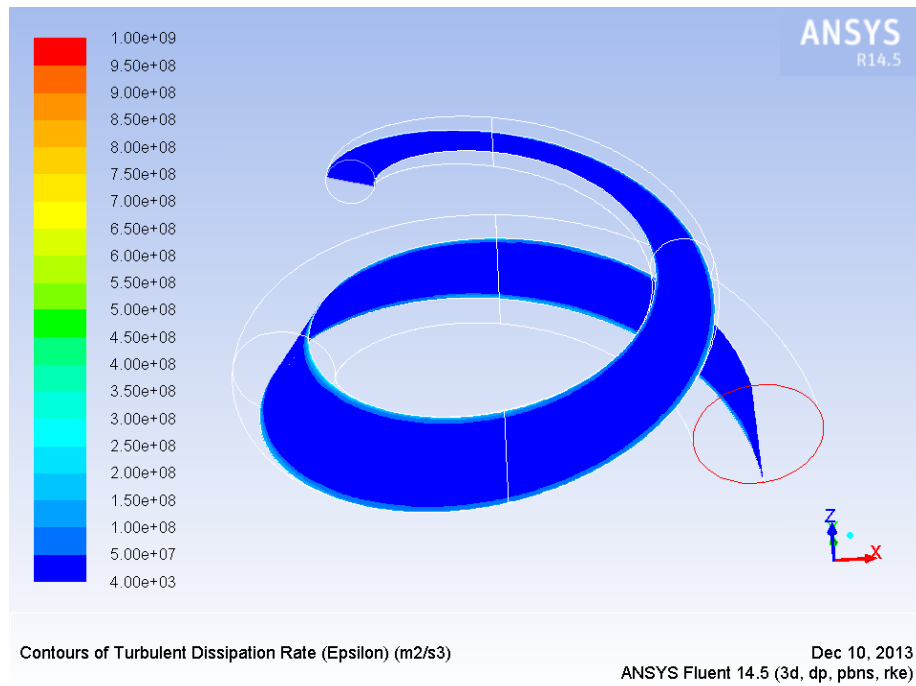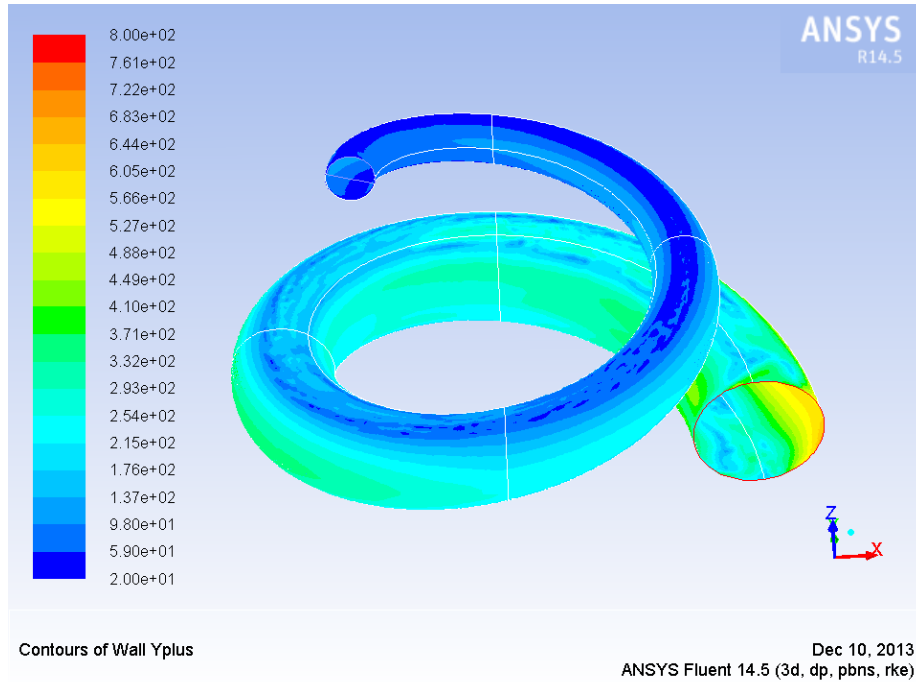

Figure 82 Concept 1, 10.000 rpm, Y+ values
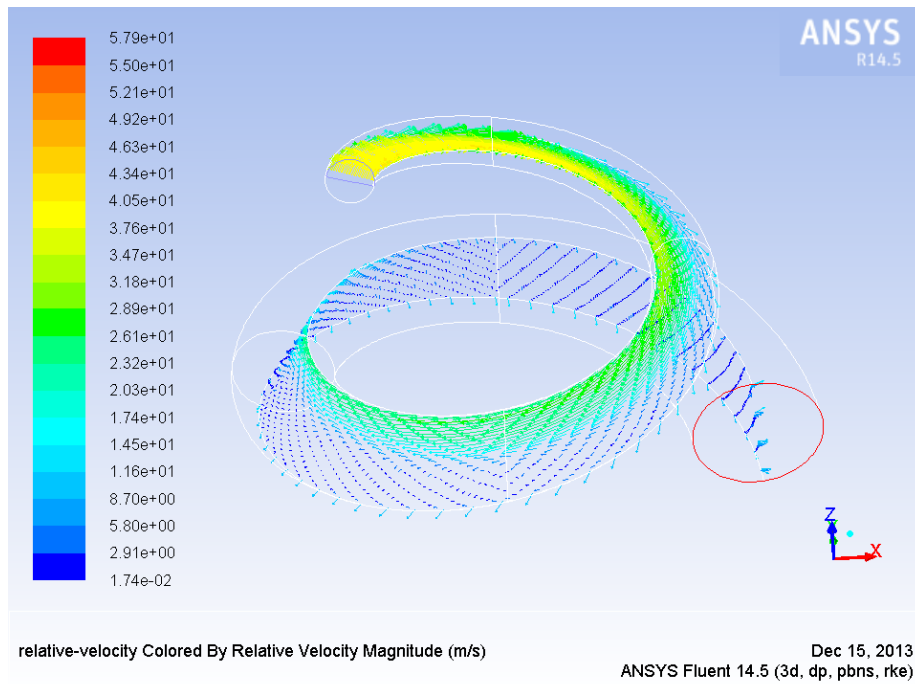
Figure 83 Concept 1, 10.000 rpm, Vectors
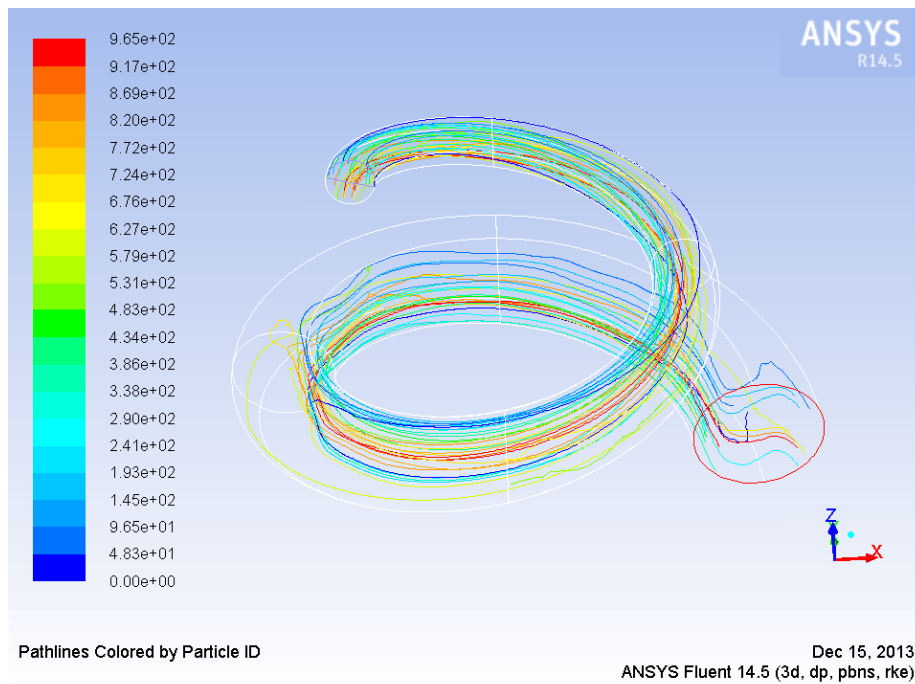
Figure 84 Concept 1, 10.000 rpm, Pathlines

CONCEPT 1 - 50.000 RPM
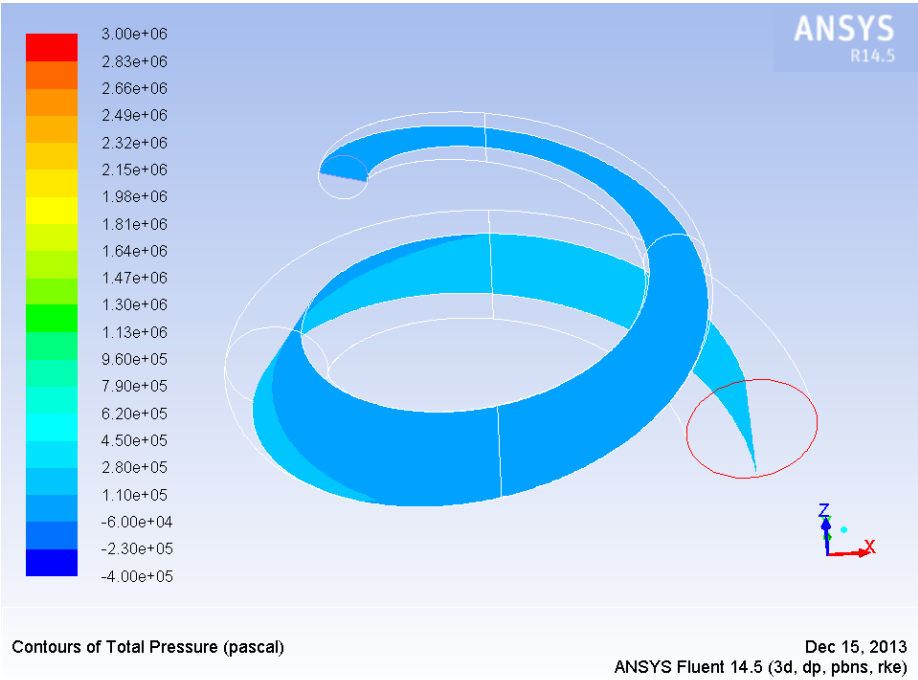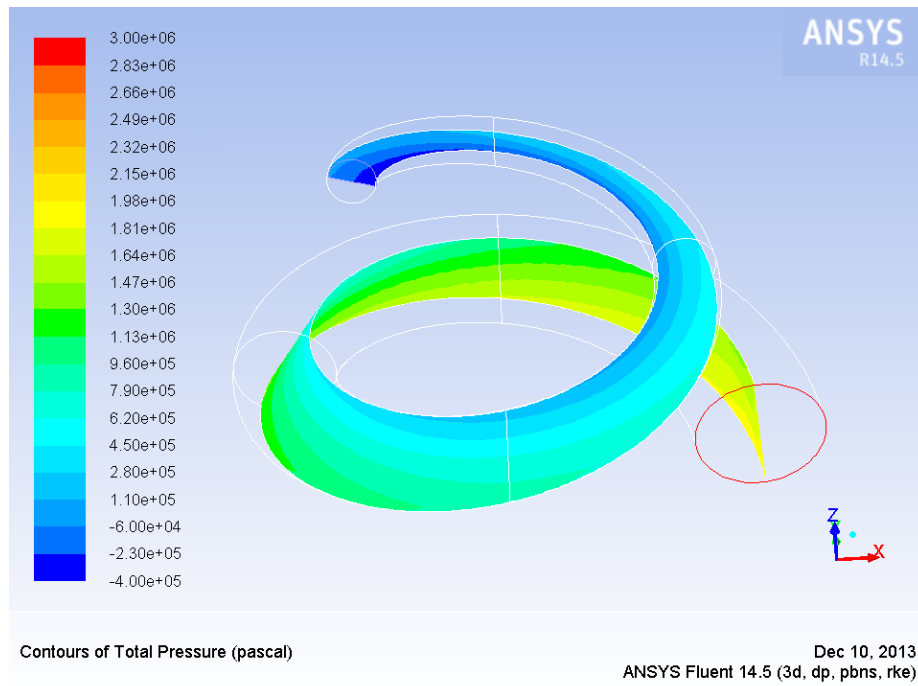

Figure 85 Concept 1, 50.000 rpm, Total pressure
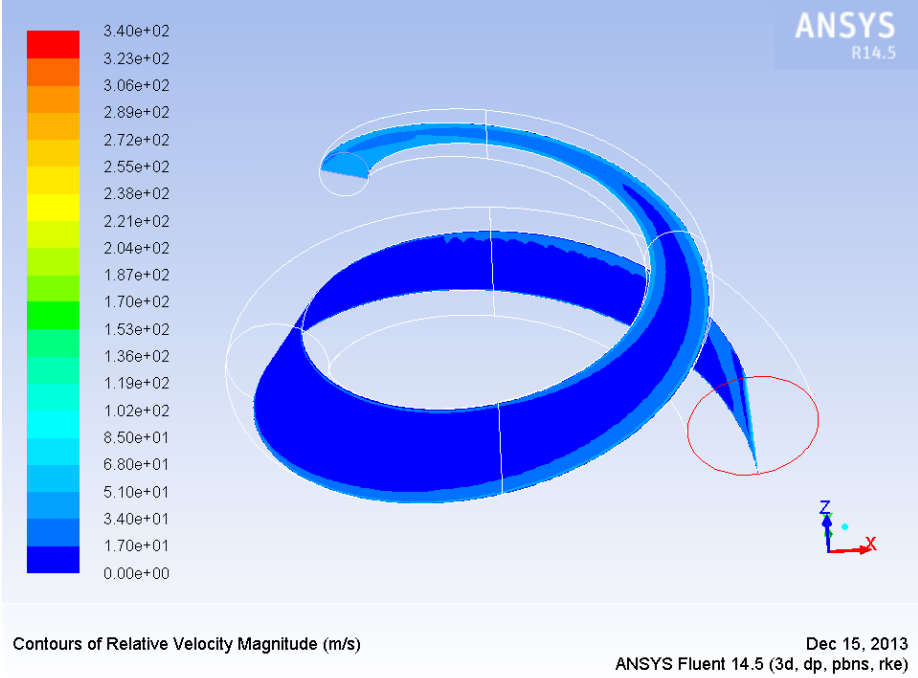
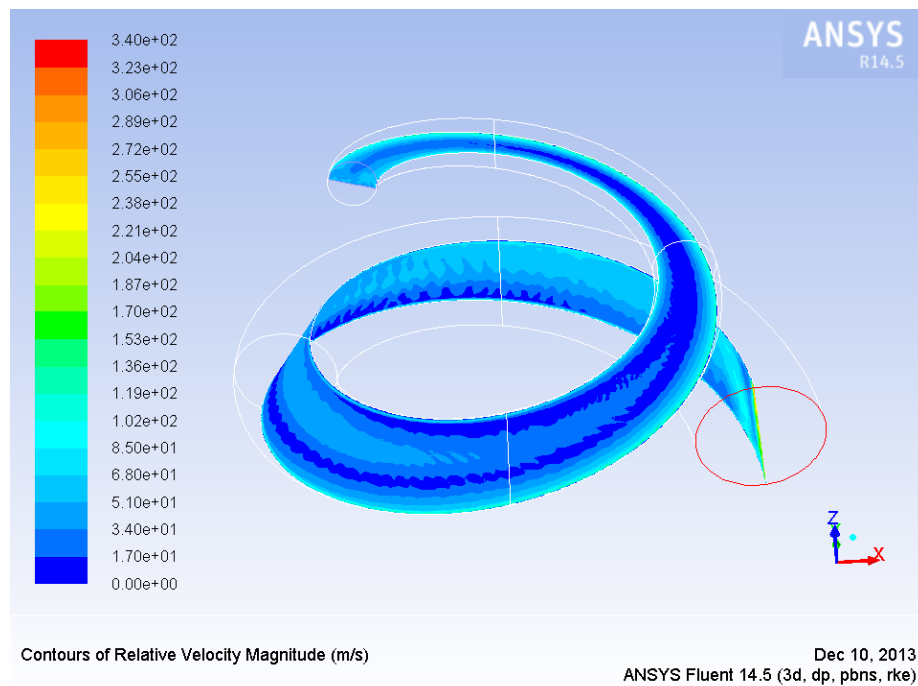Figure 86 Concept 1, 50.000 rpm, Relative velocity
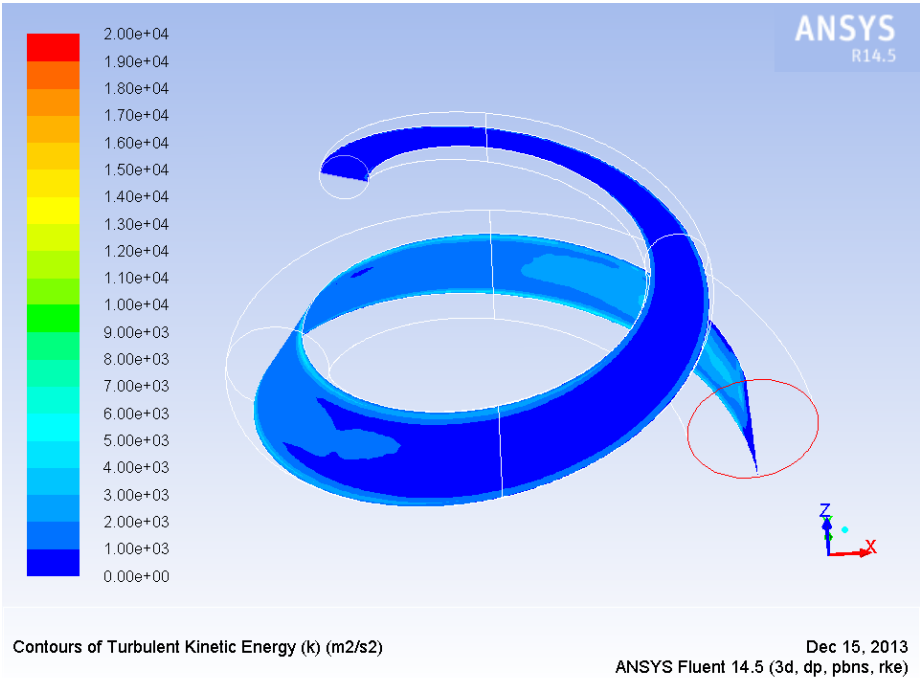
Figure 87 Concept 1, 50.000 rpm, Turbulent kinetic Energy
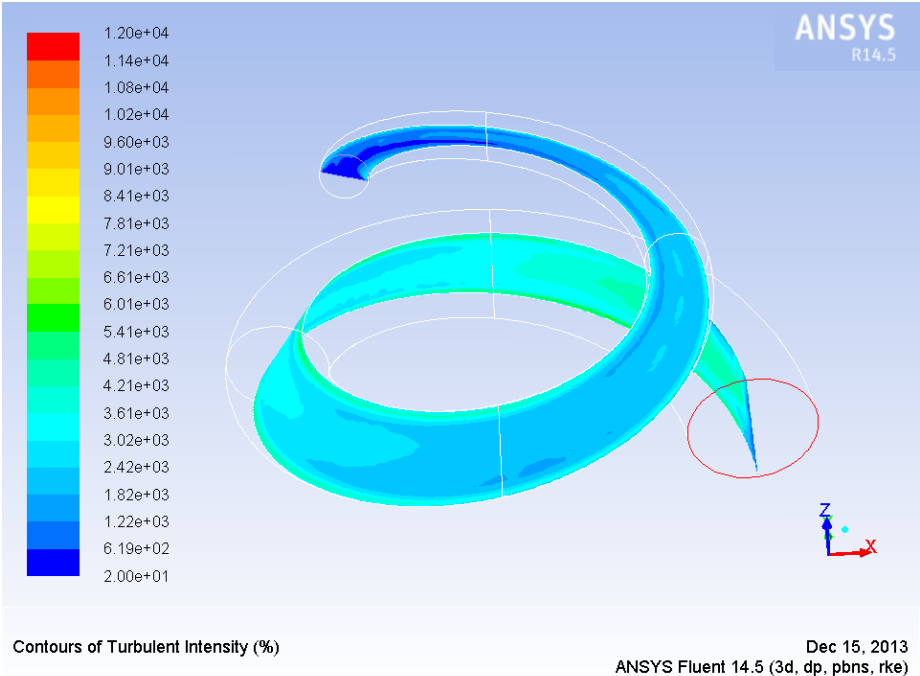
Figure 88 Concept 1, 50.000 rpm, Turbulent Intensity
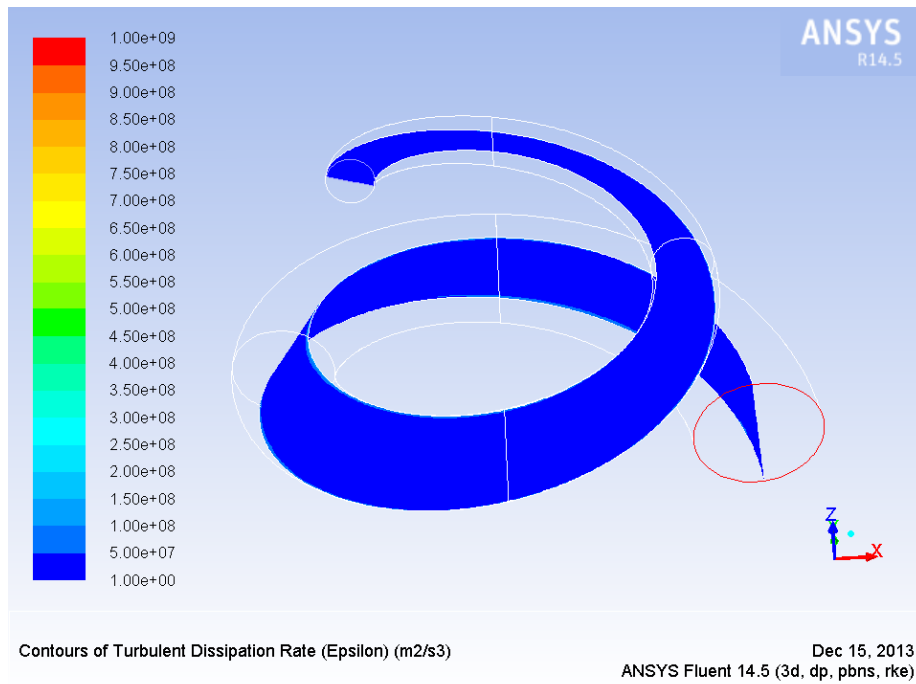
Figure 89 Concept 1, 50.000 rpm, Dissipation Rate
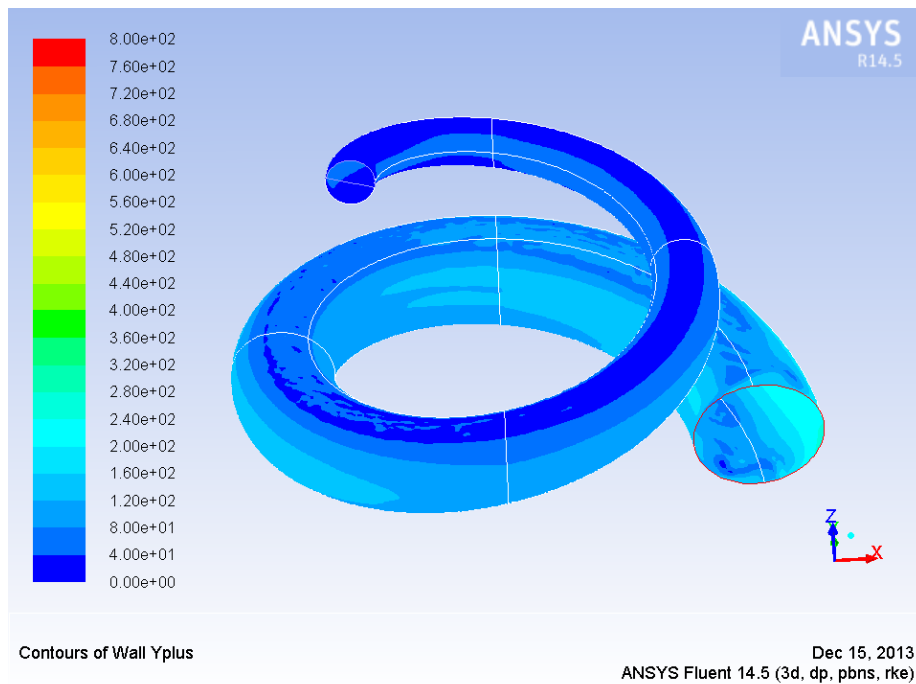
Figure 90 Concept 1, 50.000 rpm, Y+ values

CONCEPT 1 - 100.000 RPM
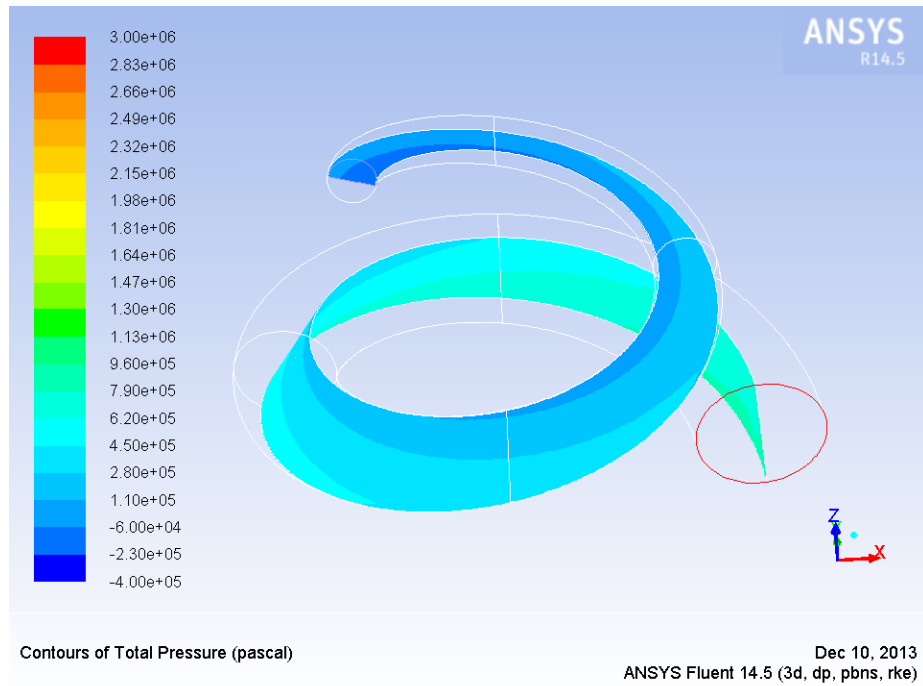
Figure 91 Concept 1, 100.000 rpm, Total Pressure
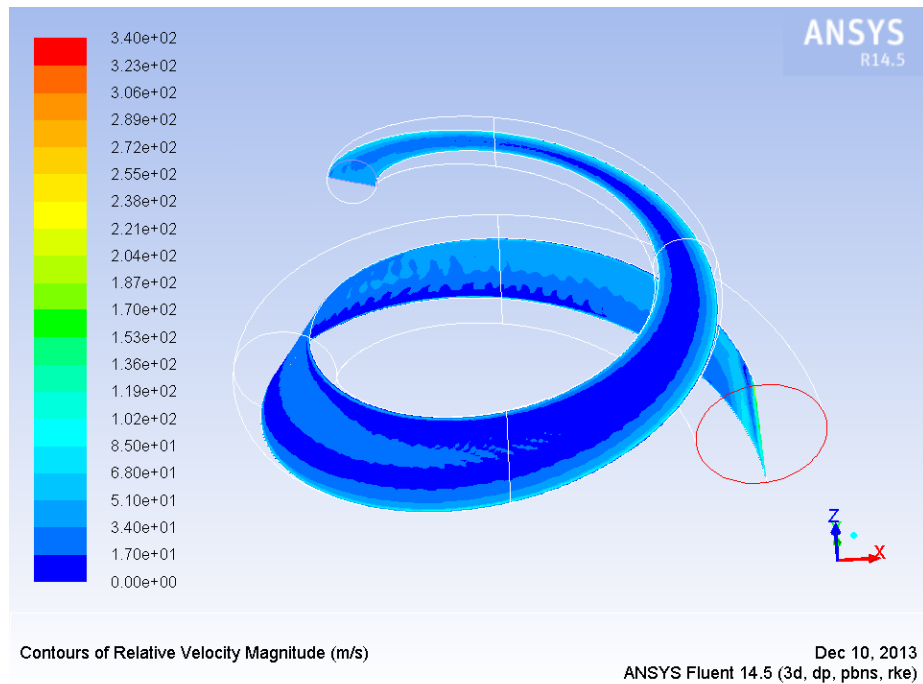
Figure 92 Concept 1, 100.000 rpm, Relative velocity
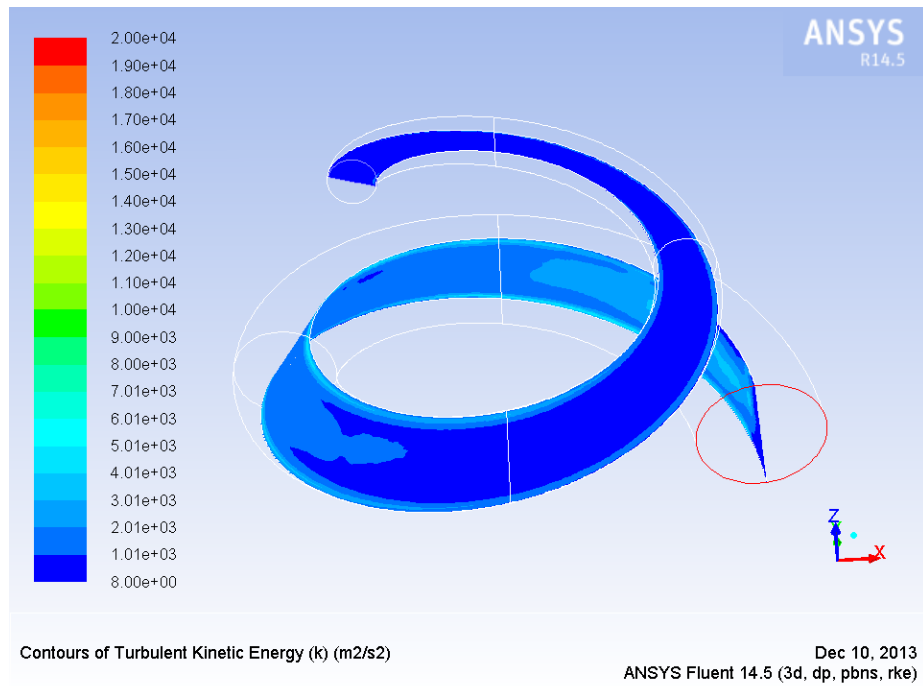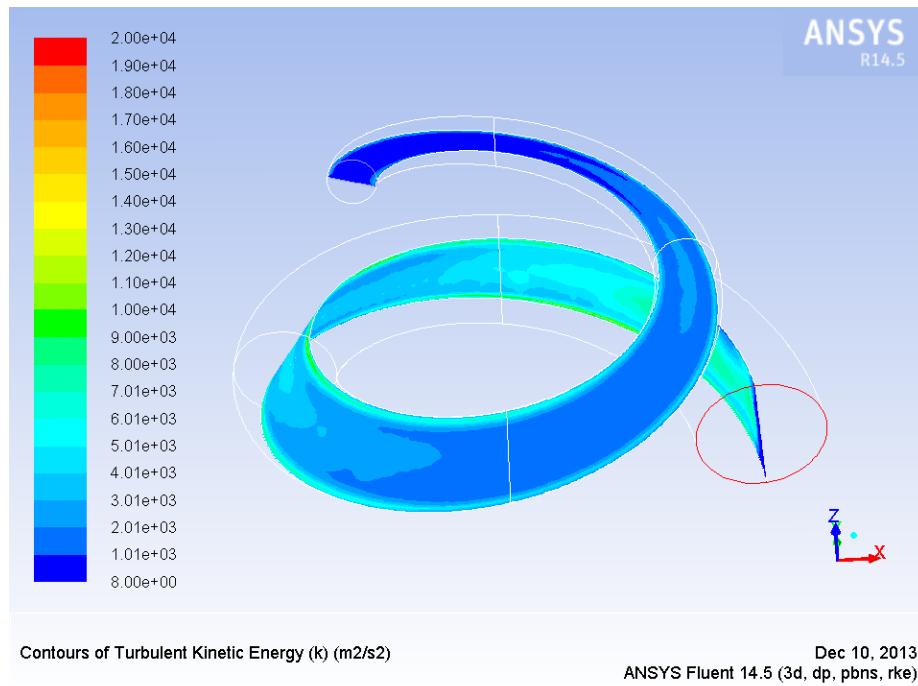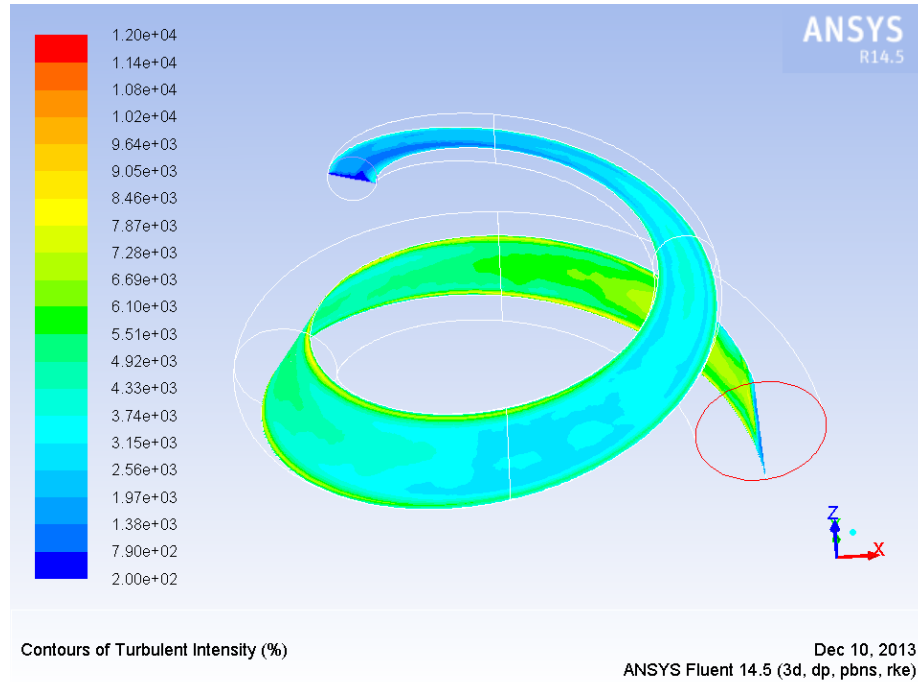
Figure 93 Concept 1, 100.000 rpm, Turbulent kinetic energy
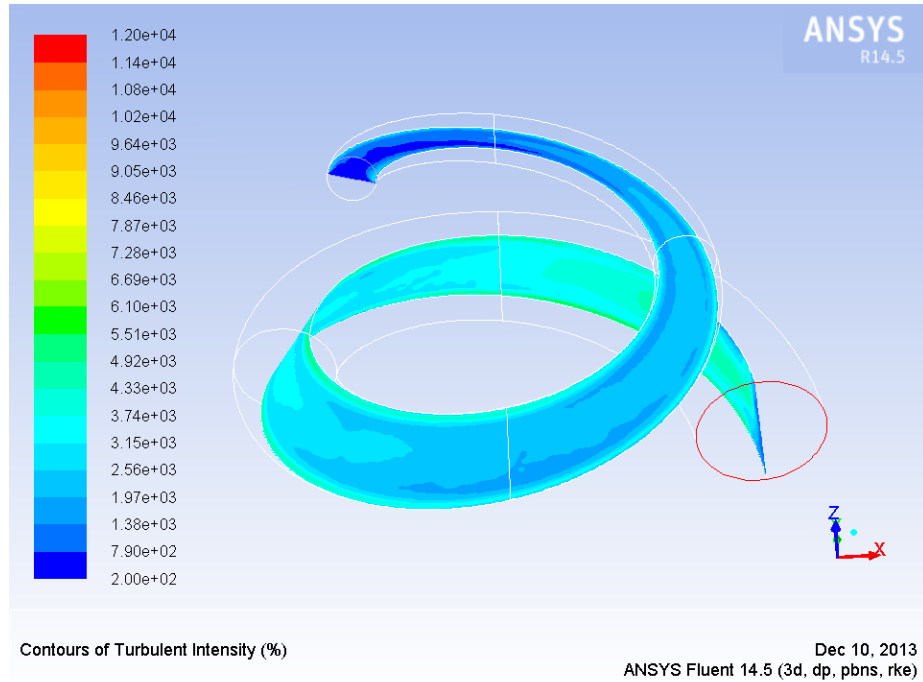

Figure 94 Concept 1, 100.000 rpm, Turbulent intensity
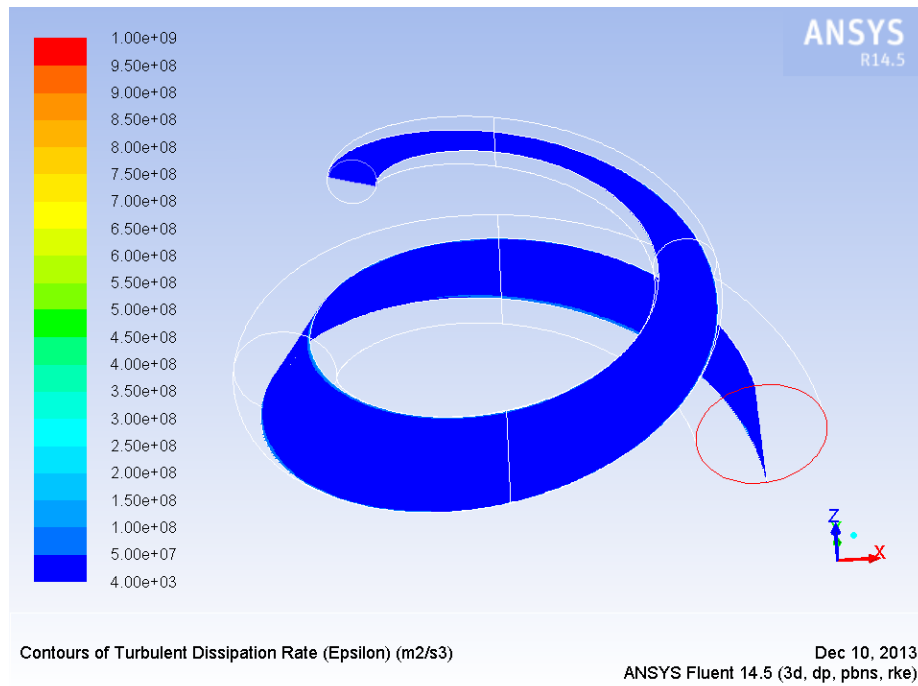
Figure 95 Concept 1, 100.000 rpm, Dissipation rate
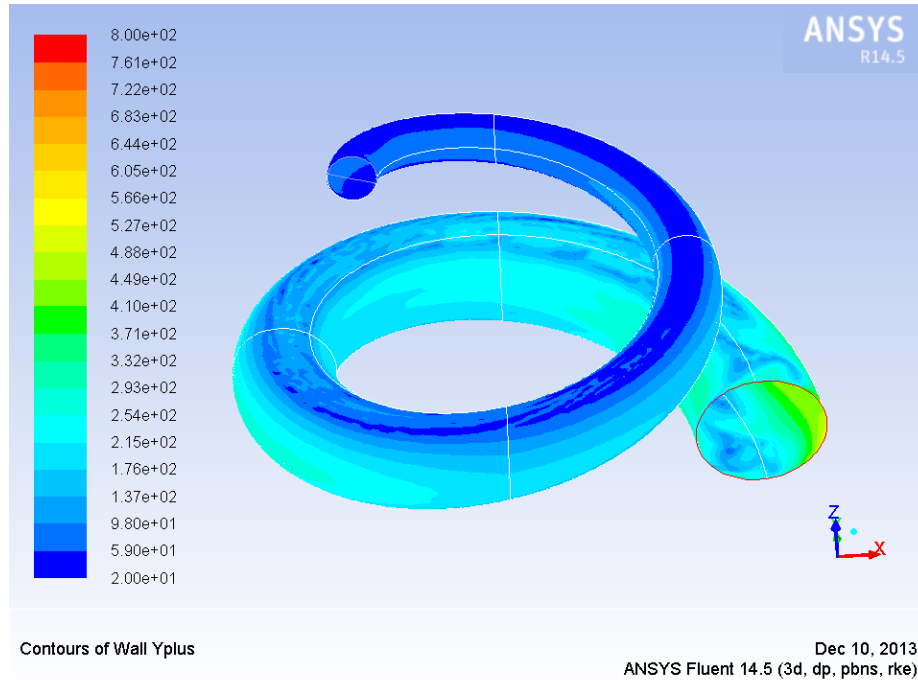
Figure 96 Concept 1, 100.000 rpm, Y+ values

Figure 97 Concept 1, 100.000 rpm, Relative velocity vectors

The vector plot of the relative velocity shows very good the suction effect at the last part of the spiral. Therefore this last element of the spiral was ignored by the evaluation of the pressure ratios before. This was done also for all other cases.

CONCEPT 1 - 130.000 RPM
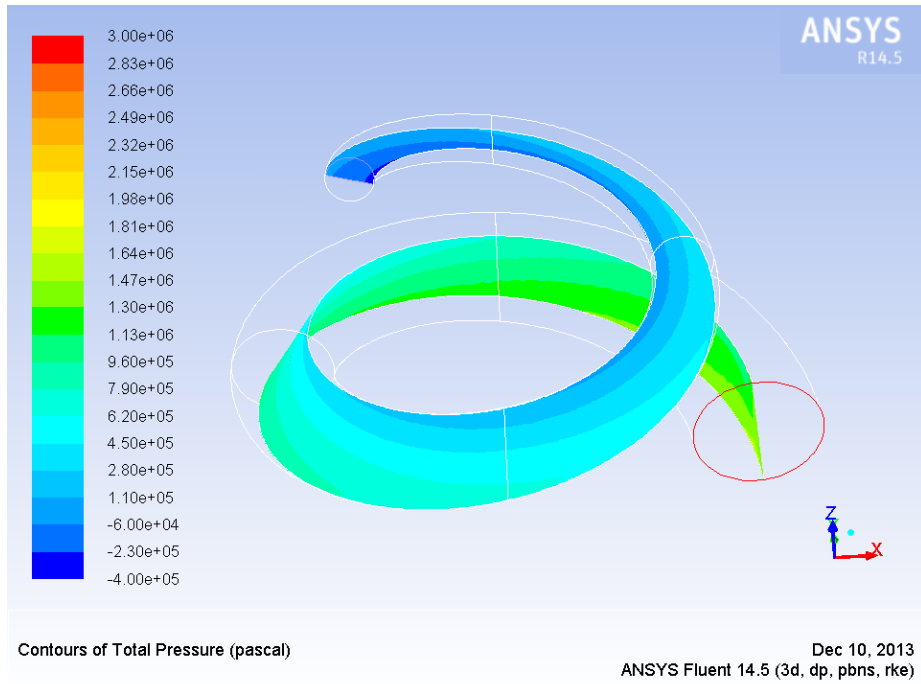
Figure 98 Concept 1, 130.000 rpm, Total Pressure
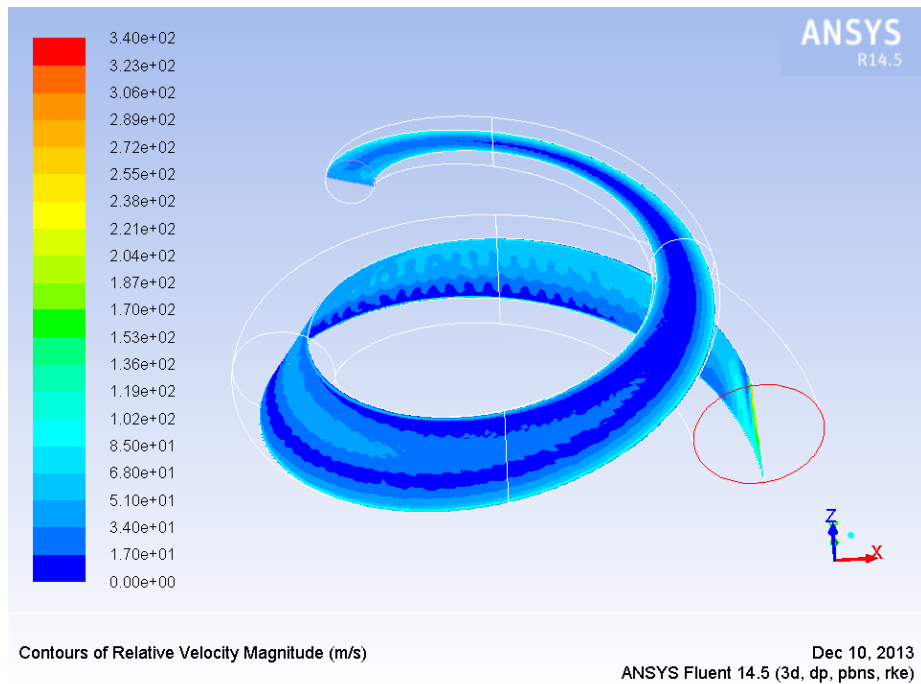
Figure 99 Concept 1, 130.000 rpm, Relative velocity

Figure 100 Concept 1, 130.000 rpm, Turbulent kinetic energy

Figure 101 Concept 1, 130.000 rpm, Turbulent intensity

Figure 102 Concept 1, 130.000 rpm, Dissipation rate

Figure 103 Concept 1, 130.000 rpm, Y+ values
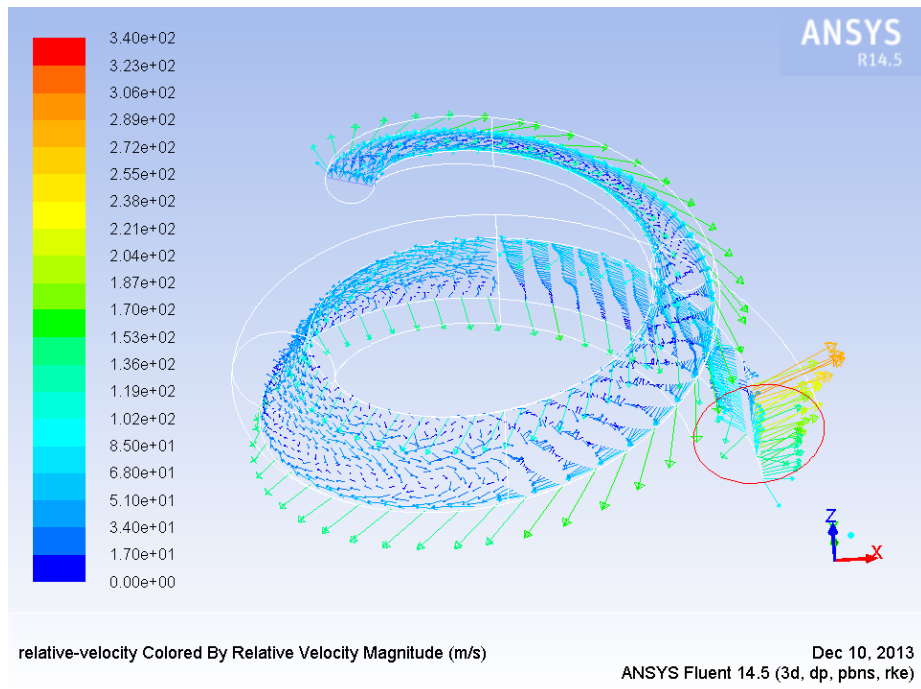
Figure 104 Concept 1, 130.000 rpm, Relative velocity vectors

CONCEPT 1 - 150.000 RPM

Figure 105 Concept 1, 150.000 rpm, Total pressure

Figure 106 Concept 1, 150.000 rpm, Relative velocity

Figure 107 Concept 1, 150.000 rpm, Turbulent kinetic energy

Figure 108 Concept 1, 150.000 rpm, Turbulent intensity
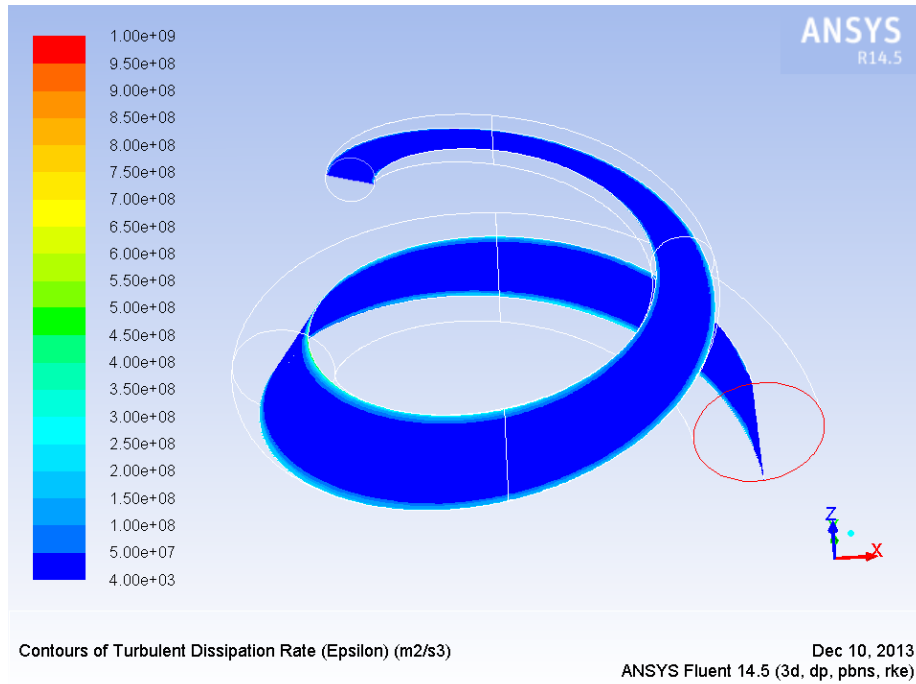
Figure 109 Concept 1, 150.000 rpm, Dissipation rate
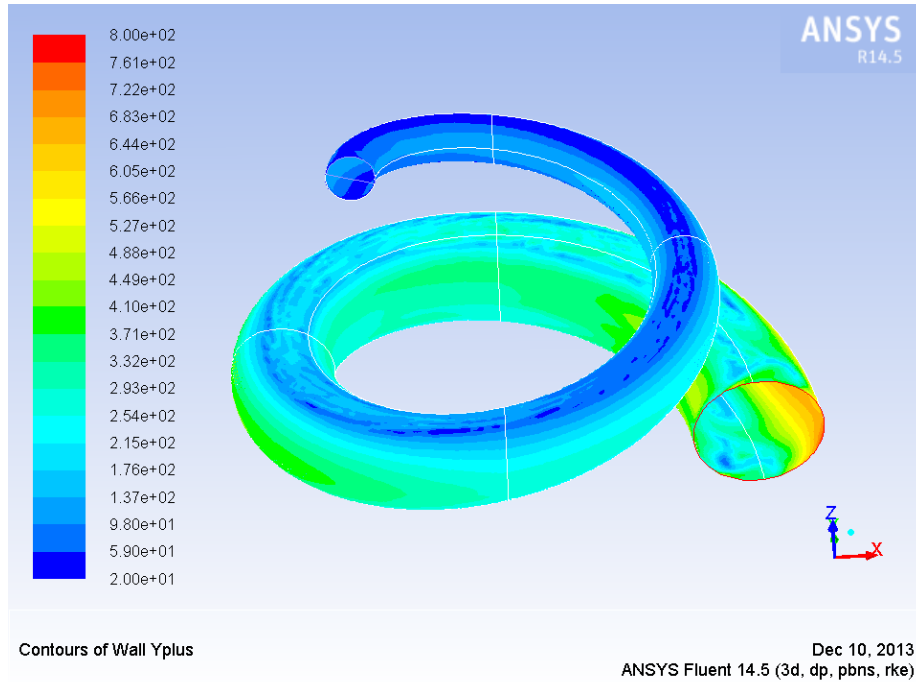
Figure 110 Concept 1, 150.000 rpm, Y+ values
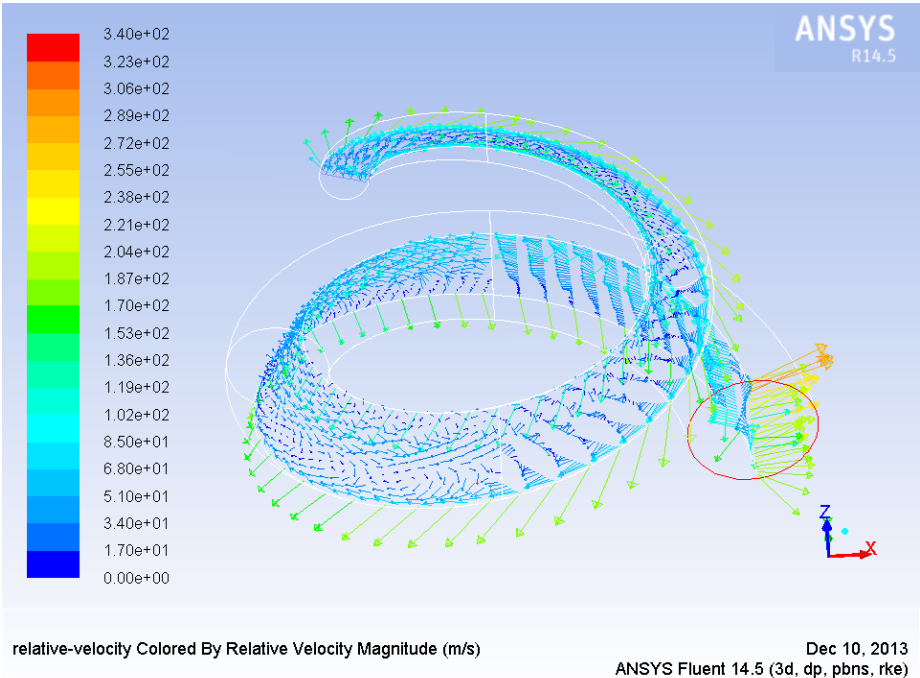
Figure 111 Concept 1, 150.000 rpm, Relative velocity vectors

6.5.2 GT4088

Because the results have shown that the spiral compressor defeats the GT1544 at lower rpm's, a second reference was used for further investigations. It's a turbocharger used in the motorsport with higher flow rates at lower revolustions per minute, the GT4088.

Figure 112 GT4088 from Garrett[85]

The specifications of the GT4088 are:

Compressor Wheel
Inducer Diameter	64,7 mm
Exducer Diameter	88,0 mm
Trim	54
A/R	0,72

Turbine Wheel
Diameter	77,6 mm
Trim	83
A/R	1,34

---

[85] Garrett - TurbochargerGuide Volume 5, p. 58
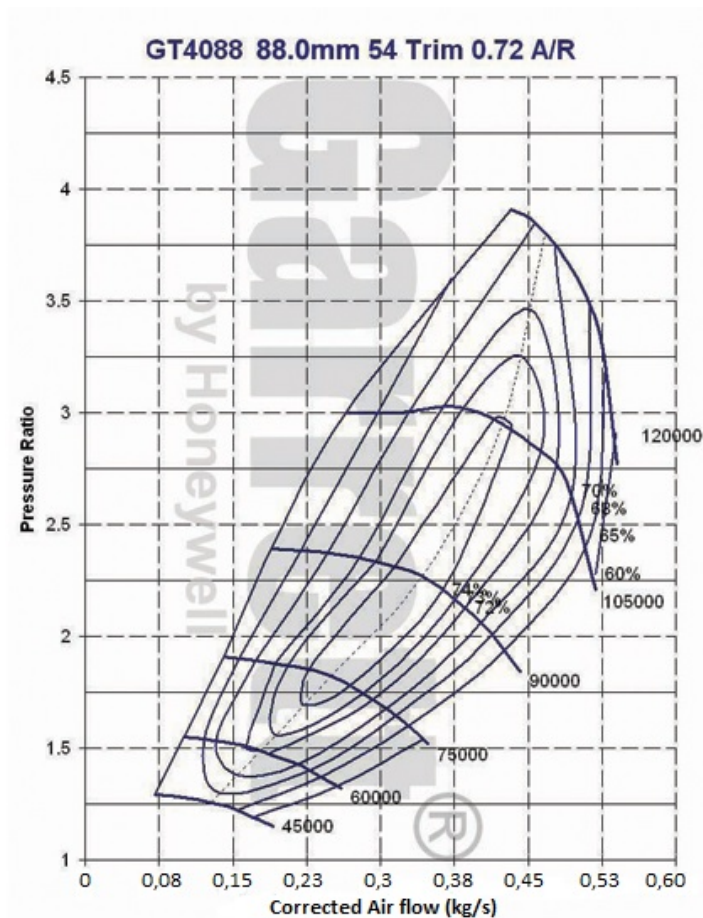
Figure 113 Compressor map from GT4088[86]

Four points in the compressor map were elected for comparing the spiral concept with the GT4088. The points are:

rpm	Air flow [kg/s]	Pressure ratio
45.000	0,14	1,25
60.000	0,18	1,5
90.000	0,34	2,75
120.000	0,47	3,75

Table 11 The reference points from the GT4088

[86] Garrett - TurbochargerGuide Volume 5, p. 58

The simulations with the new reference points (higher flow rates at lower rpm's) resulted to following values:

rpm	Air flow [kg/s]	pressure ratio		
		GT4088	one spiral	concept 1
45.000	0,14	1,25	3,11	3,35
60.000	0,18	1,5	2,00	2,14
90.000	0,34	2,75	0,51	1,33
120.000	0,47	3,75		

Table 12 Comparing to the GT4088

As it can be seen in the table, the concept is able to defeat the turbocharger again at lower rotational speeds. Therefore two more rpm cases were evaluated (10.000 and 20.000). The results illustrated in the pressure ratio versus rpm diagram:
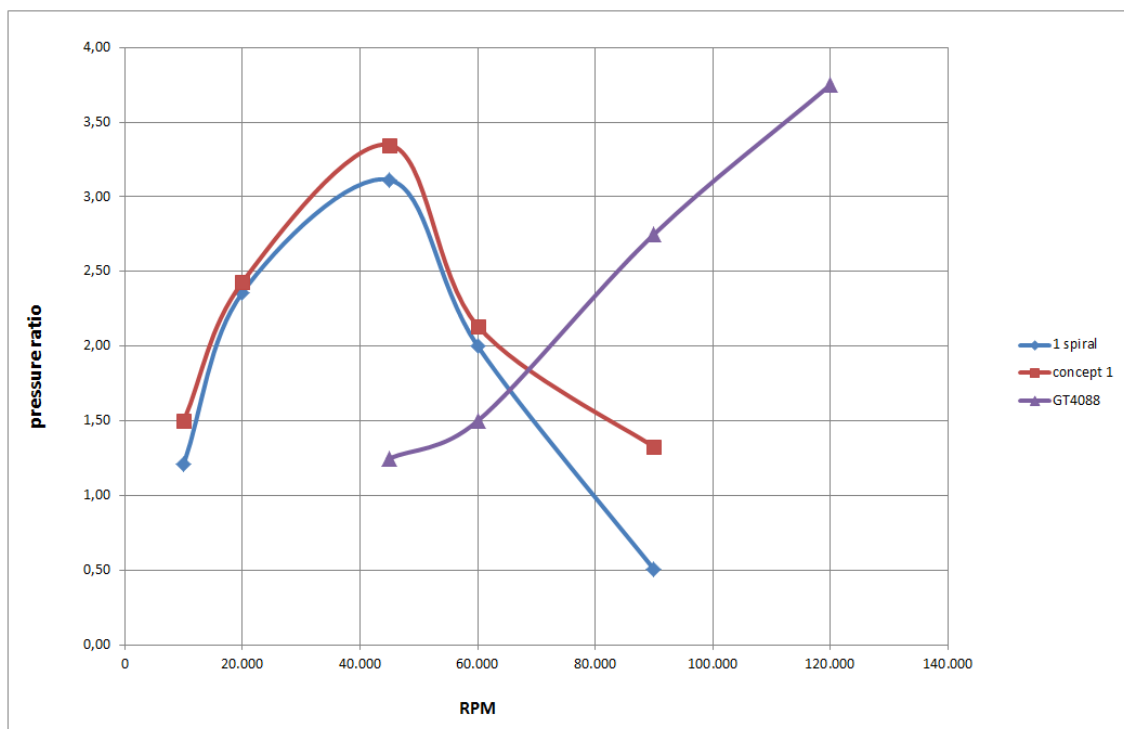
Figure 114 pressure ratios versus rpm compared to GT4088

As it can be seen, the result is the same as before by comparing it with the GT1544. At low speed the spiral concept is able to defeat the GT4088. The pressure ratio at 90.000 rpm's from the spiral compressor concept is much lower than the pressure ratio which achieves the GT4088.

The result of the simulations shows that the first considerations towards to turbochargers are proved to be false. The spiral concept should be investigated in the area of a mechanical charger, compressors/superchargers which are rotating only in the range up to 10.000 rpm's and should be compared with such a type, for example the G-Lader.
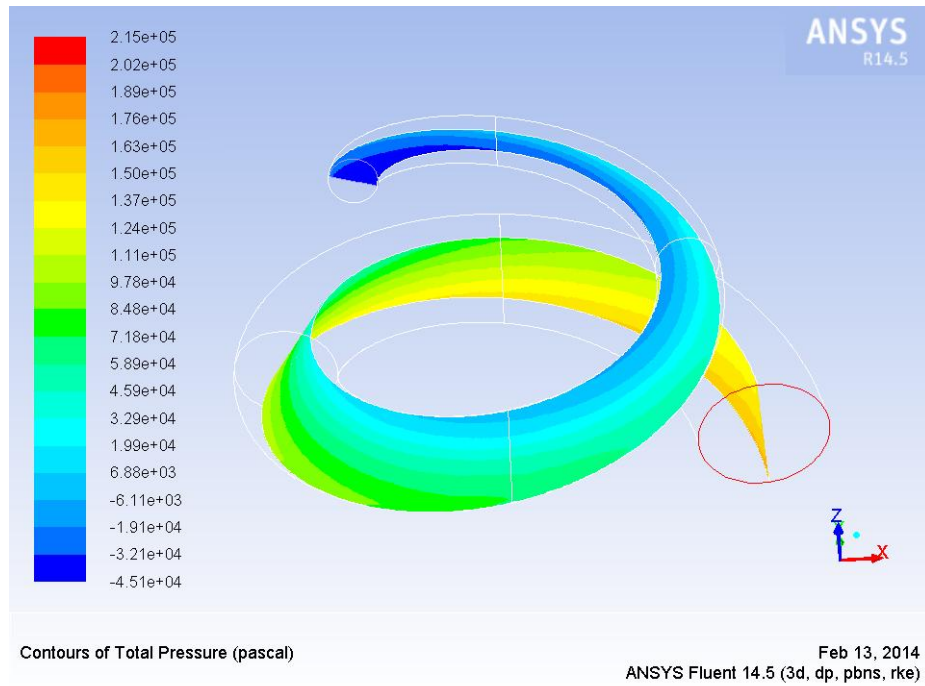
CONCEPT 1 - 45.000 RPM

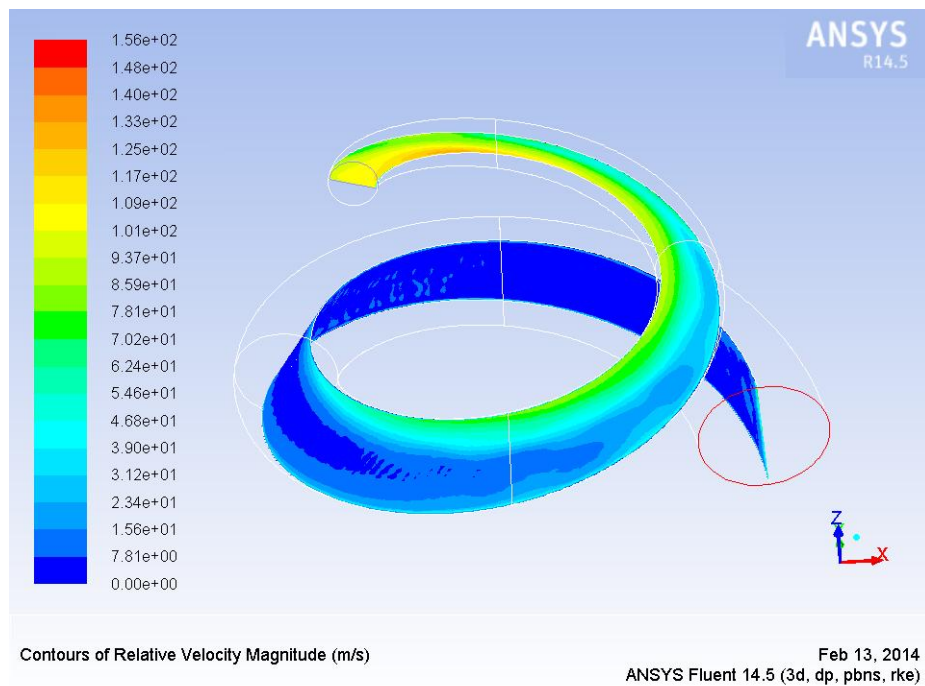Figure 115 Concept 1, 45.000 rpm, Total pressure

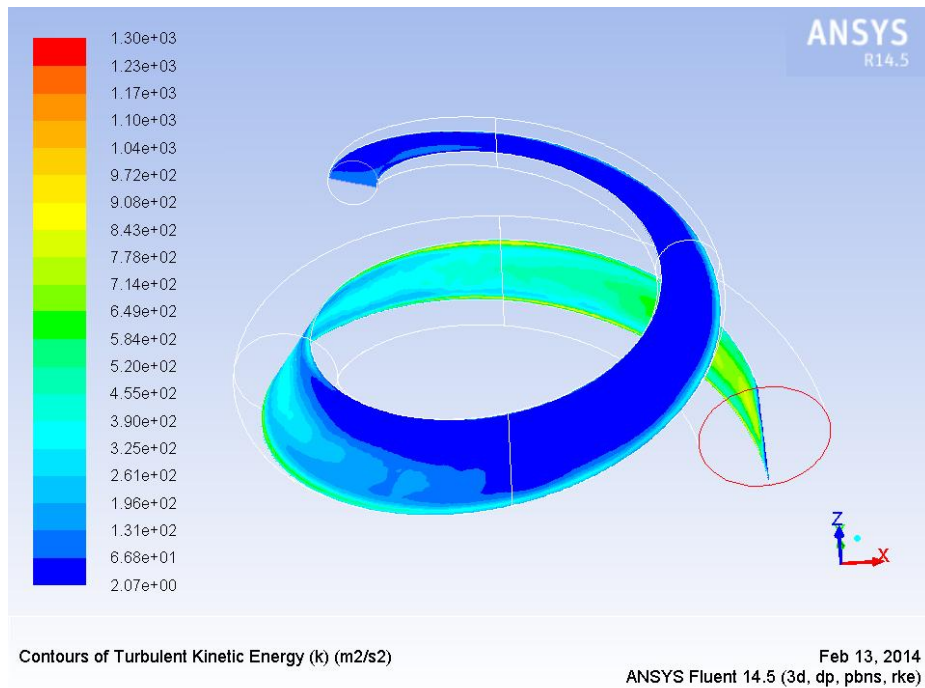Figure 116 Concept 1, 45.000 rpm, Relative velocity

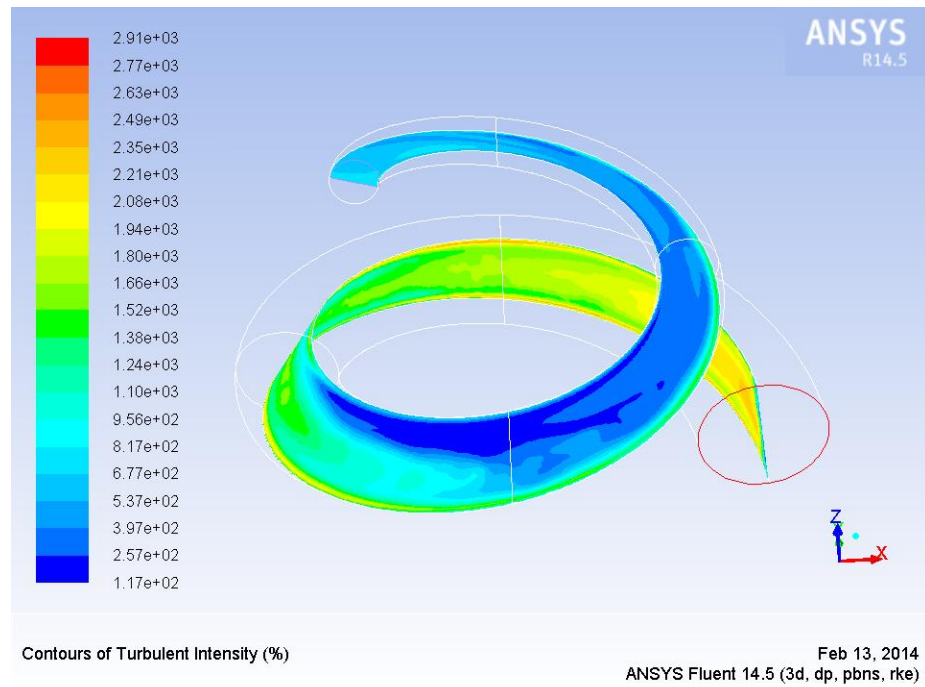Figure 117 Concept 1, 45.000 rpm, Turbulent kinetic energy

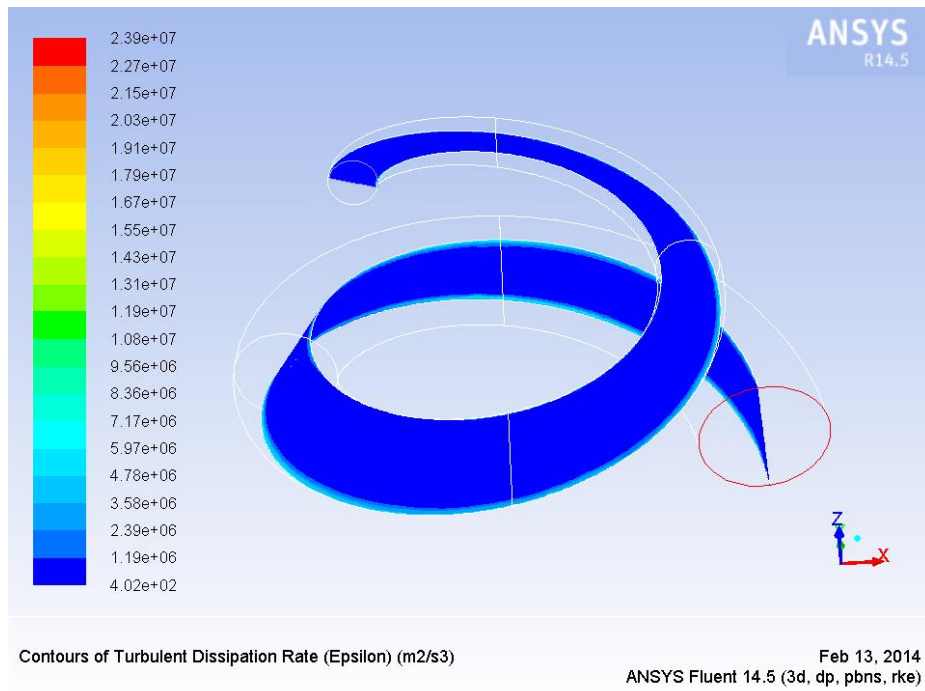Figure 118 Concept 1, 45.000 rpm, Turbulent intensity
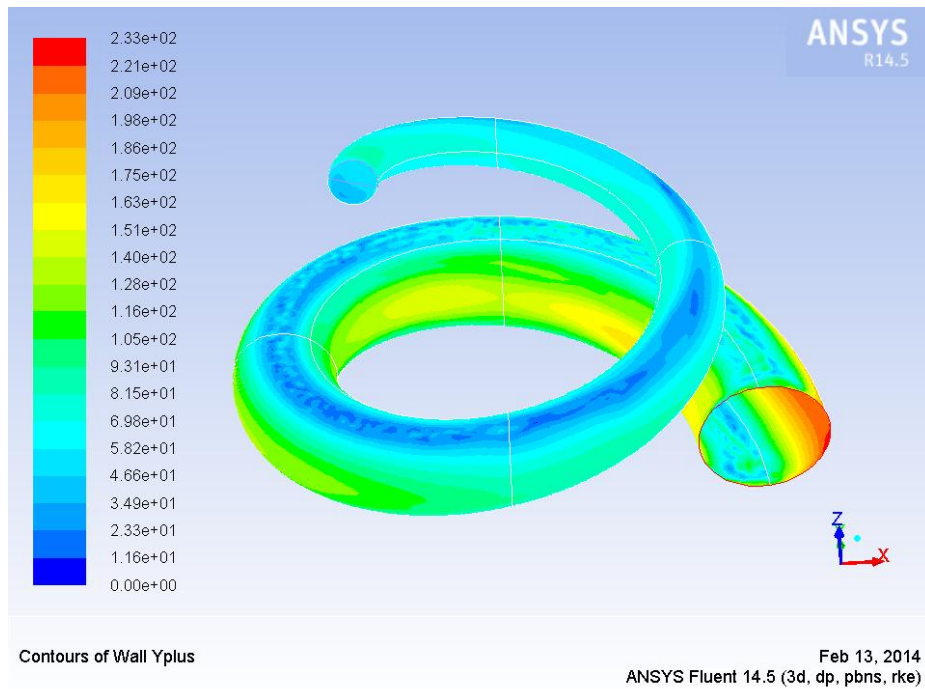
Figure 119 Concept 1, 45.000 rpm, Dissipation rate

Figure 120 Concept 1, 45.000 rpm, Y+ values
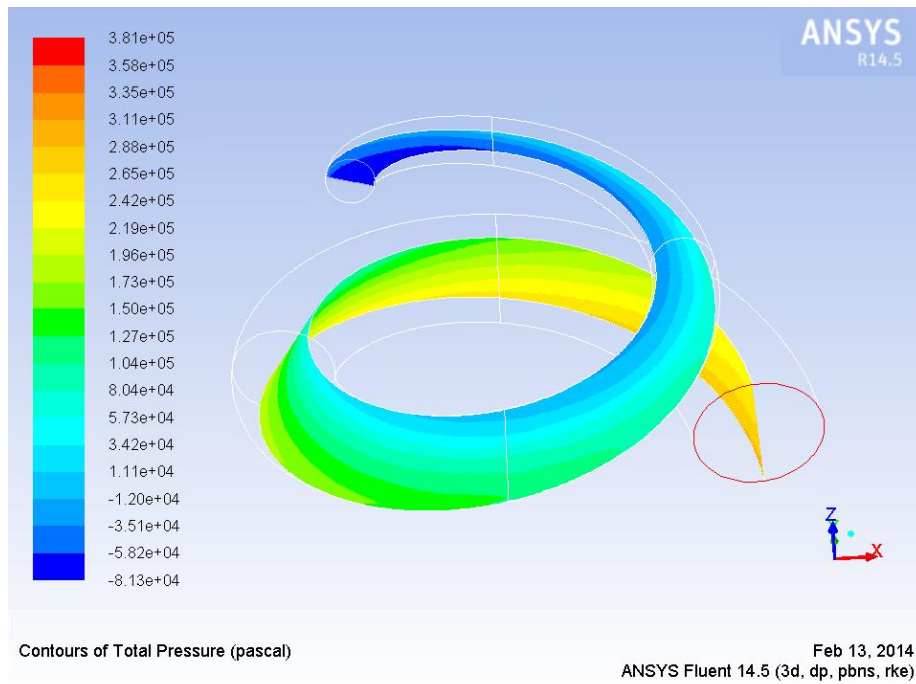
CONCEPT 1 - 60.000 RPM

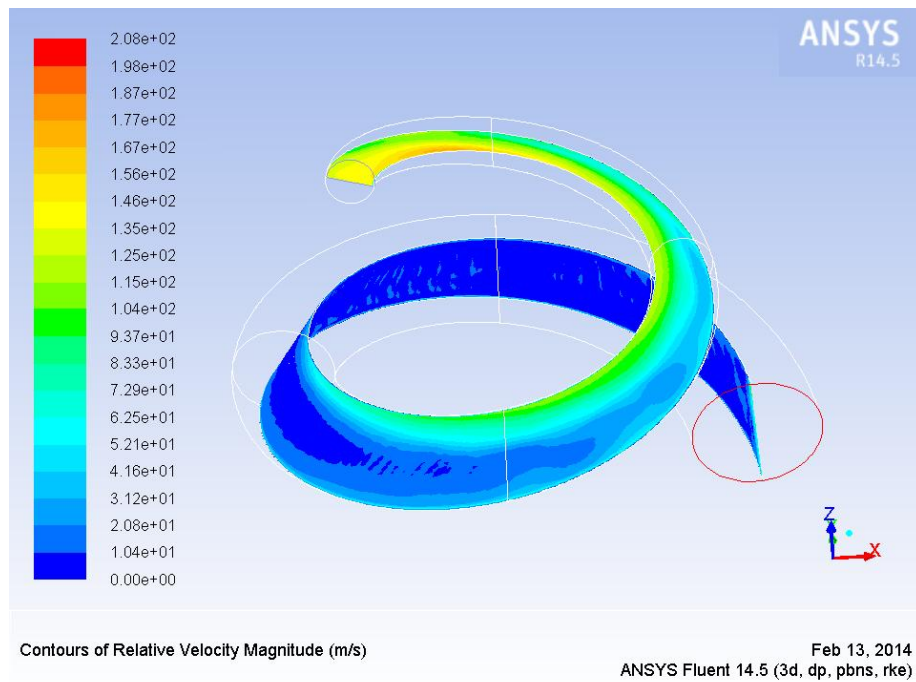Figure 121 Concept 1, 60.000 rpm, Total pressure

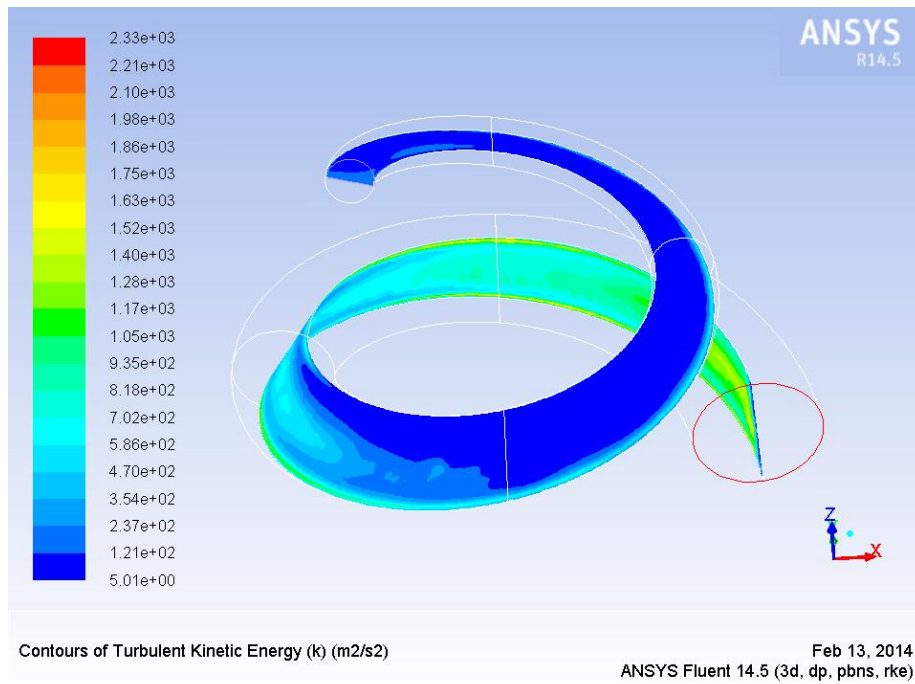Figure 122 Concept 1, 60.000 rpm, Relative velocity

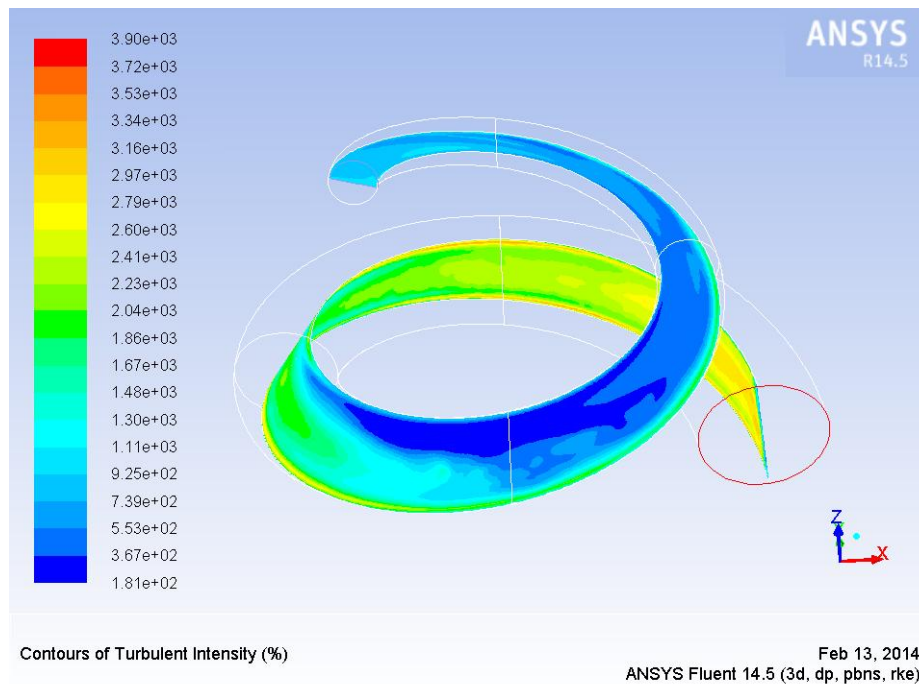Figure 123 Concept 1, 60.000 rpm, Turbulent kinetic energy

Figure 124 Concept 1, 60.000 rpm, Turbulent intensity

Figure 125 Concept 1, 60.000 rpm, Dissipation rate

Figure 126 Concept 1, 60.000 rpm, Y+ values

CONCEPT 1 - 90.000 RPM

Figure 127 Concept 1, 90.000 rpm, Total pressure

Figure 128 Concept 1, 90.000 rpm, Relative velocity

Figure 129 Concept 1, 90.000 rpm, Turbulent kinetic energy
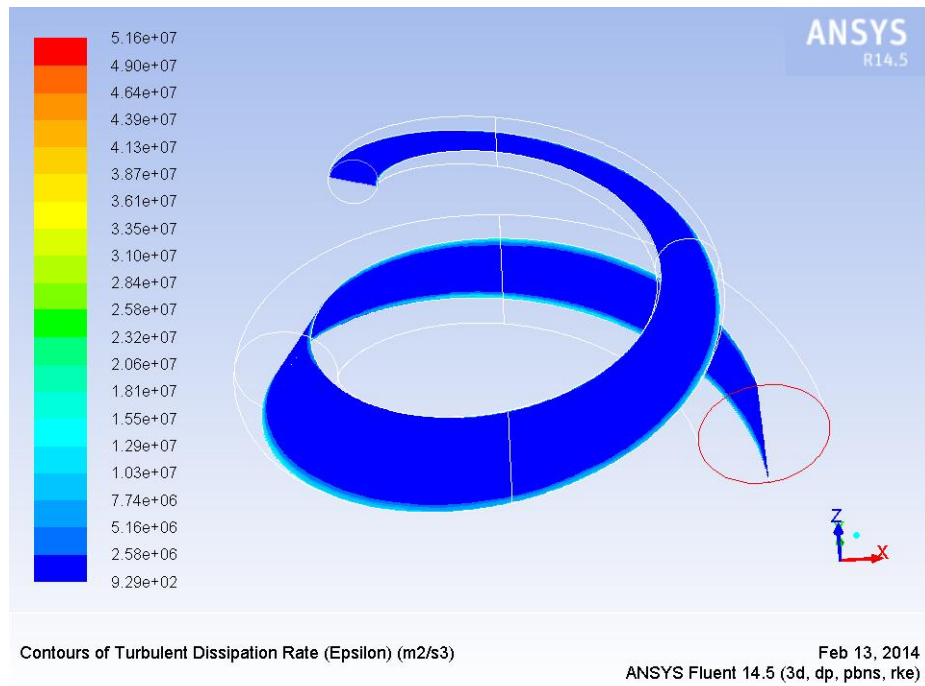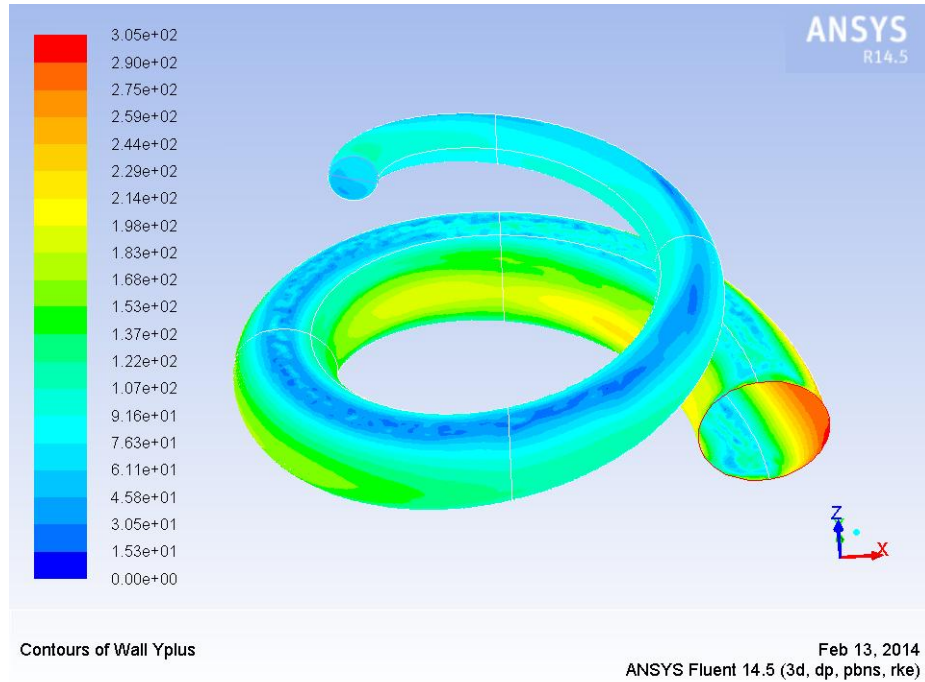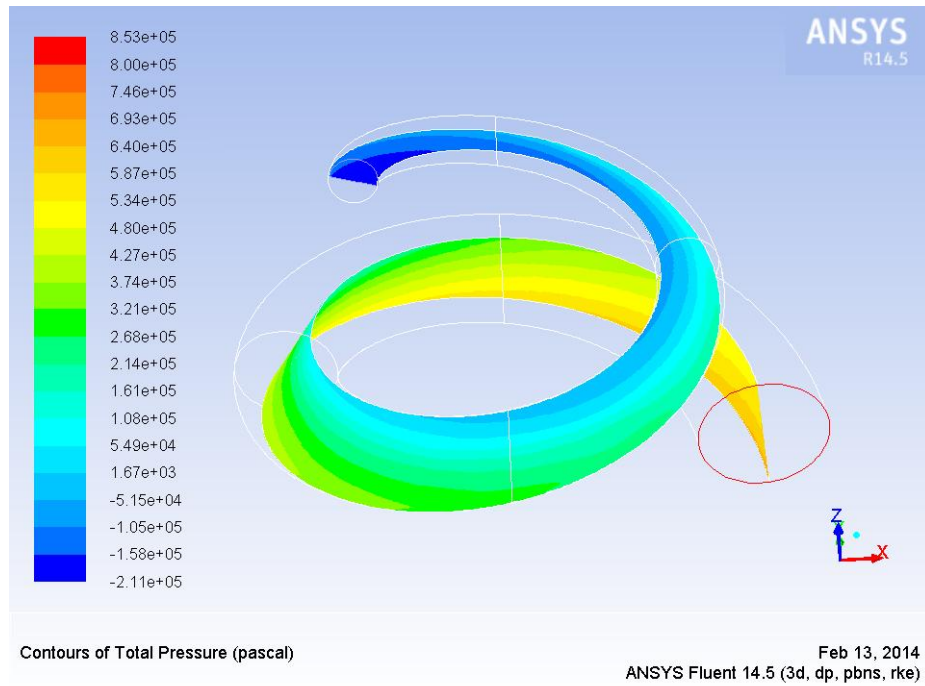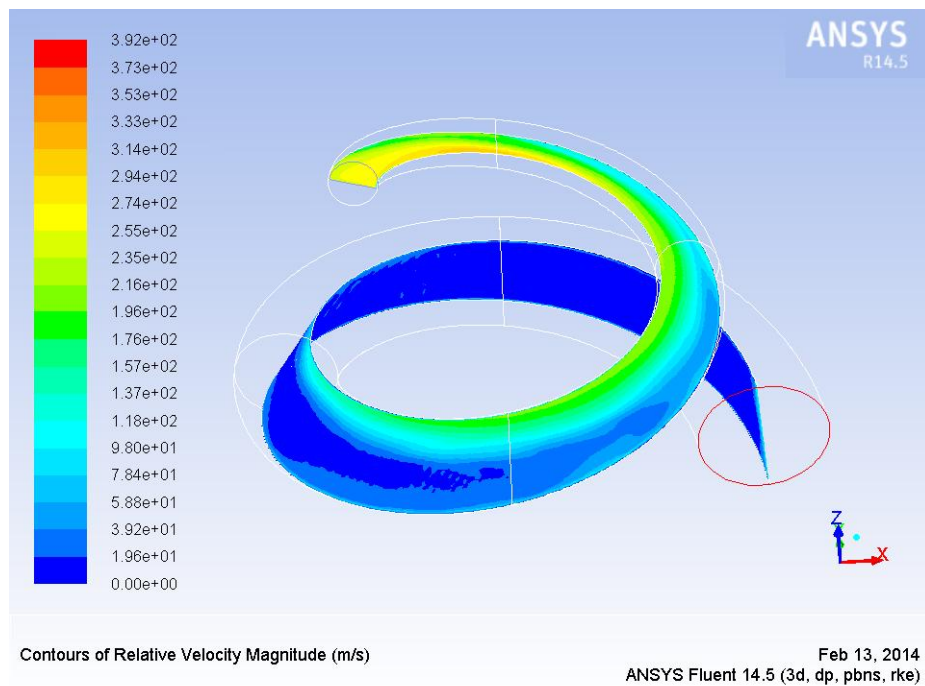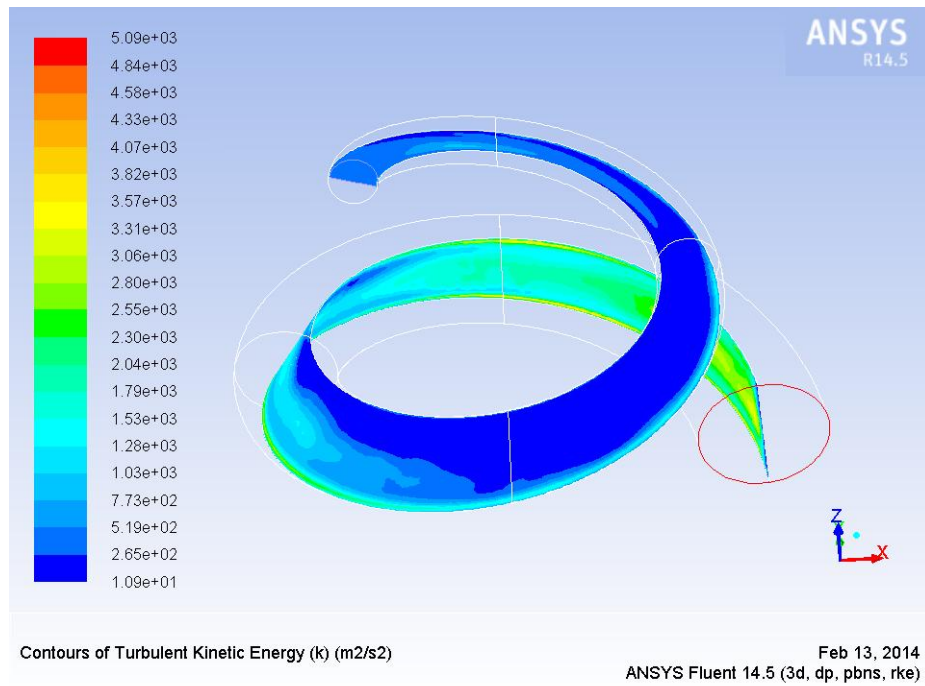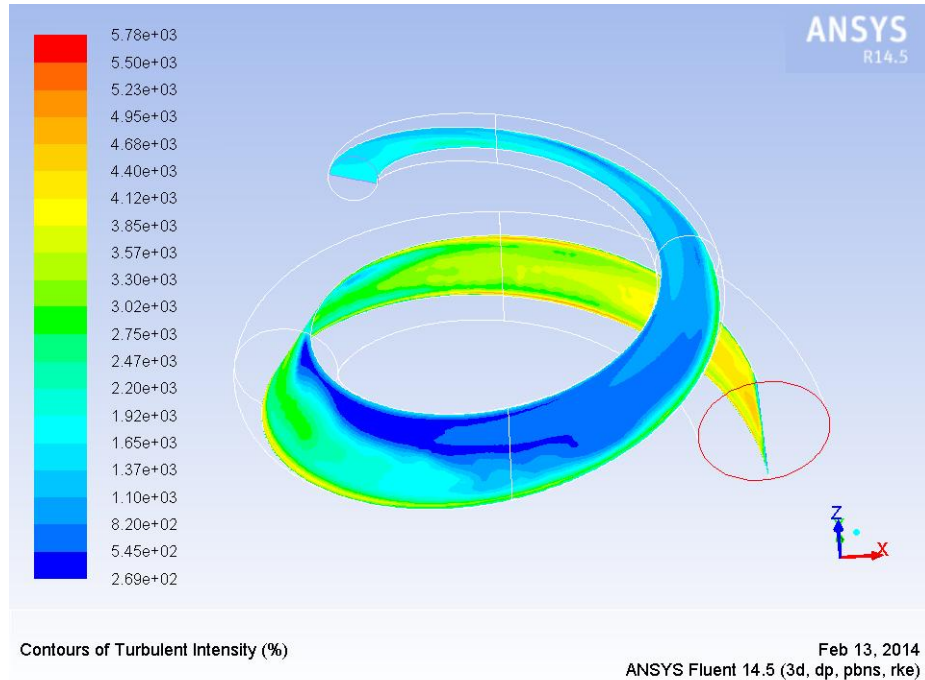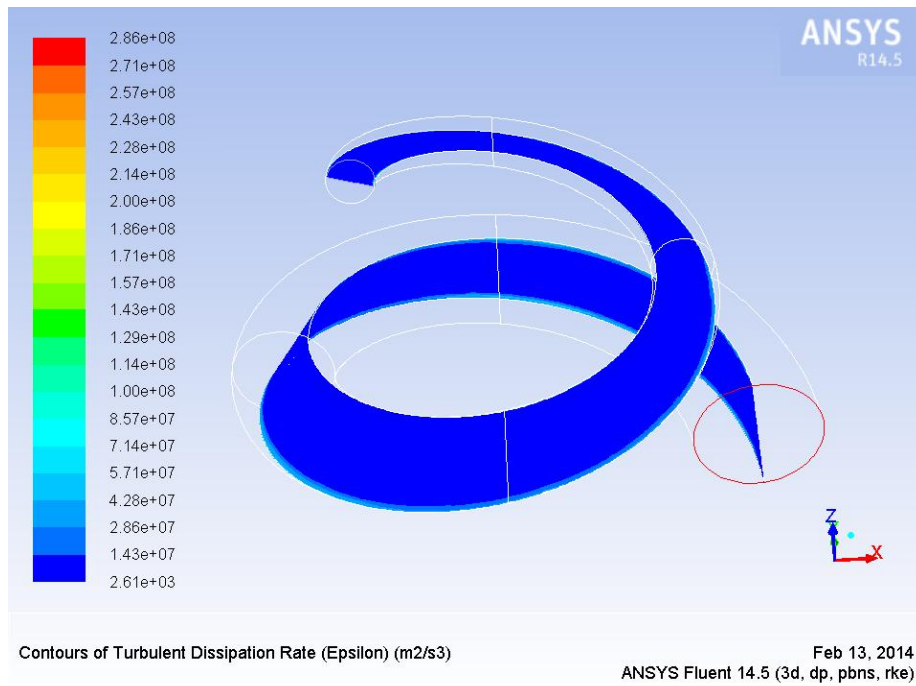

Figure 130 Concept 1, 90.000 rpm, Turbulent intensity

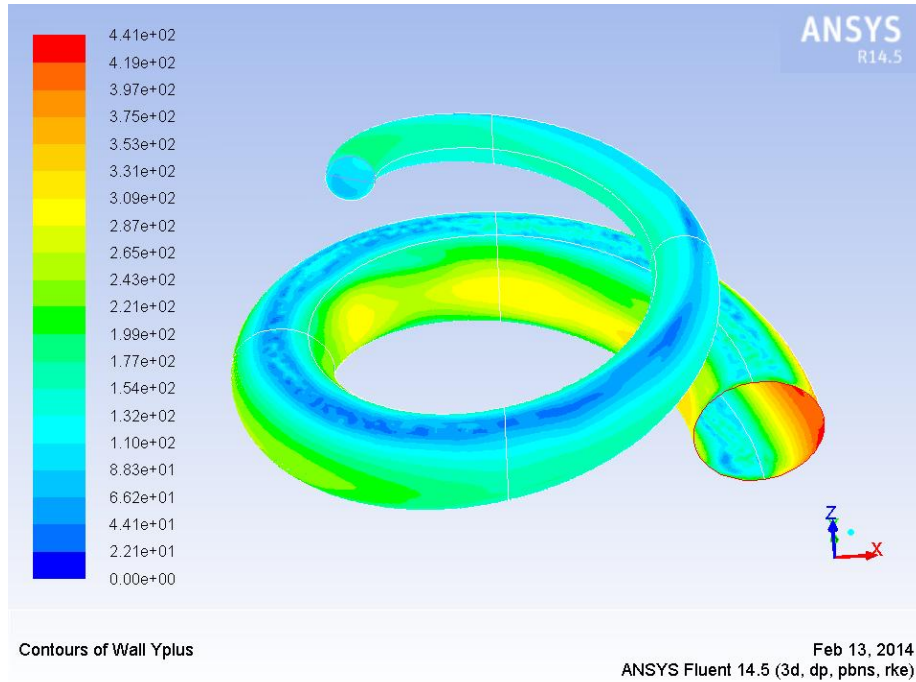Figure 131 Concept 1, 90.000 rpm, Dissipation rate

Figure 132 Concept 1, 90.000 rpm, Y+ values

7 CONCLUSION

Schauberger was ahead his time and had worth striving ideas. His best achievement was the construction of the log flumes which reduced the transport costs significantly. Unfortunately the other inventions he built were mainly prototypes and he often did not bother to develop them to the point of sellable products. The difficulty in understanding his unscientific language and thinking does not make it easier to reproduce these ideas. His theory about the ideal water movement, which was proven by the "Stuttgart experiment" with Prof. Pöpel, assumes if water can flow in an inwardly spiralling way, like it flows in the kudu-pipe which has Schauberger adapted from the horn of a kudu antelope, great losses due to resistance and friction occur.

This assertion could not be confirmed in the course of this diploma thesis. The results back in his days can only be explained by a faulty experimental set up and a very unscientific evaluation of the measurements.

The investigation to reproduce the Stuttgart experiment by using fluid flow simulation software came to the same results, as was expected according to the doctrine. The pipes with the smallest wall surfaces and thus with the lower friction areas are having the highest flow rate. The kudu-pipe shows a lower efficiency due to the large wall surface and is therefore not of interest for further investigations.

The idea of Mr. Franz Mayr, employee of the company Magna Steyr, to construct an absolutely new kind of car compressor based on the ideas of Schauberger is nevertheless a serious idea. Because of the results from the reproduced Stuttgart experiment, the construction of kudu spirals for forced induction was ignored and only a compressor with one, six and 12 simple spiral channels was analysed.

To hold the work in a reasonable framework only the spiral itself was examined, and not the whole compressor system including the housing. Also the inlet and outlet of the spiral was designed in a simple tangential way. The spiral itself was defined with one and a half turns and the ratio between the inlet diameter and outlet diameter was specified with 3:1.

The viscous model used for the simulations was the k-ε model, where the fluid flow equations for about one million cells for every simulation run were solved.

The results of the investigation shows the opposite behaviour as the GT1544, a turbocharger used as a reference compressor manufactured by GARRETT, were the pressure ratio increases with increasing revolutions per minute and air flow. The limit of the spiral compressor was identified by 130.000 rpm's, because above that value only poor pressure ratios can be reached and strong suction effects occur at the outlet of the spiral.

Below the limit better results as the reference supercharger can be achieved. The maximum pressure ratio is reached at 50.000 rpm's with a value of 2,7. The GT1544 must rotate with about 210.000 rpm's to achieve similarly high ratios. This would lead to a big advantage of the new compressor principle in terms of wear.

Because the results have shown that the spiral-compressor defeats the GT1544 at lower rpm's, a second compressor was used as a reference. A turbocharger used in motorsports, the GT4088 with higher flow rates at lower numbers of revolutions, was used to analyse the behaviour of the new concept at lower rotation speeds. But the results were pretty much the same. Again at lower rotation speed the spiral compressor defeats the reference until a certain rpm.

7.1 RECOMMENDATIONS

The results of the simulations have shown that the first considerations towards turbo-chargers were proven to be false. The spiral concept should be investigated in the area of mechanical chargers, compressors/superchargers which are rotating only in the range up to 10.000 rpm's and should be compared with such a type, for example the G-Lader.

For the present the geometry of the spiral should be retained. However, the flow conditions have to be optimized at the inlet and outlet. Innovative solutions are required for manufacturing the mechanical charger with spiral channels. Perhaps in the future the production with a 3d printer would be possible.

In terms of the simulation some improvements should be made. First the mesh could be refined. For every single case an extra mesh should be generated and checked with the resulting quality value of the simulation, thus resulting in a more accurate solution for every run. The most important change should be specifying the flow conditions at the inlet and outlet. According to the Magna Steyr concept currently an axial inflow is planned, which represents the biggest problem. This construction could cause that no air flows into the spiral channel. This was also the reason why the inlet was kept in a tangential way. To solve this problem further considerations are necessary. In order to make the concept really comparable, the whole system with housing and spiral channels should be integrated in the simulation research to be able to make a statement about the efficiency.

Generally, it would be of interest to simulate and compare the various turbulence models for spirals, which is still lacking in the literature. Therefore the k-ω and Reynold Stress model would be advisable and should also lead to a better solution.

Of course the whole study should be verified experimentally, preferable with a transparent housing. A particle image velocimetry is recommended to analyse the in- and outflow conditions.

REFERENCES

BOOKS

Alexandersson, O. (2008): *Lebendes Wasser, Viktor Schauberger rettet die Umwelt*, Ennsthaler Verlag Steyr, ISBN 978-3-85068 377-7

Bar-Meir, G. (2013): *Basics of Fluid Mechanics*, last modified: Version 0.3.4.0 July 25, 2013, www.potto.org/downloads.php

Brandstätter, W. (2011): *Geo-Engineering and Fluid Mechanics*, lecture notes, University of Leoben, Leoben

Brödel, A. (2004): *Der "Stuttgart-Versuch" Implosion Sonderheft*, Verein für Implosionsforschung und Anwendung e. V., Verlag Klaus Rauber, ISBN 3-9805725-3-6

Coats, C. (2001): *Living Energies: An Exposition of Concepts Related to the Theories of Viktor Schauberger*, Gill & MacMillan; 2nd edition, ISBN-13: 978-0717133079

Current, J.D. (2011): *Physics Related to Anesthesia*, Second Edition, PediaPress GmbH

Fitzpatrick, R.: *Fluid Mechanics*, lecture notes, University of Texas Austin, Austin

Hack, G. et al. (2003): *Turbo- und Kompressormotoren, Entwicklung und Technik*, Motorbuch Verlag, Stuttgart, 3. Auflage, ISBN 3-613-01950-7

Honeywell International Inc: Turbocharger Guide, Volume 5

Johansson, L. et al. (2002): *Self-organizing Flow Technology – in Viktor Schauberger's Footsteps*, Institute of Ecological Technology, ISBN 91-631-2611-7

Kokaly, A.: *Der goldene Pflug – 60% Mehrertrag im Feld und Garten, Entgiftung der Kunstdüngerböden, Bodengesundungen durch Spurenelemente*, Zusammengestellt nach Aufzeichnungen von Viktor Schauberger und D.I. Walter Schauberger, Nachdruck durch Verein für Implosionsforschung und Anwendung e.V., Offenburg

Lattacher, S. (2003): *Viktor Schauberger: Auf den Spuren des legendären Naturforschers*, Ennsthaler Verlag Steyr, ISBN 978-3-8506 85443

McDonough, J.M. (2009): *Lectures in elementary fluid dynamics*, Departments of Mechanical Engineering and Mathematics, University of Kentucky, Lexington, KY 40506-0503

Pangman, M. J. (2011): *Dancing with Water: The New Science of Water,* Uplifting Press, ISBN 978-0975272626

Pucher, H. (2012): *Aufladung von Verbrennungsmotoren: Grundlagen, Berechnungen, Ausführungen*,

Schauberger, V. (1933): *Unsere sinnlose Arbeit – Die Quelle der Weltkrise, Der Aufbau durch Atomverwandlung, nicht Atomzertrümmerung*, J. Schauberger Verlag, 6. Auflage 2011, ISBN 978-3-902262-00-4

Schauberger, V. (2012): *Das Wesen des Wassers*, Originaltexte, herausgegeben und kommentiert von Jörg Schauberger, AT Verlag, Deutschland, Baden und München, ISBN 978-3-03800-272-7

Schlichting, H. (1979): *Boundary-layer theory*, 8th Edition, Springer-Verlag, Berlin, Heidelberg, New York, ISBN 3-540-66270-7

Skopil, M. A. (2006): *Moderne Turboaufladung, Grundlagen der Aufladetechnik für Diesel- und Ottomotoren*, expert Verlag, Deutschland, Renningen, 2. Auflage, ISBN 978-3-8169-2721-1

Versteeg, H. K. and **Malalasekera** W. (1995). *An introduction to computational fluid dynamics – The finite volume method*, Addison Wesley Longman Limited, Edinburgh Gate, Harlow, England, ISBN 0-582-21884-5

Werdenberg, N. (2006): *Handling Water*, Executive Master of Environmental Technology and Management NDS/FH, Master Thesis, University of Applied Sciences Northwestern Switzerland

White, Frank M. (1998): *Fluid Mechanics*, Fourth Edition, Publisher McGraw-Hill College, ISBN 978-0072281927

REPORTS

PÖPEL, F. (1952): Bericht über die Voruntersuchungen mit Wendelrohren mit verschiedener Wandform, ausgeführt vom Institut für Gesundheitstechnik an der Technischen Hochschule Stuttgart, Leiter Prof. Dr.-Ing. habil. Franz Pöpel

INTERNET

en.wikipedia.org/wiki/Viktor_Schauberger (26.11.2012)

en.wikipedia.org/wiki/Greater_kudu (26.11.2012)

www.implosion-ev.de/index.html (27.11.2012)

www.pks.or.at (27.11.2012)

en.wikipedia.org/wiki/Mass_flow_rate (28.11.2012)

http://en.wikipedia.org/wiki/Supercharger (6.5.2013)

https://en.wikipedia.org/wiki/Forced_induction (6.5.2013)

APPENDIX

All results from the various simulation runs were evaluated graphically. This data can be found on the attached DVD.